DESIGN AND OPERATION OF ENZYMATIC REACTIVE CRYSTALLIZATION: APPLICATIONS IN CHIRAL PURITY AND KINETICALLY CONTROLLED SYNTHESIS

A Thesis
Presented to
The Academic Faculty

by

Luis G. Encarnación-Gómez

In Partial Fulfillment
of the Requirements for the Degree
Doctor in Philosophy in the
School of Chemical & Biomolecular Engineering

Georgia Institute of Technology
December 2015
Copyright © Luis G. Encarnación-Gómez

DESIGN AND OPERATION OF ENZYMATIC REACTIVE CRYSTALLIZATION: APPLICATIONS IN CHIRAL PURITY AND KINETICALLY CONTROLLED SYNTHESIS

Approved by:

Dr. Ronald W. Rousseau
Advisor
School of Chemical and Biomolecular
Engineering
Georgia Institute of Technology

Dr. Yoshiaki Kawajiri
School of Chemical and Biomolecular
Engineering
Georgia Institute of Technology

Dr. Charles Liotta
School of Chemistry
Georgia Institute of Technology

Dr. Andreas S. Bommarius
Co-Advisor
School of Chemical and Biomolecular
Engineering
Georgia Institute of Technology

Dr. Matthew Realff
School of Chemical and Biomolecular
Engineering
Georgia Institute of Technology

Date Approved: July 9, 2015

ACKNOWLEDGEMENTS

TABLE OF CONTENTS

Page

LIST OF TABLES

LIST OF FIGURES

Page

xiii

LIST OF ABBREVIATIONS

A_{ij}=Pitzer's model adjustable parameter $(kg/mol)^{1/2}$

[Amp]=ampicillin concentration (mM) or (g/kg H_2O)

[APA]=6-aminopenicillanic acid concentration (mM)

b = empirical nucleation rate exponent

b_M = secondary nucleation mass of crystals exponent

B_{ij}=Pitzer's model adjustable parameter $(kg/mol)^{1/2}$

B = rate of nucleation (#/min)

B_o=primary nucleation exponential constant

B_1=rate of primary nucleation (#/s m^3)

[D], [L] = concentrations of D and L enantiomers (g/kg H_2O)

[D^{sat}], [L^{sat}] = solubilities of D and L enantiomers (g/kg H_2O)

E_A = Activation energy (kJ/mol)

E_0 = initial mass of enzyme (g)

ee = enantiomeric excess

ee_{Eu} = enantiomeric excess at the eutectic point

g = growth rate exponent

G = crystal growth rate (m/s)

J=nucleation rate (#/ g/kg)

k_a =area shape factor

k_B = nucleation rate constant (#/$(g/kg)^b$·min)

k_{Bi} = primary/secondary nucleation rate constant (#/(g/kg) min)

k_B = Boltzmann's constant (m2 kg s^{-2} K^{-1})

k_G = growth rate constant (m/min)

K_M = Michealis constant (mM)

k_v = volume shape factor

$k_{o,D}$ = rate of oxidation of D-amino acids constant (mM/min·g enzyme)

k_D = net rate of consumption of D-amino acids constant (mM/min·g enzyme)

k_R = rate of reduction of DL-amino acids constant (1/mM·min)

l = crystal length (m)

l = crystal length (m)

$\bar{L}$ = average crytal length (μm)

M = mass of crystals (g)

n = number density function (#/ m·m^3)

N_A = Avogadro's number (mol^{-1})

R = gas constant (kJ/mol·K)

P = productivity (g/kg H$_2$O·min)

P = precision matrix

[PG]=D-phenylglycine concentration (mM) or (g/kg H$_2$O)

[PGME]=D-phenylglyscine methyl ester concentration (mM)

S_o=initial supersaturation (mM/mM)

s=secondary nucleation supersaturation exponent

S_i=sensitivity matrix

t = time (min)

t_N = induction period (s)

t_G = growth period (s)

T = temperature (K)

T_M = melting temperature (K)

V = covariance matrix

x_i = mole fraction (mol of i/mol total)

Greek Letters

α = synthesis vs. hydrolysis kinetic constant (dimensionless)

β_0 = synthesis vs. hydrolysis kinetic saturation constant (M^{-1})

ΔC_P = heat capacity (J/mol·K)

ΔH_M = heat of melting (J/mol)

ε = van der Waals attractive interaction parameter (m^2 kg s^{-1})

λ_{ij} = Pitzer's binary interaction parameter (kg mol^{-1})

γ = synthesis vs. hydrolysis kinetic constant (dimensionless)

σ = van der Waals diameter (m)

ρ_c = crystal density (kg/m^3)

v, v_{Max} = rate of reaction and maximum rate of reaction (mM/min)

μ_i = ith moment of number density function

SUMMARY

The work presented in this thesis is aimed to design efficient reactive crystallization operations that could potentially be implemented in the manufacture of enantiomerically pure compounds and β-lactam antibiotics. Multiple aspects of solution thermodynamics, reaction engineering and crystallization from complex solutions are involved and will be discussed in detail through the following chapters.

The first piece of this work utilizes reactive crystallization for the manufacture of enantiomerically pure amino acids. Chemo-enzymatic stereoiversion reactions are used to enrich saturated or supersaturated solutions to favor the selection of a desired enantiomer. L-Methionine and L-Phenylalanine were resolve successfully from racemic mixtures by cyclic stereoinversion. r D-amino acids were oxidized by D-amino acid oxidase (D-AAO) and the resulting ketoacid was subsequently reduced by ammonia borane producing a racemic-mixture   After the necessary enantiomeric enrichment was reached, system conditions were changed to induce supersaturation and promote crystal formation. In each case crystals with chemical and enantiomeric purities greater than 99% wt. were recovered. experimental information about reaction and crystallization kinetics was used to developed models. Such models were used to design model-based optimizations in which the productivity of the operation was enhanced by selecting an optimal temperature profile.

The second example is a reactive crystallization towards the manufacture of β-lactam antibiotics. One of the major drawbacks of the utilization of enzymes towards the manufacture of β-lactam antibiotics is the fact that the same enzyme that catalyzes the

synthesis of the antibiotic also catalyzes its hydrolysis and thus, its degradation. The reaction scheme is a kinetically controlled synthesis in which the desired product is an intermediate within the network. Hence, the focus of this work is to design an efficient reactive crystallization in which the product is crystallized before it is consumed by hydrolysis. In order to accomplish this goal we have study solution equilibria, reaction kinetics, and crystallization kinetics. Even though crystallization kinetics of ampicillin has been previously reported; the reported models are not applicable to a reactive crystallization scheme for a variety of reasons. In this work, we have developed a robust model that can be applied to multiple crystallization protocols that are consistent with the conditions at which the enzymatic reaction can be performed.

Finally, a reactive-crystallization scheme in which ampicillin was successfully recovered from solution was developed. In this work, crystal seeds were used to promote crystallization of the desired product from the complex media. The results indicated that is possible to perform the reaction and crystallization in parallel, and still recover crystals with high purity. This work is the first example in which ampicillin was produced and recovered with high purity in a single stage. Previous work on reaction crystallization of antibiotics reported ampicillin crystallization; however, this was accompanied by precipitation of by-products which greatly reduces the applicability of the operation as product purification is required after the reaction.

CHAPTER 1

Introduction

1.1 Manufacture of enantiomerically pure compounds

Enantiomers are non-superimposable mirror image compounds. As a result, these will exhibit the same chemical properties differing only on their spatial orientation. This attribute is very important since the majority of molecules in biological systems exist as a single orientation. For example, amino acids of a protein will exhibit an L-orientation. This preferred orientation is consistent through almost every molecule in life. Such topic has been an unsolved question, where researchers have been trying to explain the selective evolution towards a specific orientation (Blackmond, 2010). For this reason, enantiomeric orientation is a critical factor in the development of pharmaceuticals as different orientations will interact differently with the body. Probably, the most remarkable example of this dual interaction is thalidomide. This drug was synthesized in 1964 by CIBA pharmaceutical company, and prescribed as tranquilizer and antimetic for morning sickness (Franks et al., 2004). However, it ended up causing multiple congenital defects to approximately 10,000 children worldwide. This undesired effect is believed to be cause by one of the enantiomeric orientations. Further, examples includes a significant number of high volume prescribed medications such as Lipitor (Pfizer), Plavix (Bristol Myers-Squibb), and Advair (Glaxo Smith Kline), and common over the counter medications such as analgesics, anti-inflammatories, and acid reflux inhibitors. As a result of investigations on this area, the Food and Drug Administration (FDA) and other international regulatory agencies require both chemical and enantiomeric purity on APIs unless the counter enantiomer is proven to be unhazardous.

There are two main routes in which enantiomerically pure compounds can be obtained: (1) selective synthesis/consumption and (2) separation of racemic mixtures. In the first route (synthesis/consumption), enantioselective reactions can be achieved through the utilization of an enantioselective catalysts. These catalysts can be either organic/inorganic or biochemical. Catalysts enable reactions that can enrich the enantiomeric excess through asymmetric synthesis (i.e. just producing a single enantiomer) or by consuming one of the enantiomers of a racemic mixture (Kroutil et al., 1998; Wolf, 2007).

Alternatively, enantiomerically pure compounds can be obtained through separation and/or purification of racemic mixtures. This option is predominant due a lack of asymmetric catalysis towards the production of a significant number of compounds. Usually, when an organic synthesis is performed without the presence of a chiral catalyst there is an equal probability of synthetizing either enantiomer. As a result, the product of such reaction will be a racemic mixture that contains equal concentrations of both enantiomers. At this stage, the product can be processed through a separation train to obtain a solution or solid whose only solute is the desired enantiomer. In most cases, this separation involves chiral chromatography or chiral crystallization. Chiral chromatography involves the utilization of a stationary phase that contains chiral ligands (E. Francotte, 2009; E. R. Francotte, 2001). Recently, this principle has been extended to simulated moving beds (SMBs), where the productivity of the separation is improved by changing the inlet/outlet of the solution resulting on an optimal usage of the column (E. Francotte et al., 2002).

Enantioselective crystallization (or chiral crystallization) requires understanding the kinetics and equilibrium of the system of interest. This type of crystallization can be classified into three major groups: (1) preferential crystallization, (2) diastereoisomeric salts crystallization,

and (3) crystallization of enantioenriched solutions. The first one exploits crystallization kinetics to achieve the separation as crystallization of one enantiomer is temporarily *preferred* over its counterpart. This preference is based on seeding a solution with the desired orientation and recovering the crystals before the solution concentration returns to equilibrium. Crystallization of diastereomeric salts employs chiral reagents to form salts whose thermodynamic properties (solubility) differ from each other, thus breaking the symmetry of the system. These salts are eventually resolved with strong acids or bases to recover the pure enantiomers. Lastly, crystallization from enantioenriched solutions simply refers to crystallization from a solution in which the formation of an enantiomerically pure crystal is thermodynamically favored. Such an enantiomeric enrichment can be achieved by reactions or previous units of separation.

In this work enzymatic reactions are being used to enrich the solution with respect to the desired orientation. Enzymes have been extensively used for the synthesis of enantiomerically pure compounds as they can offer great enantioselectivity. In this project, enzymes are being used to perform enantioselective oxidations. This reaction combined with a chemical reduction allows us to completely change the orientation of the undesired enantiomer into its counterpart. Additionally, reactions are performed at concentration levels that enable the recovery of the desired product while its sill being produced. Such approach maximizes the productivity of the operation as will be explained later.

1.2 Manufacture of β-lactam antibiotics

β-lactam antibiotics are the class of antibiotics that contain a β-lactam ring within their structure. This group includes a broad range of penicillin derivatives such as ampicillin and

amoxicillin, and cephalosporins, monobactams, and carbapenems. These type of antibiotics span approximately 65% of the world market for antibiotics, with sales greater than $15 billion (Elander, 2003; Giordano et al., 2006). Commercial manufacturing of β-lactams antibiotics is usually achieved through conventional organic synthesis, where low temperatures, organochloride solvents, and protection/deprotection groups are employed (Ospina et al., 1996). As a result, a significant amount of waste is generated through the process. For example, the E-factor of cephalexin is approximately 35 kg of waste per kg of product (Wegman et al., 2001). Considering that this compound has an annual production of 3000 tons, the annual generation of waste exceeds 100,000 tons.

An alternative route for manufacturing of β-lactam antibiotics is the enzymatic synthesis by penincillin G acylase (PGA). This enzyme can catalyze the acyl transfer from an activated side chain donor to the nucleophilic β-lactam forming the desired antibiotic. For example, the enzymatic synthesis of ampicillin can be achieved by reacting 6-aminopenicillanic (6-APA) acid and D-phenylglycine methyl ester (D-PGME) in the presence of PGA. Similarly, other β-lactam can be produced by PGA simply by changing the initial reactants.

The overall reaction scheme is presented in Figure 1.1. As it can be seen in the figure, PGA does not only catalyze the synthesis of ampicillin but it also catalyze the hydrolysis of D-PGME to D-phenylglycine and the hydrolysis of ampicillin to D-phenylglycine and 6-APA. In fact, the production of 6-APA can be achieved through hydrolysis of penicillin G by PGA (Abian et al., 2003).
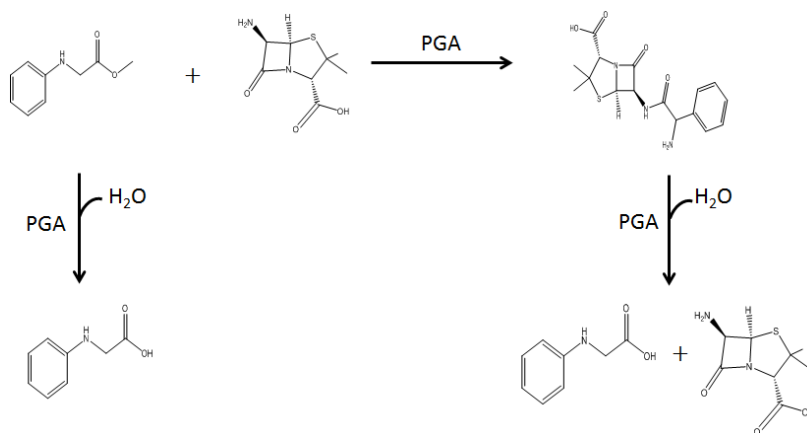
Figure 1.1: Enzymatic synthesis of ampicillin by PGA.

As it can be observed in the figure, this system is a kinetically controlled reaction, where ampicillin is an intermediate within the network. Multiple reaction engineering strategies have been used to improve the yield of 6-APA towards ampicillin.

In this work we have developed a reaction-crystallization scheme that enables the recovery of ampicillin as it is produced by the synthesis reaction. Such a process has the potential of protecting ampicillin from secondary hydrolysis, which increases the yield of the operation. Additionally, separation and purification of the desired product is achieved while is being produced. Hence, the productivity of the operation is increased as the total manufacturing time is reduced.

CHAPTER 2

Literature Review

2.1 Crystallization Fundamentals

2.1.1 Introduction

Crystallization refers to the formation of a structured (crystalline) solid phase from a supersaturated solution. Such technique has been widely used for the separation and purification of specialty chemicals, food, and pharmaceuticals. Common techniques used to induce supersaturation include cooling, evaporation, anti-solvent addition, and precipitants addition. All of these rely on changing system thermodynamics such that the solubility of the solute is reduced.

Although separation and purification can be a difficult task by itself, usually a crystallization process is design to meet not only purity and productivity targets, but crystals with the desired properties. These properties can include morphology, crystal size distribution (CSD), and minimization of impurity or solvent inclusion, etc. Such properties are considered as quality attributes as they affect the performance of the molecule. For example, it is very well know that the morphology and crystal size of an active pharmaceutical ingredient (API) affects its solubility and dissolution rate (Nagy et al., 2012). Additionally, CSD greatly affects post-crystallization operations such as filtration and drying (Wibowo et al., 2001). In order to control these properties, a thorough understanding of the crystallization process is necessary. This usually refers to obtaining information about crystallization kinetics, which relates the rate of nucleation and crystal growth to the level of supersaturation in the system (Mullin, 2001; Randolph et al., 1988).

2.1.2 Solution thermodynamics

Solubility is defined as the maximum concentration of a solute at equilibrium with a solvent at given conditions. This maximum concentration is a function of multiple variables of the process such as temperature, pH, ionic strength, co-solvent fraction, and concentration of other solutes. Using a thermodynamic framework, equilibrium can be defined using the fugacity of solutes in each phase:

$$f_{i,pure\ solid} = f_{i,solution} \tag{2.1}$$

$$f_{i,pure\ solid} = \gamma_i x_i f_{i,0} \tag{2.2}$$

where γ_i is the liquid phase activity coefficient, x_i is the solubility (mole fraction), and $f_{i,0}$ is the fugacity at standards conditions. The selection of the standard state is arbitrary; thus, the fugacity of the pure subcooled liquid can be used to relate solubility to the fugacities in the liquid and solid phases.

$$x_i = \frac{f_{i,pure\ solid}}{\gamma_i f_{i,pure\ subcooled\ liquid}} \tag{2.3}$$

Utilizing a thermodynamic cycle the ratio of the fugacities can be related to the change of free energy of the system (Prausnitz et al., 1999). This can be used to relate the fugacities with physical parameters such as heat of melting, melting temperature, and the difference in sensible heat.

$$\ln \frac{f_{i,pure\ subcooled\ liquid}}{f_{i,pure\ solid}} = \frac{\Delta H_M}{RT_M}\left(\frac{T_M}{T}-1\right) - \frac{\Delta C_p}{R}\left(\frac{T_M}{T}-1\right) + \frac{\Delta C_p}{R}\ln\frac{T_M}{T} \tag{2.4}$$

Finally, this equation can be used to relate the solubility with such physical parameters because the ratio of the fugacities is related to the solubility.

$$\ln\frac{1}{\gamma_i x_i} = \frac{\Delta H_M}{RT_M}\left(\frac{T_M}{T}-1\right) - \frac{\Delta C_p}{R}\left(\frac{T_M}{T}-1\right) + \frac{\Delta C_p}{R}\ln\frac{T_M}{T} \qquad (2.5)$$

By assuming ideal solution and neglecting the effect of sensible heat, Equation 2.5 can be reduced to the commonly used Van't Hoff equation, which relates solubility with the temperature of the system.

$$\ln\frac{1}{x_i} = \frac{\Delta H_M}{RT_M}\left(\frac{T_M}{T}-1\right) \qquad (2.6)$$

This expression is commonly used in the design of cooling crystallization protocols, as the temperature of the system is reduced to induce supersaturation.

2.1.3 Phase diagrams

For practical purposes, the solubility of a particular solute in a solvent can be represented with a phase diagram. This type of diagram presents useful information related to the solubility of the compound of interest as a function of process variables such as temperature, pH, composition, and others. Figure 2.1 shows a generic phase diagram for a single component as a function of temperature. In such diagram we can identify the concentration at equilibrium at any particular temperature. The solubility curve divides the diagram in two possible phases; below the curve an undersaturated region exist where only a liquid phase is present, while above the curve the solution is supersaturated and a solid and liquid phase can coexists.
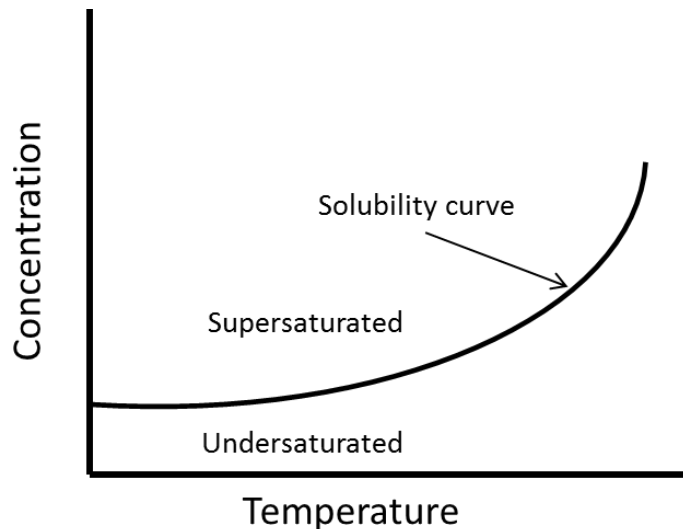
Figure 2.1: Pure component phase diagram as a function of temperature.

Similarly, phase diagrams can be constructed using different variables such as pH, ionic strength, or composition. If multiple solutes can crystallize at the range of operation, a multicomponent phase diagram is necessary to describe the system. In future sections, such a diagram will be used to describe the solubility of chiral compounds as a function of temperature and counter-enantiomer.

2.1.4 Nucleation

The formation of new crystals from a supersaturated solution is referred as nucleation. This event can be classified as primary or secondary nucleation. Primary nucleation occurs when new crystals are created in the absence of previously formed crystals (seeds), while secondary nucleation refers to the creation of new crystals in the presence of seeds. Primary nucleation can be sub-classified in two categories: (1) homogeneous and (2) heterogeneous nucleation (Randolph et al., 1988). Homogeneous nucleation is refer to a spontaneous nucleation event that is not induced by the presence of foreign solid bodies (Mullin, 2001). On the other hand, heterogeneous primary nucleation is induced by the presence of foreign solid bodies (other than seeds). Although in

9

multiple processes primary nucleation is assumed to be homogeneous, it is difficult to guarantee that the surface area of the crystallizer, blades, baffles, etc. are not influencing nucleation.

The formation of new stable nuclei requires organization and clustering of solute molecules in solution (Larson et al., 1986b). However, prior the onset of nucleation an interchange of molecules between the cluster and solution will take place. This cluster would remain in solution until a nuclei critical size is achieved. Such critical size can be derived from solution thermodynamics by considering the change in free energy of the system (Larson et al., 1986a). First, the contributions of solute surface area and volume are considered as the total change in free energy of the system.

$$\Delta G = \Delta G_A + \Delta G_V \tag{2.7}$$

The contribution of the surface area to the change in free energy of the system it is assumed to be proportional to the change of total area times its surface tension.

$$\Delta G_A = A_n \gamma \tag{2.8}$$

Additionally, the contribution of the volume it is associated to the specific free energy change of the liquid-solid phase transformation.

$$\Delta G_V = -\left(1-\alpha+\nu\alpha\right)V_n C_c R T ln \frac{C}{C*} \tag{2.9}$$

Finally, by substituting the respective expressions in the total change in free energy of the system, an expression that relates this change with the dimensions of the nuclei can be obtained.

$$\Delta G = A_n \gamma -\left(1-\alpha+\nu\alpha\right)V_n C_c R T ln \frac{C}{C*} \tag{2.10}$$

Nuclei critical size can be obtained by differentiating the change in free energy respect to length and equating this expression to zero.

$$L_c = 4\gamma / \left(\left(1 - \alpha + \nu\alpha\right) RTc_c \ln \frac{C}{C^*} \right)$$ (2.11)

Figure 2.2 shows the change in free energy as a function of nuclei size. As it can be observed, whenever the positive contribution of the surface area is predominant, the nuclei will not reach its critical size and will remain in solution. This barrier is overcome when the supersaturation of the system it is high enough to make the volume contribution predominant. After this, the energy of the system will decrease by the creation of a new phase.
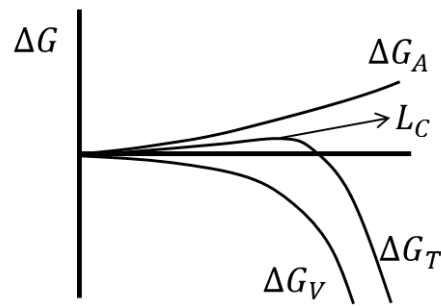
Figure 2.2: Change in free energy of the system as a function of nuclei length.

2.1.5 Growth

Crystal growth refers to the accumulation of solute molecules in an already existing crystal, resulting in an enlargement of the crystal size. As in nucleation, such a process is driven by the supersaturation in the system. There are multiple theories that explain this mechanism such as diffusion-reaction, surface energy, and layer adsorption theories. Diffusion-reaction explains the process by two steps. In the first step solute molecules diffuse from the bulk to the crystal surface, while in the second step solute molecules react with other molecules at the surface of the nuclei. Surface energy theory is based on the hypothesis that crystals will grow in the shape that minimize the surface energy of the crystal (Mullin, 2001). Finally, layer adsorption theory emphasizes the

importance of surface imperfections to facilitate the deposition of solute molecules into the crystal lattice.

2.1.6 Crystallization process

In the previous sections solution thermodynamics, nucleation, and crystal growth were discussed; in this section, this information will be used to discuss crystallization processes. Figure 2.3 shows a phase diagram as a function of temperature. It can be observed that the phase diagram it is divided in three different zones. The undersaturated region represents conditions that only a liquid phase can exist as the solubility has not been reached. The metastable region represents conditions in which the solution it is supersaturated (i.e. concentration>solubility) but this supersaturation it is not sufficiently high to induce instantaneous nucleation. After the metastable limit, the liable region it is reached. In this region, supersaturation is sufficiently high to induce instantaneous nucleation. This process can be explained from classical nucleation theory. As discussed in Section 2.1.4, the change in free energy of the system is composed of area and volume effects. These effects are inherently associated with the supersaturation of the system. However, this process explains only primary nucleation. In fact, if a solution within the metastable is seeded with crystals of the solute, nucleation is possible at the surface of these seeds through secondary nucleation mechanisms. This technique is used for the separation of compounds with similar solubility curves, as it is the case of enantiomeric compounds (Rodrigo et al., 2004). .
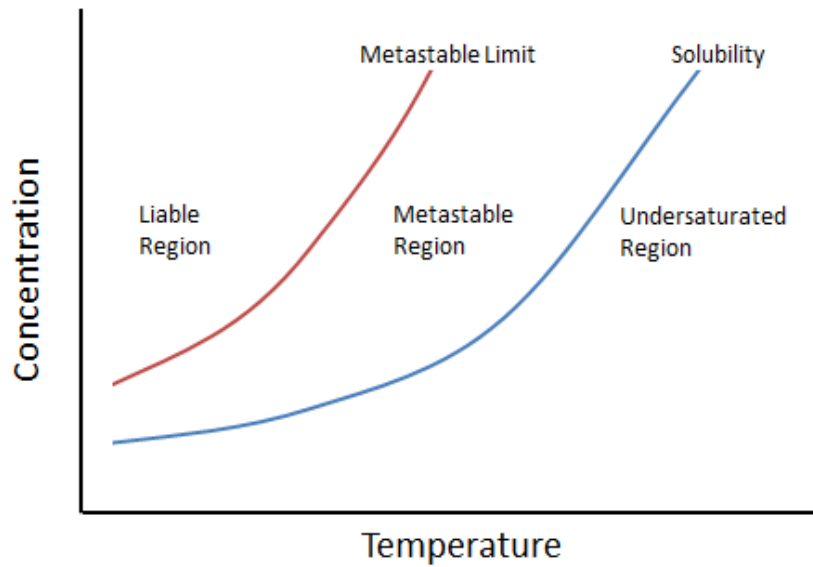
Figure 2.3: Solubility curve and metastable limit.

To illustrate the process let's consider Figure 2.4. The figure shows a cooling crystallization experiment of L-methionine (Encarnacion-Gomez et al., 2015). As it can be observed, at the beginning of the experiment the solubility curve it is above the solution concentration curve. Hence, at this point the solution is undersaturated and it is not possible to crystallize any product. As the temperature of the system is reduced, the solubility of the system changes accordingly to its temperature dependence. At some point, the solubility curve meets the concentration curve and the system enters the metastable region. As the solubility is still decreasing, supersaturation builds until the metastable limit is reached and nucleation occurs. After the first nuclei is created, supersaturation is depleted by a combination of nucleation and crystal growth. However, usually, as the concentration curves gets closer to the solubility curve crystal growth is the predominant mechanism.
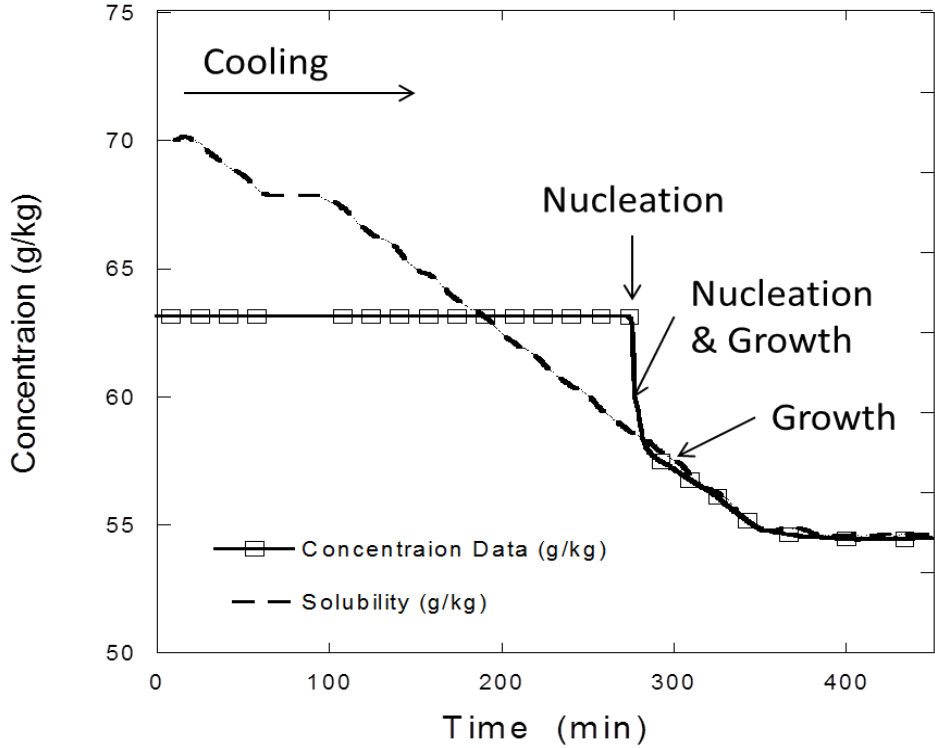
Figure 2.4. Crystallization of L-methionine steps.

2.1.6 Population balance and crystallization kinetics

The formation of solid particles in a crystallizer can be described by population balance equations(Randolph et al., 1988). Equation 2.12 represents the evolution of the number of particles of a particular size as a function of time and its size.

$$\frac{\partial n}{\partial t} = -\frac{\partial (nG)}{\partial L} \tag{2.12}$$

where:

$$n = \lim_{\Delta L \to 0} \frac{\Delta N}{\Delta L} = \frac{dN}{dL} \tag{2.13}$$

This equation is a partial differential equation; thus, both initial and boundary conditions are required for its solution. Equations 2.14 and 2.15 are the typical conditions used to solve the population balance equations. The initial condition represents the initial population at the beginning of the process and for unseeded crystallization it is equal to zero. The boundary

condition can be derived from a material flux analysis and it represents the creation of a particle of a negligible size that is growing in some characteristic direction.

$$n(L,0) = n_0 \tag{2.14}$$

$$n(0,t) = \frac{B}{G} \tag{2.15}$$

Numerical solution of PBE is achieved through multiple discretization methods as discussed elsewhere (Chang, 1995; Qamar et al., 2006). Such methods deal with the high non-linearity of crystallization processes increasing the reliability and robustness of the models.

Solution to population balance equations can be simplified by applying the method of moments. In this method, the moments of the distribution are related with cumulative properties of the system. For example, the zeroth moment represents the total number of particles with a dimension of zero (nuclei). The first moment represents particles of one-dimension; hence, it represents the summation the length of the particles in the system.

$$\mu_i = \int_0^\infty n(t,L) L^i dL \tag{2.16}$$

Differentiation of the moments leads to expressions that contain nucleation and growth kinetics:

$$\frac{d\mu_0}{dt} = J \tag{2.17}$$

$$\frac{d\mu_i}{dt} = iG\mu_{i-1} \tag{2.18}$$

This method has been extensively employed to model batch crystallization kinetics as the partial differential equation is transformed to an ordinary differential equation that can be easily solved with the appropriate initial conditions (Qiu et al., 1994).

2.2 Synthesis and separation of enantiomerically pure compounds

2.2.1 Enzymatic synthesis and resolution of chiral compounds

Biocatalysts are commonly used to manufacture enantiomerically pure compounds because of their high enantioselective. Enzymes can perform different reactions such as reductions, oxidations, transaminations, and others. Usually, these reactions are performed at mild conditions in comparison with their chemical counterparts. Simon et al.(Simon et al., 1985) discussed the utilization of different microorganisms for the reduction of multiple aldehydes, carboxylic acids, ketones, and carboxylates. The selectivity of such reactions was found to be completely dependent on the substrate of interest. Bommarius et al. discussed the utilization of isolated enzymes towards the manufacture of enantiomerically pure amino acids (Bommarius et al., 1998, 2001). In their work, multiple processes such as hydantoinase/carbamoylases and reductive aminations are discussed. Hydantaoinase/carbamolyse is a two-step process; a hydantoin is first hydrolyzed to a carbamoylic acid and then converted to the amino acid. One of the key attributes of this process is that it can be easily adopted for the production of either L or D amino acids. This attribute is critical as D-amino acids are not common in nature and have great utility in the synthesis of pharmaceutical compounds. Another route discussed is the reductive amination of keto acids to amino acids by amino acid dehydrogenases. Further examples include the production of chiral amines by amine dehydrogenases (Abrahamson, Bommarius, et al., 2012; Abrahamson, Vazquez-Figueroa, et al., 2012). Instead of accepting keto acids as an amino acid dehydrogenase, ketones are accepted as a substrate yielding chiral amines as a product. Although these reactions are of great utility in the manufacture of enantiomerically pure compounds, half of the raw materials is lost if the initial substrate is a racemic mixture. Nevertheless, in multiple cases it is economically attractive to follow such approach (Wolf, 2007).

16

A significant number of chiral reactions deal with the transformation of a single enantiomer. In order to alleviate this issue, processes in which most of the racemic mixture is utilized have been developed. A remarkable example of such a process is seen in the manufacturing of aspartame. The yield of this operation can be double by the racemization of the undesired D-phenylalanine methyl ester (Boehm et al., 1984). In this process, the undesired D-phenylalanine methyl ester is continuously recycled and racemized. After multiple cycles, most of the undesired enantiomer has been converted and used in the final product.

A different approach that can be used to obtain enantiomerically pure compounds is stereoinversion of undesired enantiomers (Alexandre et al., 2002; Gruber et al., 2006; Soda et al., 2001). For example, amino oxidase has been used in combination of chemical reactions to obtain enantiopure products. This process can achieve streoinversion of chiral amino acids into a single enantiomer by a cyclic chemo-enzymatic stetroinversion. The process starts by oxidizing the undesired enantiomer into an achiral amino acid by using an enantioselective oxidase. Depending on enantiomer of interest, it is possible to oxidize different orientation as both D and L amino acid oxidases are available. Later, the achiral amino acid can be reduced into a racemic mixture through a chemical reduction. Alexandre et al. discussed the advantage of using amine-boranes for this purpose as less initial material is necessary to achieve the reduction (Alexandre et al., 2002). Additionally, models to predict and enhance the performance of this cyclic stereoinversions have been developed (Findrik et al., 2005; Kroutil et al., 1998). As mentioned before, these processes require the utilization of reduction agents. Therefore, process cost-effectiveness will be linked to the price of substrate vs. reducing agents.

2.2.1 Crystallization and purification of chiral compounds

Crystallization is one of the predominant techniques for the resolution of chiral compounds because of its robustness, simplicity, and cost effectiveness (Lorenz et al., 2014). As any crystallization process, separation of enantiomers it is driven by supersaturation at some conditions. However, the similarity of the enantiomers introduces complexity, as enantiomers are mirror images compounds that exhibit the same physical and chemical properties.

The vast majority of enantiomeric compounds are categorized as conglomerates or racemic compounds forming systems (Eliel, 1983). Ternary phase diagrams of such systems are illustrated in Figure 1 where solubility curves are presented at two different temperatures (i.e. two superimposed phase diagrams).
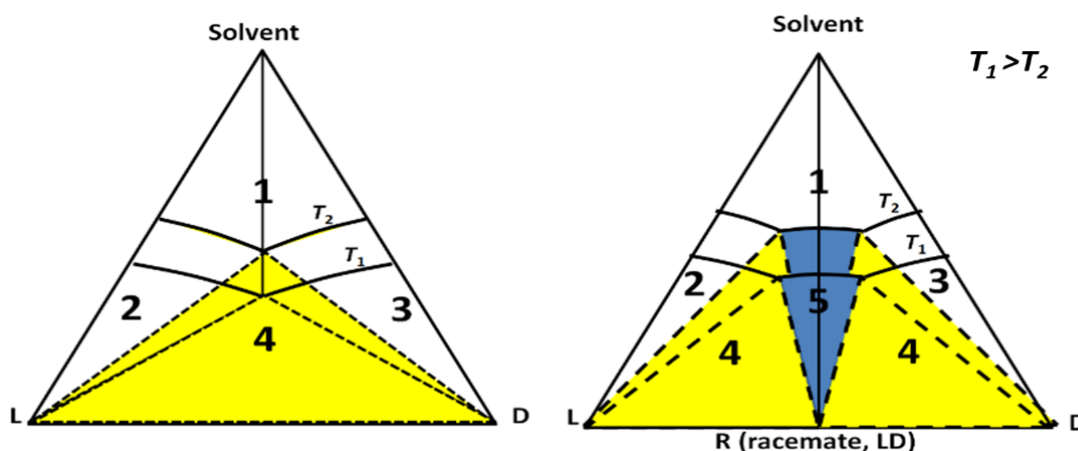
Figure 2.5: Conglomerate-forming (left) and racemic-compound-forming (right) systems.

Vertices of the triangles represent pure components with solvent at the top and the enantiomers at the bottom. The sides of the triangle represent the solvent-enantiomer or enantiomer-enantiomer systems. In both diagrams, Zone 1 represents undersaturated solutions; Zones 2 and 3 correspond to saturated solutions in equilibrium with enantiomerically pure crystals; Zone 4 represents saturated solutions in equilibrium with a physical mixture of crystals of the enantiomer and the racemate. The distinguishing characteristic of a racemic-compound-forming

system is Zone 5, which has saturated solutions coexisting with crystals of a racemate compound. Such crystals incorporate both enantiomers in a single crystal lattice.

Multiple techniques have been developed for the resolution of racemic mixtures (Lorenz et al., 2014). One that has been extensively applied for the resolution of conglomerate forming systems is preferential crystallization. Preferential crystallization simply refers to the utilization of seeds of the desired enantiomer to promote its nucleation over the counter enantiomer. In order to explain the process, let's assume that the conditions in Figure 2.5 are that the solution is supersaturated with respect both enantiomers, but this supersaturation is not enough to induce spontaneous nucleation. However, as explained in Section 2.1, at these conditions it is still possible to reduce supersaturation through secondary nucleation and/or crystal growth. Hence, if a solution is seeded with crystals of some orientation, we can *preferentially* promote secondary nucleation of these crystals. As shown in Figure 2.6, the solution concentration will move through a tie line indicating crystallization of a single enantiomer. However, at some point the enantiomeric imbalance will be high enough that crystals of the counter enantiomer will nucleate and the concentration will move towards equilibrium, which is at the middle of the ternary phase diagram. It is therefore necessary to understand crystallization kinetics to optimize this operation (Chaaban et al., 2014; Rodrigo et al., 2004).
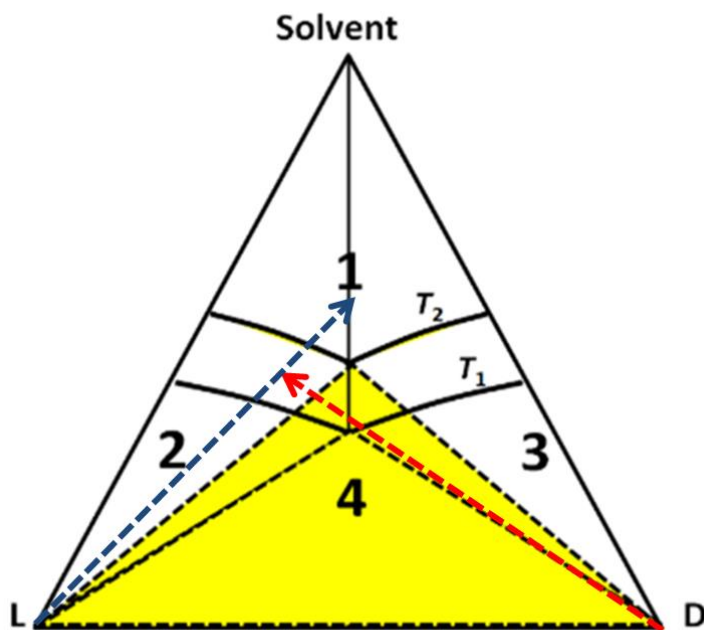
Figure 2.6: Preferential crystallization process. Red line: Tie line of D-

enantiomer. Blue: Tie line of L-enantiomer.

In order to enhance the efficiency of this technique multiple hybrid systems have been

developed. For example Svang-Ariyaskul et al. developed a system in which membranes and

crystallization separations were integrated (Svang-Ariyaskul et al., 2012). The process consists

of connecting two crystallizers through a membrane that allows migration of the enantiomers

from one crystallizer to the other. Seeding each vessel with a different enantiomer enables

preferential crystallization in the vessel. As crystallization of each enantiomer proceeds, their

respective concentrations will decrease. Hence, in order to maintain chemical equilibrium

interchange of enantiomers will occur through the membranes. Elsner et al. developed a similar

system in which each crystallizer is connected to a shared dissolution vessel that feeds both

crystallizers with a racemic mixture (Elsner et al., 2009). These processes rely on controlling the

enantiomeric imbalance so that nucleation of the undesired enantiomer is controlled. As a result,

both processes can be run continuously without worrying about nucleation of the undesired

enantiomer. Unfortunately, preferential crystallization cannot be applied to racemic compound forming systems. Resolution of racemic compound forming systems requires changing the thermodynamics of the system via salt formation or enriching the solution respect to the desired enantiomer.

Salt formation was discovered by Pasteur in 1853 and it still is one of the most employed processes to obtain optically active crystals. This resolution method consists in the formation of a salt between a racemic acid and an optically active base or a racemic base with an optically active acid (Eliel, 1983). As shown in figure 2.7, salt formation breaks the symmetry of the system, enabling crystallization of a single diastereomers at the middle of the ternary phase diagram. Finally, the new salt has to be broken in order to obtain the pure enantiomer from the purified diastereomer. Jaques et al. described several methods as decomposition by mineral acids, inorganic bases, alumina and ion exchange resins that could be used to obtain the final product.
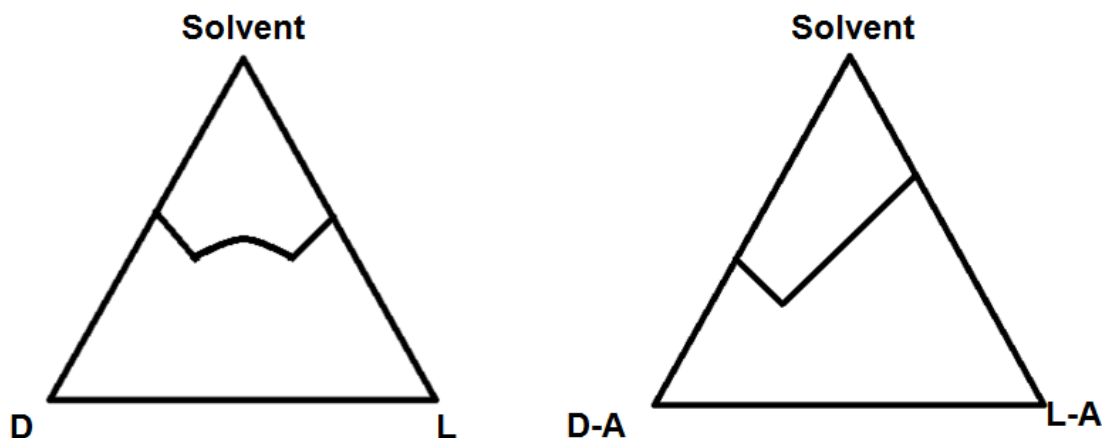
Figure 2.7: Phase diagrams of racemic compounds forming system (left) and diastereominc salts of racemic compound forming system (right).

Another technique that can be used to enrich solutions with desired enantiomer is the utilization of chiral chromatography prior crystallization. This can be achieved by feeding a

racemic mixture to a chromatographic bed that contains a chiral stationary phase. However, classic batch chromatography does not provide high productivities, which inhibits its utilization. In order to make the process cost effective the integration of simulated moving beds (SMBs) and crystallization had been studied (E. Francotte, 2009; E. Francotte et al., 2002; E. R. Francotte, 2001). This process consists of alternating the feed and outlet position of the beds, simulating the movement of the stationary phase. Such process maximizes the utilization of the bed, increases productivity, and enhances the separation.

2.3 Synthesis and separation of β-lactam antibiotics

β-lactam antibiotics are the class of antibiotics that contain a β-lactam ring within their structure. This group includes a broad range of penicillin derivatives such as ampicillin and amoxicillin, cephalosporins, monobactams, and carbapenems. This type of antibiotic spans approximately 65% of the world market for antibiotics, with sales greater than \$15 billion per year (Elander, 2003; Giordano et al., 2006). Commercial manufacture of β-lactams antibiotics usually is achieved through conventional organic synthesis where low temperatures, organochloride solvents, and protection/deprotection groups are employed (Ospina et al., 1996). As a result, significant amount of waste is generated through the process.

An alternative route for the manufacture of β-lactam antibiotics is the enzymatic synthesis by penincillin G acylase (PGA) or amino ester hydrolases (AEH). Although both enzymes can performed this reaction PGA had been more extensively used and studied (Blum et al., 2010). This enzyme can catalyze the acyl transfer from an activated side chain donor to the nucleophilic β-lactam forming the desired antibiotic. For example, the enzymatic synthesis of ampicillin can be achieved by reacting 6-aminopenicillanic (6-APA) acid and D-phenylglycine methyl ester (D-PGME) in the presence of PGA. Similarly, other β-lactam can be produced by PGA simply by changing the initial reactants.

As mentioned in chapter 1, PGA not only catalyzes the synthesis of ampicillin but it can also catalyzes the hydrolysis of D-PGME to D-phenylglycine and the hydrolysis of ampicillin to D-phenylglycine and 6-APA. In fact, the production of 6-APA can be achieved through hydrolysis of penicillin G by PGA (Abian et al., 2003). Hence, this system is a kinetically controlled reaction where ampicillin is an intermediate within the network. Multiple reaction engineering strategies had been used to improve the yield of 6-APA towards ampicillin. These strategies can be classified into thermodynamically controlled reactions or kinetically controlled reactions. The first one relies on medium optimization to shift the microscopic reversibility of the enzymatic reaction towards the synthesis reaction. Based on the fact that the undesired reaction is a hydrolysis reaction, organic co-solvents have been used to shift equilibrium towards synthesis (Abian et al., 2003; Illanes et al., 2002; Kim et al., 1996). This approach has been demonstrated to improve the equilibrium constants, but the kinetics and yield of reaction are drastically reduced. A different approach relies on optimization of reaction kinetics to enhance the synthesis of ampicillin.

Multiples studies have been done in order to understand the mechanisms of the synthesis of β-lactam antibiotics by PGA (Giordano et al., 2006). Youshko et al. work was used to describe the complexity of this reaction by considering multiple possibilities of enzyme-substrate-product interactions (Youshko, Chilov, et al., 2002; Youshko & Svedas, 2000). Their minimal kinetic model demonstrated that synthesis of ampicillin proceeds through the formation of an acylenzyme-nucleophile complex. This complex has two potential routes of product unbinding. In the first one, the nucleophile and primary hydrolysis products are released as independent products (6-APA and D-phenylglycine), while in the second one the antibiotic is released as a product. It is interesting that secondary hydrolysis proceeds through the same mechanism but in

a different direction. This can be explained as enzymatic microscopic reversibility since binding and unbinding can occur in both directions.

Reactor design and optimization of the synthesis of ampicillin has been an area of extensive research (Elander, 2003). Ospina et al. investigated the effect of pH on the synthesis of ampicillin by PGA. Ferreira et al. investigated the utilization of non-conventional reactor design towards the synthesis of ampicillin (Ferreira, 2007). In their work, a fed-batch with gel matrix for enzyme immobilization was utilized. In this wok, high concentrations of substrate enable precipitation of ampicillin, but D-phenylglycine was also present in the solid phase. In a similar work, Youshko et al. developed a semi-batch reactive system in which D-phenylglycine methyl ester was feed at multiple points through the reaction (Youshko et al., 2001). This maximized the substrate utilization as the rate of primary hydrolysis was controlled by maintaining relatively low concentrations of D-phenylglycine methyl ester.

CHAPTER 3

Reactive crystallization of selected enantiomers: chemo-enzymatic stereoinversion of amino acids at supersaturated conditions

3.1 Introduction

As mentioned in Chapter 2, the different thermodynamic regions indicate that is necessary to maintain the solution with an enantiomeric excess greater than the one at the eutectic point if an enantiomerically pure crystal is desired (Eliel, 1983). This can be assured only if the solution from which the crystals are formed has a solution concentration within the boundaries of either Zone 2 or Zone 3 of Figure 2.4. Accordingly, solutions of racemic mixtures must be enriched in the desired enantiomer beyond the eutectic point in a supersaturated solution; in other words, the enantiomeric excess (ee) must exceed that at the eutectic (ee_{Eu}), where $ee = 100\% \times (x_L - x_D)/(x_L + x_D)$ and x_D and x_L are mole fractions of the D and L enantiomers. In recognition of these requirements the present work has the following objectives:

1. Formulate a strategy for chemo-enzymatically enriching an initially racemic mixture in one enantiomer at the expense of the other. The enantiomeric enrichment must be accomplished at solution compositions appropriate for subsequent crystallization of the desired enantiomer.

2. Demonstrate the feasibility of the strategy on two amino-acid systems: methionine and phenylalanine. This will require several intermediate steps:

    a. Appropriate equilibrium data and models for the two systems must be obtained so that we can determine the regions in which crystallization is feasible and set targets for enantiomeric enrichment.

b. Identify an appropriate enzyme and test its effectiveness at the temperatures and high solute concentrations essential to the success of the strategy. Use the enzyme with the two model systems to obtain data sufficient for development of a model for the reaction kinetics.

c. Perform cooling crystallization experiments to verify that crystals of high enantiomeric purity can be obtained. Use the data from *in situ* measurements of solute concentrations during crystallizations to obtain rudimentary models of nucleation and growth kinetics.

d. Combine the models of reaction and crystallization kinetics to demonstrate how these two steps can be sequenced to produce the desired isomer.

e. Use the two-step model to show how the productivity of the process can be enhanced through initiating crystallization while enzymatic enrichment is occurring.

Figure 3.1 is a visual representation of the objectives of the present work. The required equilibrium data (Objective 2a) is illustrated in Figure 3.1. This can be summarized as obtaining the solubility of the enantiopure compound and the racemate as a function of temperature and enantiomeric excess, and the enantiomeric excess at the eutectic points along its temperature dependence. Step 1 shows how the system composition is to be adjusted by enantiomeric enrichment (Objective 2b) using specific chemo-enzymatic stereoinversion reactions. Demonstration of enzyme stability in supersaturated solutions is a major challenge to the success of Step 1, and we show experimentally how this challenge was met. In Step 2, the temperature of the system is reduced to crystallize the desired product of the reaction (Objective 2c). We describe experiments demonstrating the success of Steps 1 and 2 and also formulate models of both the chemo-enzymatic reaction and the crystallization kinetics. Using these models,

which have not been refined, we show how they can be combined with equilibrium behavior to develop a sequential two-step process (Objective 2d) and a process in which reaction and crystallization occur simultaneously (Objective 2e), which is illustrated in Step 3 of Figure 2. The actual path followed in Step 3 depends on the specific temperature vs. time relationship followed, and we illustrate the effect of multiple temperature profiles on the productivity and enantiomeric purity of the desired crystals.
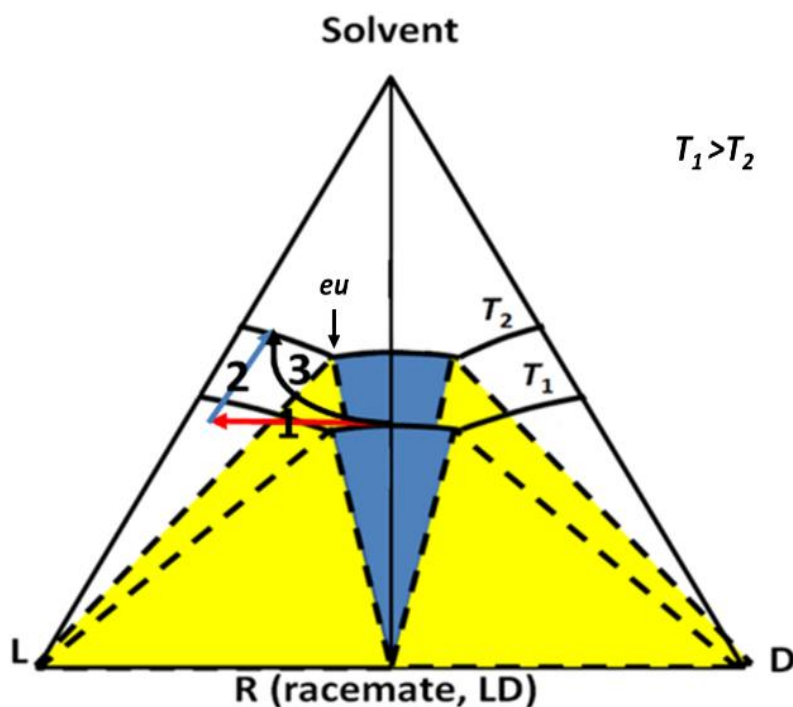
Figure 3.1: Reactive crystallization process. At **1** a reaction transforms D into L enantiomers, then at 2 the crystallization takes place reducing L-enantiomers concentration. 3 represents a reaction-crystallization rourte where both reaction and crystrallization occur simultaneusly.

3.2 Materials and Methods

3.2.1 Chemicals and analytical methods

DL-phenylalanine, DL-methionine, ammonia borane complex, potassium phosphate monobasic and dibasic, bovine serum albumin, porcine kidney catalase, and flavin adenine dinucleotide were purchased from Sigma Aldrich USA (St. Louis, MO) and used without further

purification. Porcine kidney D-amino acid oxidase (D-AAO) was purchased from Calzyme Inc. (San Benito, CA).

The concentration of each of the enantiomers was determined by a Shimadzu (Kyoto, Japan) high-pressure liquid chromatography system using a Chirex 3126 (Length 150 mm, particle size 5 µm, and internal diameter 4.6 mm) from Phenomenex (Torrance, CA) and an Astec Chirobiotic T (250 mm, particle size 5 um, and internal diameter 4.6 mm) from Sigma Supelco (St. Louis, MO) chiral columns. Calibration curves were prepared using both internal and external standards. A polarimeter and a refractometer were used during the crystallization experiments. Calibrations of both instruments were obtained by measuring the specific optical rotation and refractive index as functions of the solution composition.

3.2.2 Chemo-enzymatic stereoinversion

Chemo-enzymatic stereoinversion of D-amino acids using D-AAO and ammonia borane were used to enrich racemic solutions of DL-phenylalanine and DL-methionine into their respective L-amino acids. These amino acids had shown a high degree of activity and enantioselectivity with D-AAO towards their respective imino acids [11]. The reactions were performed in a 100-mL jacketed reactor in which the temperature was maintained at 37 ℃ by a recirculating water bath. Potassium phosphate buffer (0.1 M) was used to maintain the pH at 7.5, which was selected based on the literature [12]. Flavin adenine dinucleotide was added because it is the cofactor of D-amino acid oxidase, catalase was used to decompose hydrogen peroxide, and bovine serum albumin was used to enhance the mechanical stability of the enzyme. The reactions were started

by adding 1 mL of a concentrated enzyme solution to saturated or supersaturated solutions of the racemic amino acids.

3.2.3 Solubility

The solubilities of L- and DL-phenylalanine were determined through isothermal experiments at multiple temperatures and compositions. This was performed by adding an excess of the desired compound at a specific enantiomeric excess to water and allowing the resulting slurries to equilibrate at the desired temperature for at least 24 h. Samples of solution were withdrawn with a syringe through a 0.45 μm filter to ensure that only the liquid phase was analyzed. Sequentially withdrawn samples were analyzed to ensure that equilibrium was achieved.

3.2.4 Crystallization kinetics

We developed a monitoring system to obtain crystallization kinetics for the batch operation. It consisted of a 500-mL jacketed vessel in which the temperature was controlled by a recirculating water bath. A small stream was withdrawn continuously from the vessel through a 0.1-μm filter by a peristaltic pump that circulated the solution through tubing to a polarimeter and refractometer in series and then back to the reactor. Temperature-controlled heating tape was wrapped around the tubing to prevent crystallization in the lines. The optical rotation, refractive index, and temperature were stored as a function of time in a computer. Prior starting each cooling phase, the temperature was raised (5 ℃) to ensure crystals dissolution. The L-methionine cooling crystallization experiments were performed starting at approximately 40 ℃ and cooling the solution to 20 ℃ at rates of 0.06 ℃/min and 0.1 ℃/min. In the case of L-phenylalanine, the temperature range was from 35 ℃ to 15 ℃ with a cooling rate of 0.1 ℃/min. Since the rates of crystallization were determined for enantiopure solutions, a single signal (from either the

refractometer or the polarimeter) was enough to obtain the concentration of the amino acid in solution. However, when both enantiomers of a given system are present in solution (as when the reactive crystallization is taking place), both the refractometer and the polarimeter are necessary to determine the concentration of each enantiomer.

3.2.5 Crystal recovery

After reaching a high enantiomeric excess (i.e. where the ee > ee$_{eutectic}$) using the reaction network described in Section 3.2.2, the solution was cooled from 37 °C to 10 °C to crystallize the desired enantiomer. While this recovered the desired enantiomer, we decided to increase the yield by first isothermally evaporating approximately 15% of the solvent, which, of course, increased the concentration of the amino acid in solution. The solution was then cooled 10 °C to bring about crystallization of the desired enantiomer. Finally, the crystals were recovered by microfiltration through a 0.45 μm filter and then redissolved in deionized water for HPLC analysis.

3.3 Results and Discussion

3.3.1 Solubility

The solubilities of L- and DL-phenylalanine were measured in the range of 10 °C to 60 °C, while the solubilities of L- and DL-methionine were obtained from the literature (Polenske et al., 2009) . Both sets of data were fit using a Van't Hoff equation

$$\ln x = \frac{A}{T} + B \qquad (3.1)$$

with the results shown in Figures 3.2a and 3.3a; values of the parameters A and B for each species are reported in Table 3.1.

The solubility at the eutectic point represents the total solute in solution, and it can be related to the solubilities of the pure enantiomers and the racemate compound using the

approximations developed by Klussmann et al.(Klussmann et al., 2006). In that approach a

parameter (η) defined as the ratio of the solubility of the racemate compound to that of the pure

enantiomer is used to estimate the solubility and enantiomeric excess at the eutectic using the

following equations:

$$\eta = \frac{[\mathrm{DL}^{\mathrm{Sat}}]}{[L^{\mathrm{Sat}}]} \tag{3.2}$$

$$[\mathrm{Eu}^{\mathrm{sat}}] = [\mathrm{L}^{\mathrm{sat}}]_{\mathrm{Eu}} + [\mathrm{D}^{\mathrm{sat}}]_{\mathrm{Eu}} = [\mathrm{L}^{\mathrm{sat}}]\left(1 + \eta^2/4\right) \tag{3.3}$$

$$\mathrm{ee}_{\mathrm{Eu}} = \frac{1 - \eta^2/4}{1 + \eta^2/4} \tag{3.4}$$

The left axis of Figures 3b and 4b shows the measured solubilities of the enantiopure compound

and racemate, and the calculated solubility at the eutectic point (Equation 3.3). In the right axis

of theses plots, the calculated enantiomeric excess at the eutetectic point is presented (Equation

3.4). Based on the proximity of the calculated solubility and enantiomeric excess with the

experimental data reported by Polenske and Lorenz (Polenske et al., 2009), we used the values

calculated from Equation 3.3 in the following work.
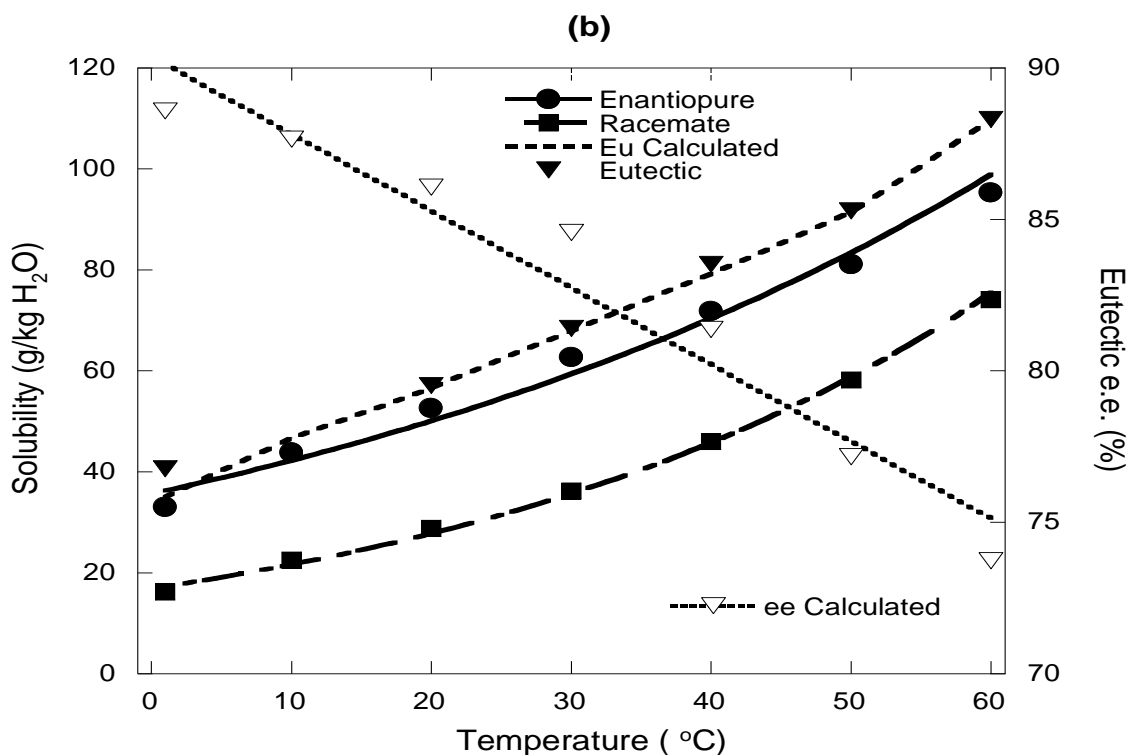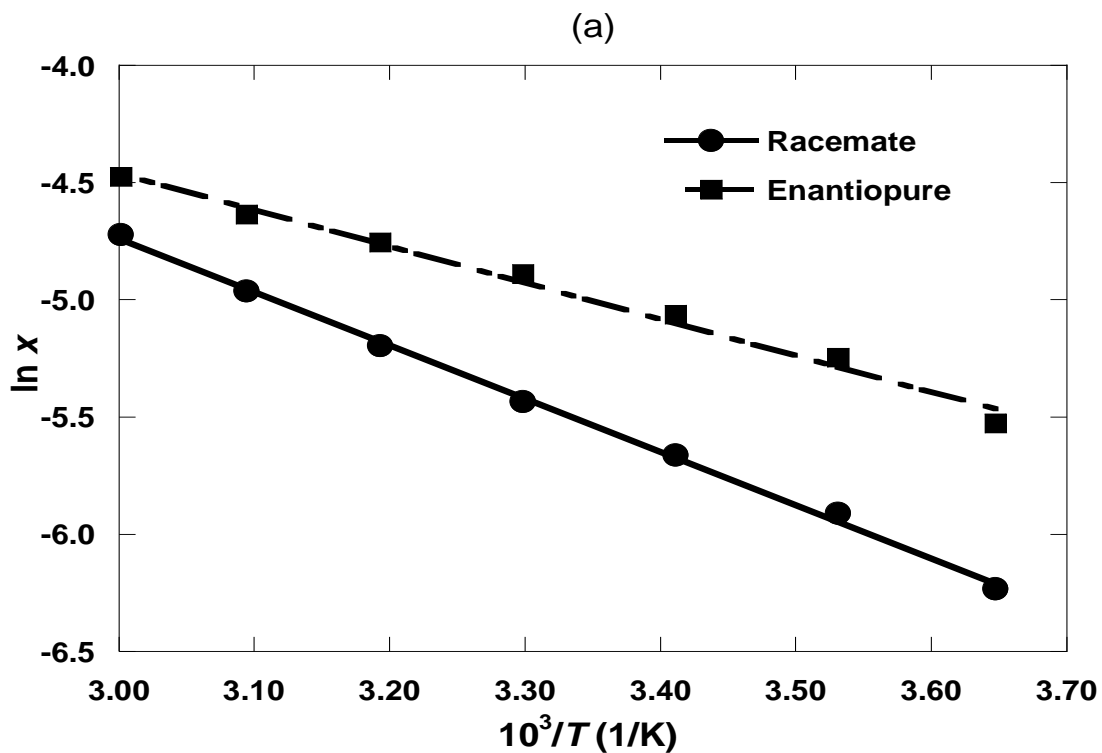
Figure 3.2: (a) Solubilities of L- and DL-methionine. (b) Solubilities of L- and DL-methionine, solution concentration at the eutectic point (experimental and calculated by Equation 3.3), and the enantiomeric excess at the eutectic point estimated from Equation 4. Data are from (Polenske et al., 2009).

(a)

(b)
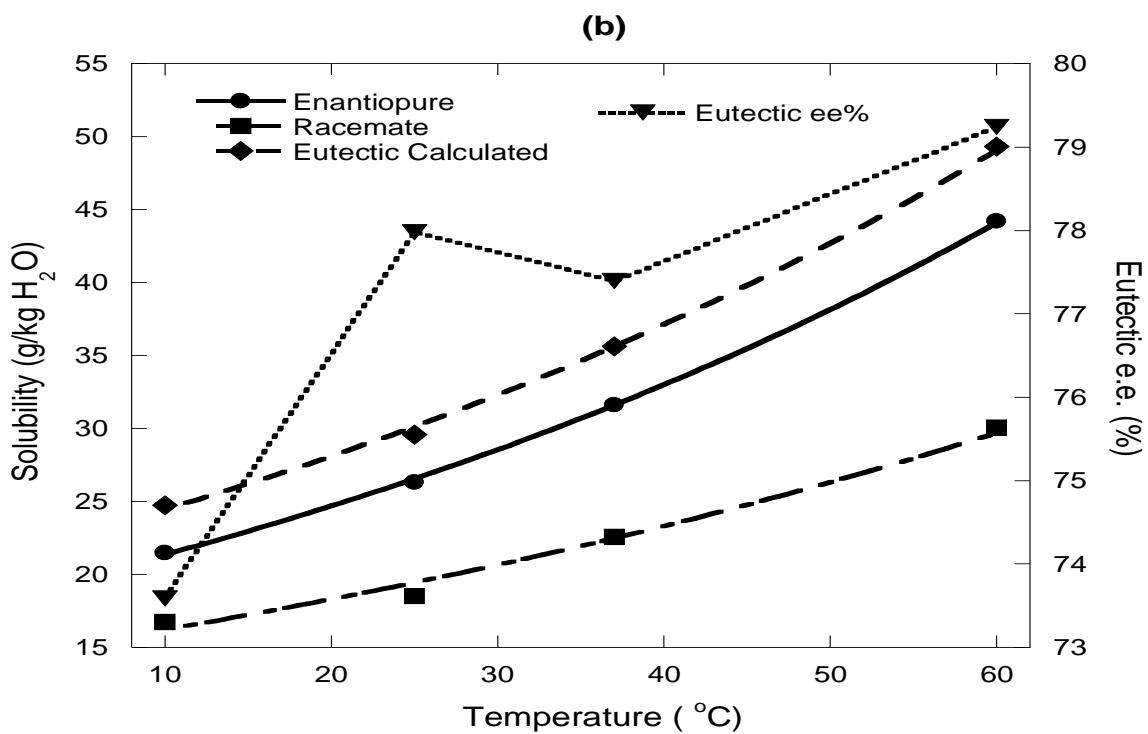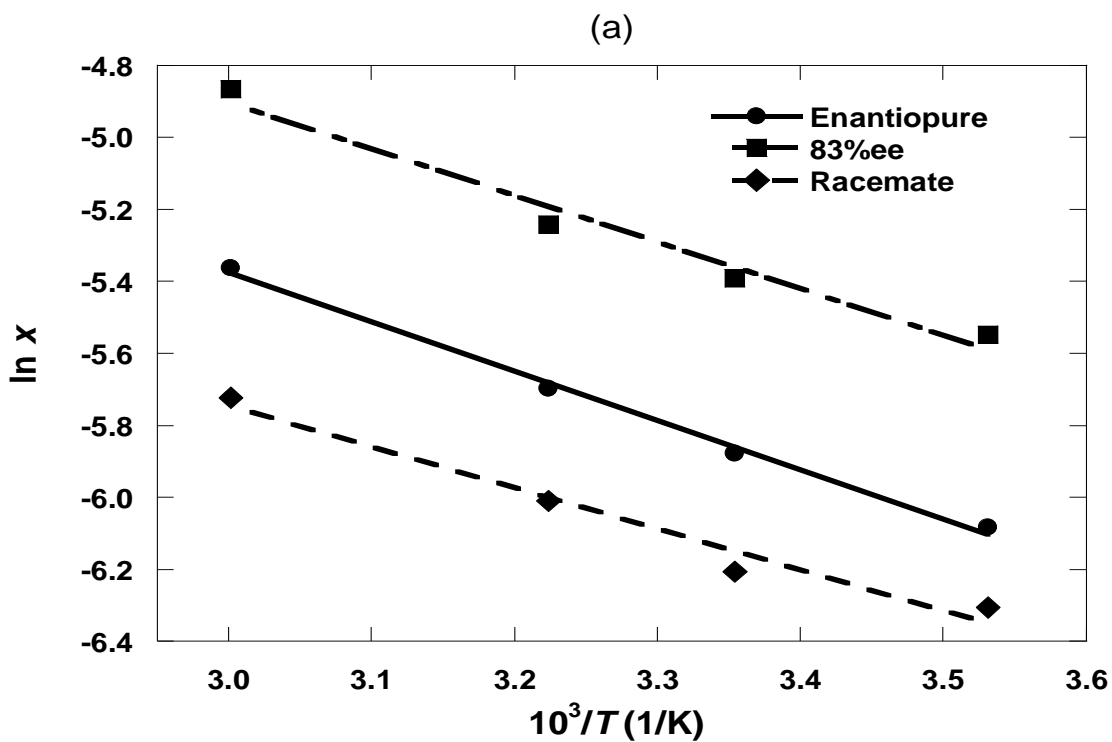
Figure 3.3: (a) Solubilities of L- and DL-phenylalanine, solution concentration at 83% ee. (b) Solubilities of L- and DL-phenylalanine, and the ee at the eutectic point estimated from Equation 3.4.

Table 3.1: Parameters obtained from fitting solubility data for methionine and phenylalanine to the Van't Hoff equation (Equation 1).

	$A(10^3)$	B	R^2
DL-Phenylalanine	−1.1353	−2.3396	0.9698
L-Phenylalanine	−1.3650	−1.2573	0.9956
DL-Methionine	−2.2721	2.0758	0.9982
L-Methionine	−1.5500	0.1899	0.9892

Finally, since the solubilities are to be used in extensive modeling described later in the manuscript, they were correlated as functions of temperature and enatiomeric excess (ee) using the following equation:

$$[S] = C + DT + ET^2 + F\,(ee)^2 \tag{3.6}$$

where [S] is the solubility of either the pure L enantiomer or the racemate DL compound. Table 3.2 provides the parameters obtained by fitting the equation to the available data.

Table 3.2: Parameters obtained from fitting solubility data for methionine and phenylalanine to Equation 3.6.

	C	D	E	F	R^2
DL-Phenylalanine	13.460	2.166×10^{-3}	7.932×10^{-2}	4.111×10^{-3}	0.964
L-Phenylalanine	27.850	-9.593×10^{-4}	2.276×10^{-1}	3.632×10^{-3}	0.997
DL-Methionine	10.080	4.106×10^{-3}	6.620×10^{-1}	8.290×10^{-3}	0.971
L-Methionine	54.900	-2.295×10^{-3}	9.024×10^{-1}	2.679×10^{-3}	0.994

3.3.2 Chemo-enzymatic stereoinversion

Chemo-enzymatic stereoinversions of phenylalanine and of methionine were achieved using D-AAO and ammonia borane in the reaction cycle shown in Figure 3.4;

D-AAO oxidizes the D-amino acid in the mixture to the achiral imino (AI) acid, which is then

then reduced by the reducing agent (RA) ammonia borane to a racemic mixture of the original

amino acid (Alexandre et al., 2002; Soda et al., 2001)
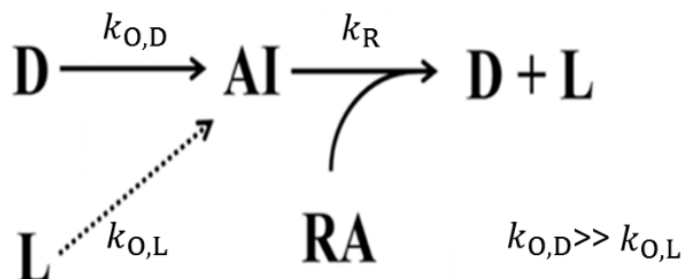
Figure 3.4: Reactions for chemo-enzymatic stereoinversion.

Since the first reaction is selective for the D enantiomer, the combination of both

reactions enriches the solution in the L-enantiomer by consuming two units of D and producing

one unit of D and one of L. Undesired oxidation of the achiral imino acids to keto-acids is

possible (Alexandre et al., 2002), but our experiments determined that maintaining a high

concentration of ammonia borane (4 mol ammonia borane/mol DL-amino acid) suppressed such

oxidation and enhanced the rate of reduction of the imino acids to amino acids.

Racemic supersaturated solutions of phenylalanine and methionine at 37 °C were

subjected to the stereoinversion reaction scheme. The resulting data shown in Figure 6 illustrate

one of the key features of the present work: namely, the feasilibilty of performing the reactions at

supersaturated conditions. As far as we know, the present work is the first example where this

has been demonstrated. Moreover, the concentrations of both D-phenylalanine and D-methionine

are shown to approach extinction, demonstrating that high enantiomeric excesses of the L

enantiomers can be achieved. Therefore, the solution can be moved from Zone 5 to Zone 2 of

Figure 3.2(b) where crystallization of the desired enantiomer can be performed.

As expected, the concentrations of D and L amino acids in Figure 6 move in opposite directions; the concentration of D is decreased due to oxidation while the concentration of L increased as it was formed by the reaction cycle. In a perfect execution of the reaction cycle, the increase in L would be a reflection of the decrease in D. While this was approximately true for the phenylalanine data in Figure 6(a), it was not for the methionine data in Figure 6(b). We attribute this lack of symmetry to the system being deficient in ammonia borane, which limited the reduction rate of the achiral imino acid into L-methionine. Nevertheless, it was still possible to recover enantionmerically pure L-methionine from the reaction products because the intermediate imino acid was more soluble than methionine.

Assuming the reactions in Figure 3.4 follow a Michaelis-Menten mechanism, the rate of reaction (v) can be described by Equation 3.7. Assuming this model, it is easy to show the advantage of performing the reaction at supersaturated conditions, provided there is enzyme stability at these conditions. At high values of the substrate concentration, i.e. $[S] \gg K_M$, the rate of reaction is maximized at v_{max}.

$$v = \frac{k_{o,D} E_0 [S]}{K_M + [S]} = \frac{v_{Max} [S]}{K_M + [S]} \approx v_{max} \qquad for \quad [S] \gg K_M \qquad (3.7)$$
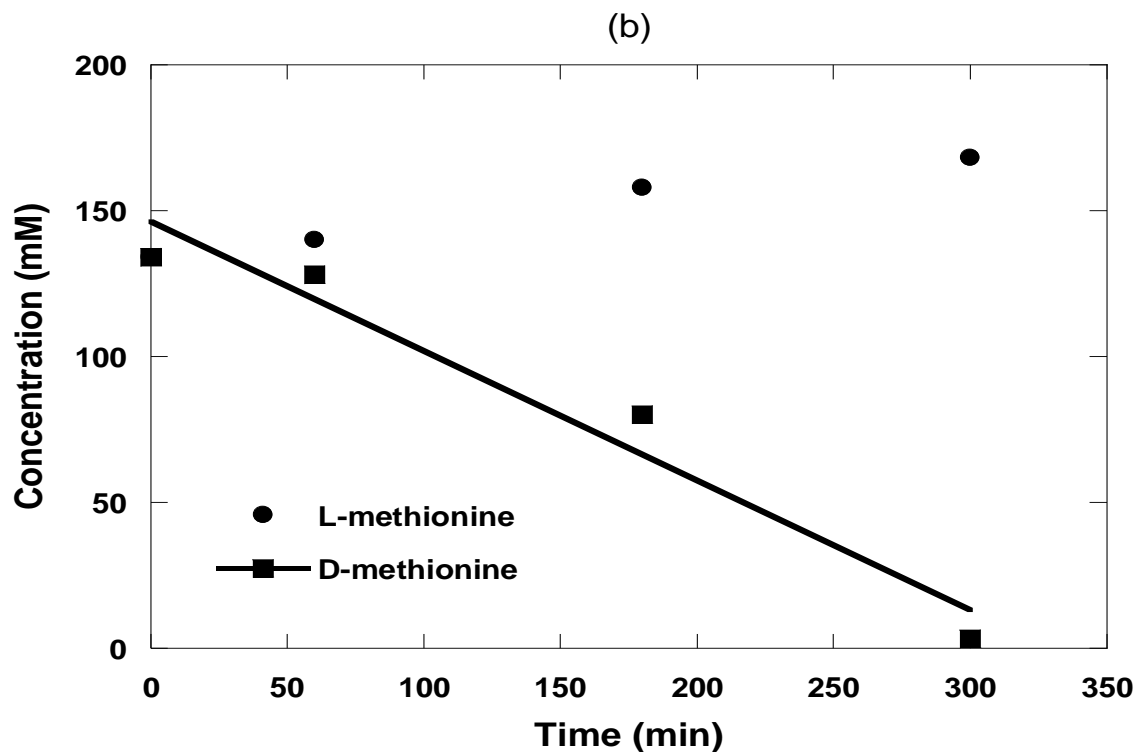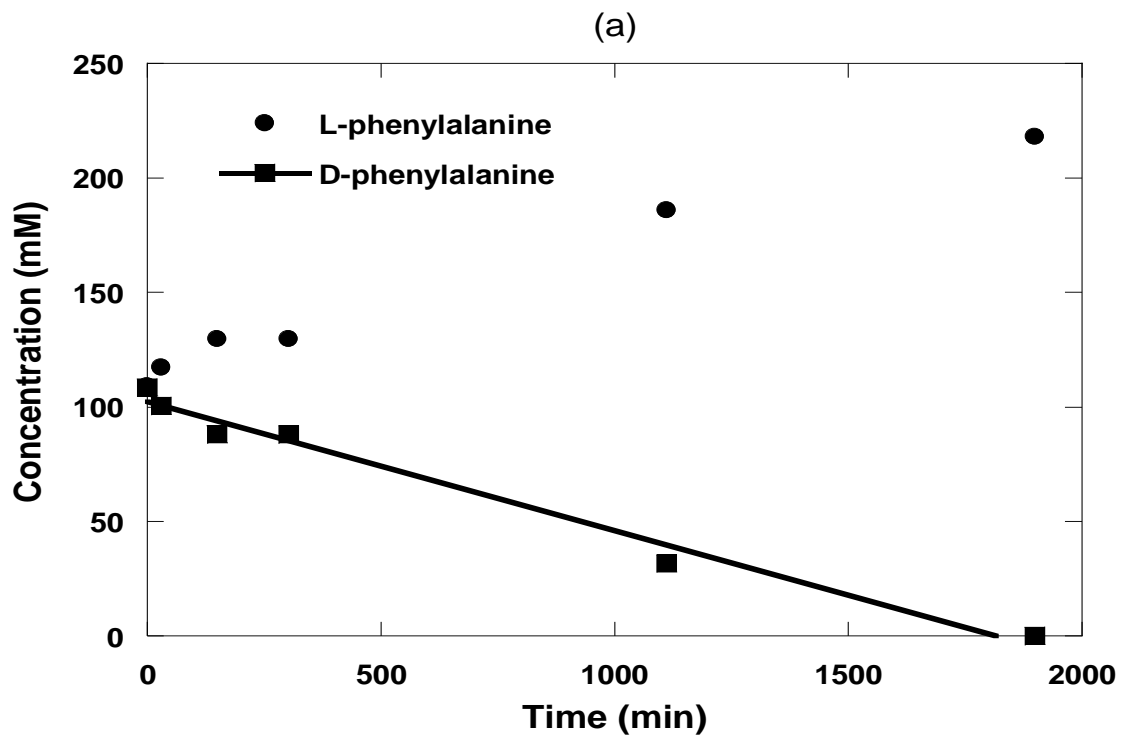
Figure 3.5: Chemo-enzymatic stereoinversion of (a) phenylalanine and (b) methionine. Lines show linear fits to D-amino acid concentration. (*Note:* The increase in L-methionine production does not track D-methionine consumption for reasons explained in the text.)

The rates at which concentrations of the D enantiomers decreased were

determined from the data in Figure 3.5. The consumption of D-phenylalanine followed

the zero-order kinetics embodied by the approximation in Equation 3.7, but this was true

only early in the process for D-methionine. Even so, the data for both systems were

linearized and used to estimate the specific (i.e. normalized by enzyme mass) reaction

rate constants of phenylalanine and methionine. These were found to be 10.6 and 10.7

mM/(min·g enzyme), respectively. The methionine reaction was performed using a

higher concentration of enzyme, which ris why D-methionine was consumed faster than

D-phenylalanine even though that the reaction rate constants are similar.

The observable rates of oxidation determined during our experiments are similar

to those reported by the manufacturer (Calzyme Inc.) and others (Findrik et al., 2005) for

the oxidation of amino acids by D-amino acid oxidase. However, overall conversions of

the D-amino acids into L-amino acids involves both oxidation and reduction. Since we

found that the rate of generation of L-phenylalanine tracked the consumption of D-

phenylalanine by oxidation and because the rate of reduction can be increased by

increasing the concentration of ammonia borane, we assumed in our subsequent analyses

that the rate of oxidation was the controlling step in the process.

Table 3.3 lists the parameters obtained by fitting the concentration of D-amino acids as a

function of time, where the rate of reaction constant (k_D) was approximated from the slope and

the Michealis constant (K_M) from the literature (Findrik et al., 2005). This rate of reaction

constant is factoring in the fact that for every 2 moles of D-amino acid consumed, one mol of L-

amino acid will be produced (i.e. $k_D = k_{o,D}/2$). The activation energy (E_A) of D-amino acid oxidase

with D-methionine as the substrate was obtained from the literature (Massey et al., 1966) and
assumed to be the same for D-phenylalanine.

Table 3.3: Rate of reaction of D-methionine and D-phenylalanine by D-AAO.

	D-methionine	D-phenylalanine
k_D (mM·min^{-1}·g E_o^{-1})	10.7	10.6
K_M (mM)	2.5	2.5
E_A (kJ/mol)	38.2	38.2
R^2	0.95	0.98

3.3.3 Crystallization kinetics

Enantiomerically pure reaction products were crystallized as described in Section 3.2.5.
For both the phenylalanine and the methionine systems, the crystals obtained had chemical and
enantiomeric purities over 99% . In fact, HPLC analysis of the recovered crystals was unable to
detect reaction by-products or opposite enantiomers. These results demonstrate the feasiblity of
performing the reactions at crystallization conditions (i.e. in supersaturated solutions) and of
recovering enantiomerically pure crystals from the reaction products.

The rates of crystallization of L-phenylalanine and L-methionine were determined
experimentally by coupling solute and population balances through the method of moments
(Randolph et al., 1988)where moments of the population density function are given by

$$\mu_i = \int_0^\infty n(\ell,t)\,\ell^i\,d\ell \tag{3.8}$$

The zeroth, first, second, and third moments are related to the total number, length, area, and
volume of crystals, respectively. Derivatives of the moments are given by

$$\frac{d\mu_0}{dt} = B \tag{3.9}$$

$$\frac{d\mu_i}{dt} = iG\mu_{i-1} \qquad (3.10)$$

where B and G are respectively the nucleation and growth rates. Kinetic expressions for

nucleation and growth were expressed as

$$B = k_B \left([L] - [L^{sat}]\right)^b \qquad (3.11)$$

$$G = k_G \left([L] - [L^{sat}]\right)^g \qquad (3.12)$$

where k_B, k_G, b, and g are system-dependent parameters. Finally, a solute mass balance gives

$$\frac{d[L]}{dt} = -\rho_c k_v \frac{d\mu_3}{dt} = -3\rho_c k_v G\mu_2 \qquad (3.13)$$

where ρ_c is crystal density (set at 1000 kg/m^3) and k_v is the volume shape factor (set at 0.1),

which are approximated based on the fact that the particles are elongated but do not affect

significantly the simulation outcome.

The concentrations of enantiomers during batch operations must be known to

estimate the rate of crystallization. This was achieved using a monitoring system similar

to that of Rodrigo et al. (Rodrigo et al., 2004); as described earlier, the solution was

withdrawn, circulated through a polarimeter and a refractometer, and returned to the

crystallizer. Concentrations of both enantiomers in the crystallizer were determined using

appropriate calibrations of the two instruments. The measured temperature was combined

with the solubility models developed Section 3.3.1 to estimate the solubility during a run.

Finally, the experimental concentration was compared to that calculated from the mass

balance in Equation 3.13.

Estimation of parameters in the kinetic expressions was performed using the

following objective function:

$$\min{}_p E = \sum_{j=1}^{N\exp} \sum_{i=1}^{Nx} (x_{i(t,p)} - x_{i(t)}^{\exp})^2 \qquad (3.14)$$

where $x_{i(t,p)}$ represents the modeled concentration at some set of parameters $p = [k_b \ b \ k_g \ g]$, $x_{i(t)}^{\exp}$

represents the set of concentrations determined experimentally, N_x is the number of data points,

and $N_{\exp}$ the number of experiments. (For methionine $N_{\exp} = 2$ and for phenylalanine $N_{\exp} = 1$.)

The probability of being trapped in a local minimum was reduced by performing two consecutive

minimizations. First, a stochastic minimization (*MATLAB simulannealbnd*) was used to identify

the best set of parameters among multiple combinations of parameters. Then, that set of

parameters was used as the starting point of a deterministic minimization (*MATLAB fminsearch*)

that refined the parameters and further reduced the error.

The robustness of the identified set of parameters was quantified by the confidence

interval of each parameter calculated using the recommendation of Nagy et al. (Nagy et al.,

2008). The confidence intervals of the parameters obtained were narrow, which means that the

estimated set of parameters provides a good approximation of the true set. However, these

confidence interval are based on concentration data which is easier to fit than CSD or moments

data. Is expected that if particle information is included, the confidence intervals should be much

broader. Results of the fitting procedure are given by the parameters in Table 3.4. As expected,

nucleation exponent are large since the empirical equation is capturing primary nucleation. It is

important to notice that these parameters were estimated from concentration data, and they

should only be used accordingly. Estimations of crystal size distribution would require including

CSD data in the parameter-estimation procedure. However, since the purpose of the present work

is focused on the mass of species produced and not CSD, the estimated parameters are sufficient

for our purposes.

Table 3.4: Parameters used to model crystallization kinetics.

Parameters	L-methionine	L-phenylalanine
k_B (#/(g/kg)^b·min)	$2.03 \times 10^8 \pm 5.72 \times 10^6$	$7.08 \times 10^5 \pm 2.32 \times 10^4$
b	12.21 ± 0.14	7.56 ± 0.12
k_G (m/(g/kg)^g·min)	$4.86 \times 10^{-8} \pm 9.17 \times 10^{-10}$	$1.99 \times 10^{-7} \pm 6.07 \times 10^{-9}$
g	0.67 ± 0.01	1.36 ± 0.03

Comparisons between experimental concentrations at run conditions given in Section 3.2.4 and those obtained from the fitting procedure are shown in Figures 3.6 and 3.7. Clearly, the fit to each data set is satisfactory as the corresponding model describes the change in solute concentration during the course of a run and, by mass balance, facilitates prediction of the yield of each species. Again, however, we point out that the parameters were estimated using solute concentrations data and may give poor estimates of the corresponding crystal size distributions.
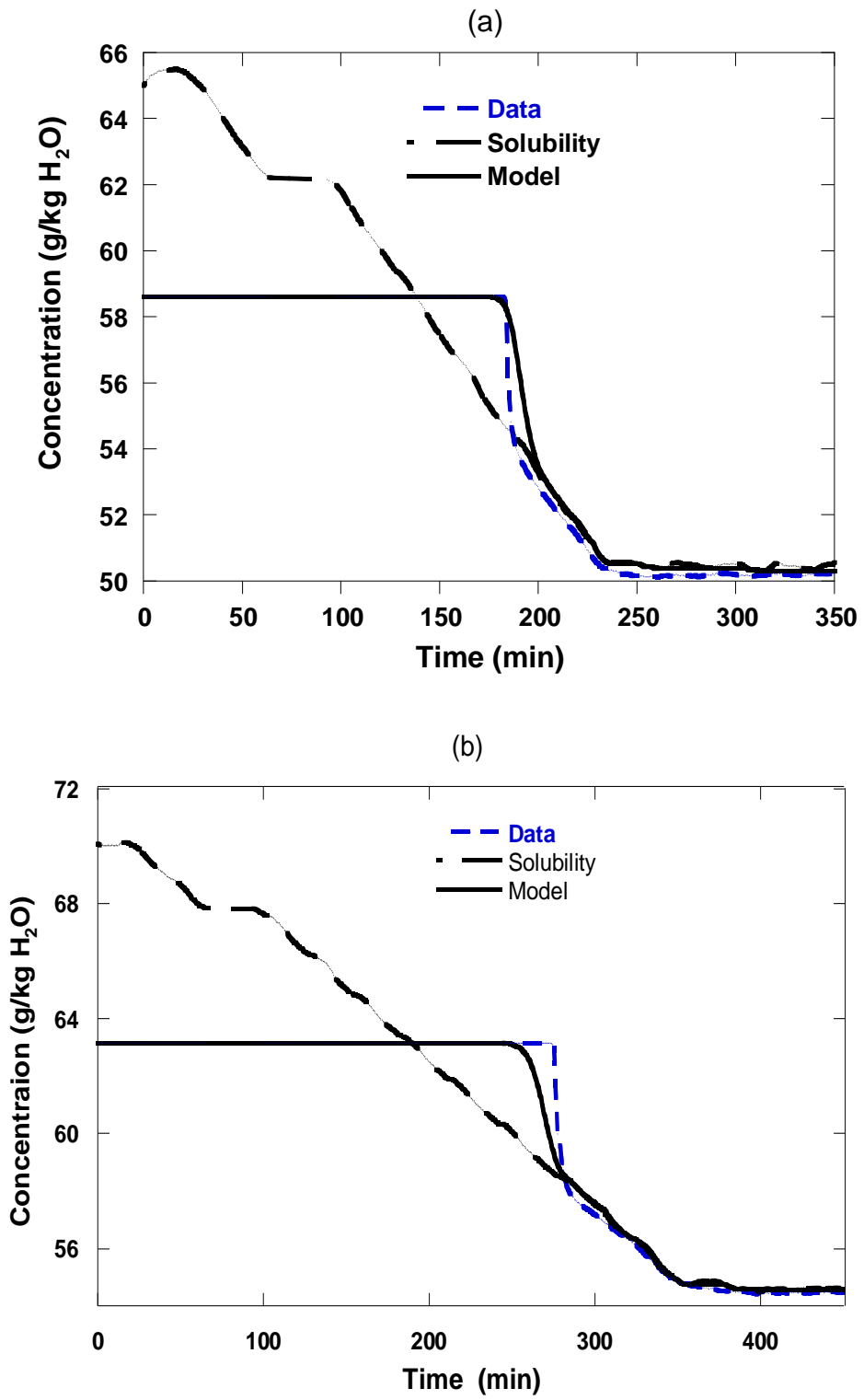
Figure 3.6: Experimentally determined and modeled concentration profiles of L-methionine for batch cooling crystallizations at two different cooling rates, (a) 0.10 °C/min and (b) 0.06 °C/min.
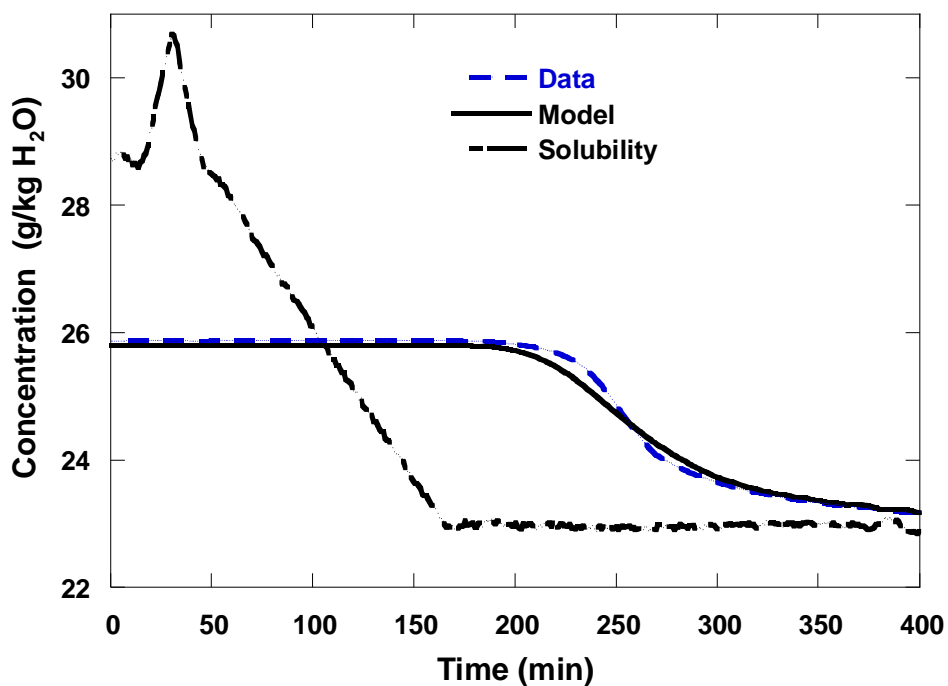
Figure 3.7: Experimentally determined and modeled concentration profiles of L-phenylalanine for batch cooling crystallization at a cooling rate of 0.1 °C/min.

3.3.4 Process modeling

In the previous sections we demonstrated and modeled the elements of the process proposed for the separation of enantiomerically pure isomers from racemic mixtures. To recap the two key steps of the process: (1) chemo-enzymatic stereoinversion to enrich the concentration of one of the enantiomers in an originally racemic mixture so that the solution composition is relocated to Zone 2 of Figure 1(b) ; (2) crystallization of the desired enantiomer from the solution formed by chemo-enzymatic stereoinversion. Such steps represented in Figure 2 as 1 and 2, were determined experimentally in Section 3.3.2 (Figure 3.5) and 3.3 (Figure 3.6 and 3.7). In this section, we show that the separately modeled steps in the overall process of enantiomer recovery can be combined and that the

44

combined model can be used to guide optimization of the process. This model is used to simulate the path named 3 in Figure 3.1, where different routes in which reaction and crystallization occur simultaneously are explored.

We first show how to combine the solids formation described by crystallization kinetics with mass balances on D and L enantiomers, the reducing agent RA, and the achiral imino acid AI involved in the reaction cycle shown in Figure 3.4. The species balances are given by

$$\frac{d[\text{D}]}{dt} = \frac{-k_{\text{o,D}} E_0 [\text{D}]}{K_{\text{M}} + [\text{D}]} + k_{\text{R}} [\text{AI}][\text{RA}] \tag{3.15}$$

$$\frac{d[\text{L}]}{dt} = k_{\text{R}} [\text{AI}][\text{RA}] \tag{3.16}$$

$$\frac{d[\text{RA}]}{dt} = -2k_{\text{R}} [\text{AI}][\text{RA}] \tag{3.17}$$

$$[\text{AI}] = [\text{D}_\text{o}] + [\text{L}_\text{o}] - [\text{D}] - [\text{L}] \tag{3.18}$$

where the rate of oxidation of L-amino acids ($k_{\text{o,L}}$) has been set to zero.

Analytical solutions for similar models are discussed elsewhere, but combining these expressions with crystallization kinetics results in a set of stiff differential equations. Since none of the stiff differential-equation solvers in MATLAB (*ode15s*, *ode23s*, and *ode23tb*) gave accurate solutions to the equations, we simplified the reaction kinetics and combined the results with crystallization kinetics to design the reaction-crystallization operation.

In the following approach, we assumed that the chemo-enzymatic stereoinversion occurs in a single reaction for the direct conversion of D-amino acids into L-amino acids; in other words, we ignore the intermediates AI and other reactants RA. Such an approximation is justified if RA is in excess (i.e. [RA] is large) and if [AI] is minimized by enhancing the rate of reduction. The reaction was modeled using a Michaelis-Menten expression that represents the net

45

conversion of D-amino acids, represented by the net rate of reaction constant (k_D).

Notice that the mechanism of the reaction works in a way that for every 2 moles of D-amino acid, only one is converted into L-amino acid and the other one into D-amino acid. Additionally, an Arrhenius expression is used to take into account the decay of the rate of reaction during the cooling phase.

$$\frac{d[L]}{dt} = \frac{k_D E_0 [D]}{K_M + [D]} \tag{3.19}$$

$$\ln\left(\frac{k_D}{k_{D,0}}\right) = \frac{-E_A}{R}\left(\frac{1}{T} - \frac{1}{T_0}\right) \tag{3.20}$$

Rates were estimated as discussed in Section 3.3.2, and modeling the effect of temperature was needed to account for the reaction-rate reduction during cooling, which occurs when crystallization and reaction are combined. By coupling the solids balance (Equation 3.13) and with the balance on L (Equation 3.19), we obtain

$$\frac{d[L]}{dt} = \frac{k_D E_0 [D]}{K_M + [D]} - \frac{d[L]_{solid}}{dt} \tag{3.21}$$

where $[L]_{solid}$ represents the mass of solids divided by the initial amount of solvent, and

$$\frac{d[L]_{solid}}{dt} = 3\rho_c k_v G \mu_2 \tag{3.22}$$

The resulting system of differential equations was solved in MATLAB by a stiff ordinary differential equation solver (*ode15s*).

The validity of the modeling approach was tested by comparing predictions of the combined model with segments of experimental data on each of the constituent steps in the process; in other words, the model was initiated at the same temperature and concentration as the experiment reported in Figure 3.5(a) and allowed to proceed until enrichment in L-phenylalanine brought the solution composition to the initial crystallization conditions given in Figure 3.7. That

took approximately 600 minutes. At that point, cooling was initiated and followed the protocol

for the experiment in Figure 3.7. The two sets of experimental data (one for reaction, the other

for crystallization) are shown in Figure 3.8 along with the model predictions. In other words,

during the first 600 minutes the model is compared against reaction data at the same conditions,

and from 600 to 1200 minutes crystallization data is compared against the model using the same

temperature profile. It can be seen that the model does fit both the reaction section (first 600

minutes) and crystallization section (last 600 minutes) with good accuracy.
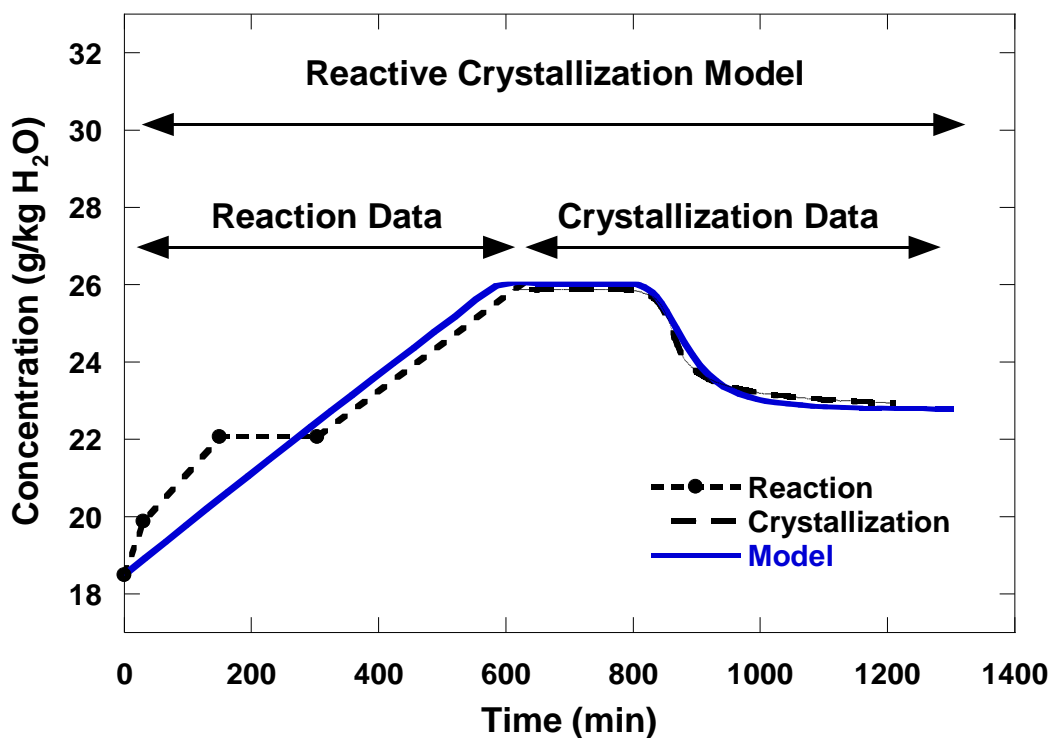
Figure 3.8: Experimental and modeled crystallization
concentration profiles of L-phenylalanine.

Given the success of the model in reproducing system behavior, it was used to examine

the effects of different cooling strategies on the productivity and enantiomeric purity of the

recovered crystals. For example, consider the illustration of a base case in Figure 3.9. Here the

chemo-enzymatic reaction was allowed to proceed until essentially all of the D amino acid was

consumed and then the system temperature was reduced at a constant rate of 0.1 °C/min. Note how the concentration of the desired L enantiomers increased from the initial racemic conditions while concentrations of the D enantiomers fell to zero. Then, as crystallization began, the concentration of the L enantiomer in solution decreased in correspondence to the increase in L enantiomer crystals. Also note that there is a substantial period of time when there is little change in the system concentrations: between 300 and 600 minutes for phenylalanine and between 600 and 800 minutes for methionine. These base cases represent the path composed by steps 1 and 2 in Figure 3.1. We now use the model to simulate processes that follow a reaction crystallization route (as path 3 on Figure 3.1) and to demonstrate how the overall process can be made more efficient by following such a route.
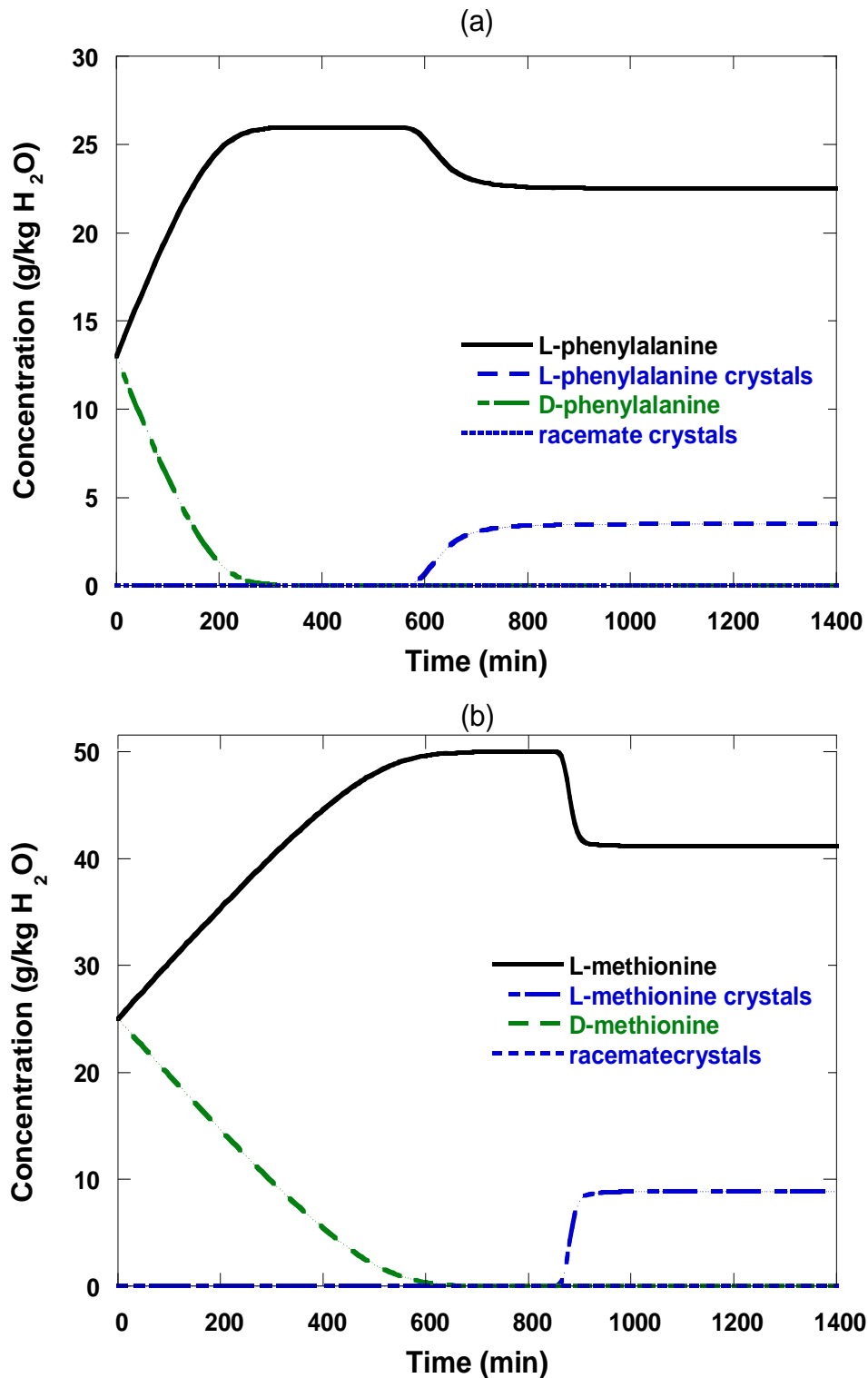
Figure 3.9: Modeled reactive-crystallization of (a) phenylalanine and (b) methionine.

A series of simulations were performed with identical cooling rates between identical initial and final temperatures, but with different times at which cooling was initiated. The initial temperature of the reaction mixture was maintained high at the beginning of the process so as to enhance the rate of the stereoinversion, but then decreased to crystallize the desired enantiopure amino acid. If cooling is initiated too soon, crystallization of the racemate or co-crystallization of the racemate and enantiopure compound will take place.Figure 3.10 shows accumulations of crystals of pure L-phenylalanine for initiation of cooling at various times. In all of these runs, the production of DL-phenylalanine was miniscule and could be ignored, indicating the preferred operation would initiate cooling so that the overall run time was minimized. For the results in Figure 3.10, that would correspond to initiating cooling after about 200 minutes of run time.
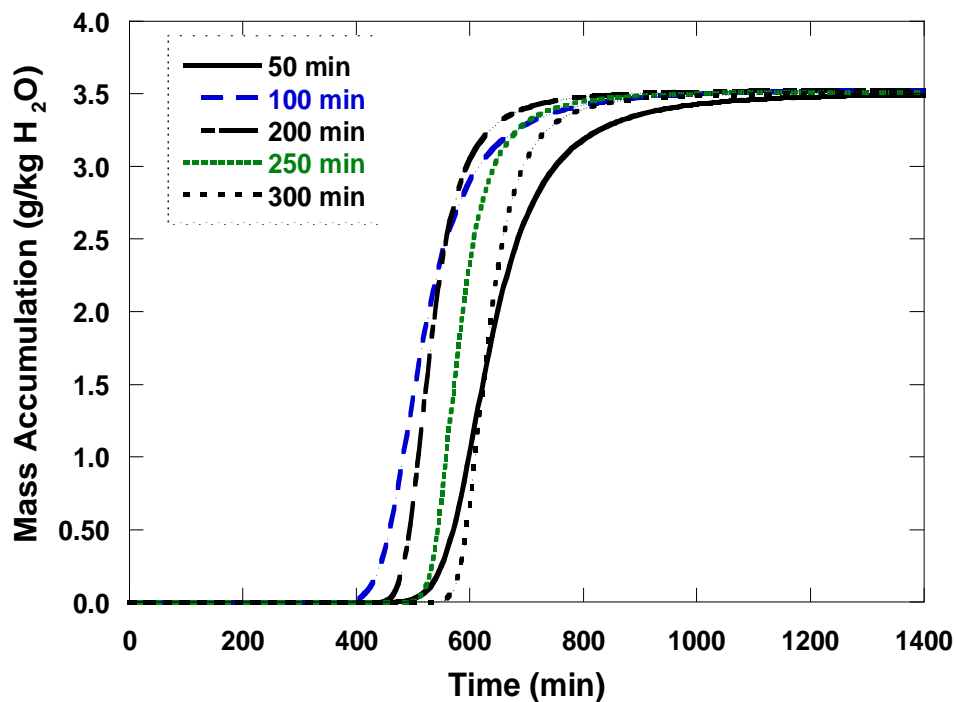
Figure 3.10: Accumulation of L-phenylalanine crystal mass when initiating cooling at various times after the start of a run.

Simulations similar to those described for phenylalanine were also performed for methionine and gave a significantly more complicated outcome, as shown in Figure 3.11. The figure shows that is some runs both L- and DL-methionine were produced. Note that the curves for 100 minutes are for both enantiomers, and DL-methionine is produced in significant amounts, starting at about 200 minutes; on the other hand, essentially no L-methionine is produced until around 1100 minutes. These results demonstrate that initiating cooling prior to inadequate enrichment by stereoinversion leads to crystallization of the undesired racemic compound. Starting the cooling at 200 minutes or later led to recovery of pure L-methionine.
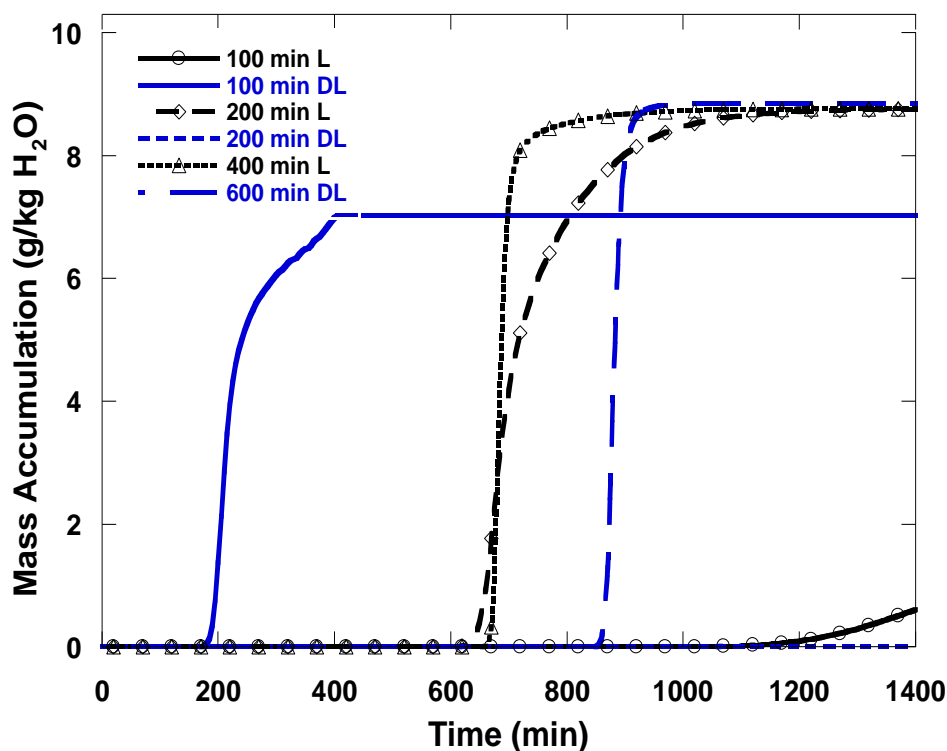
Figure 3.11: Accumulation of L- and DL-methionine crystal mass when initiating cooling at various times after the start of a run.

The different cooling profiles shown in Figures 3.10 and 3.11 were evaluated by calculating a process productivity based on the total amount of crystals obtained at a time, where productivity P is defined by

$$P = \frac{[L]_{solid}}{t} \tag{3.23}$$

The total elapsed run time is t and $[L]_{solid}$ is the mass of enantiopure crystals per unit mass of solvent.

Figures 3.12(a) and 3.13(b) show, respectively, the productivities of L-phenylalanine and L-methionine at multiple cooling profiles that led to high enantiomeric excesses of the desired products. There is a clear maximum in each of the productivity plots, which represents the most efficient use of the system; at times beyond the maxima, productivities decrease since the yield of crystals remains essentially constant. Moreover, comparison among the protocols for each solute demonstrates superiority of one over the other; i.e. for L-phenylalanine the most productive protocol has cooling being initiated 200 minutes after the process was started, while the most productive for L-methionine calls for initiating cooling after 400 minutes.
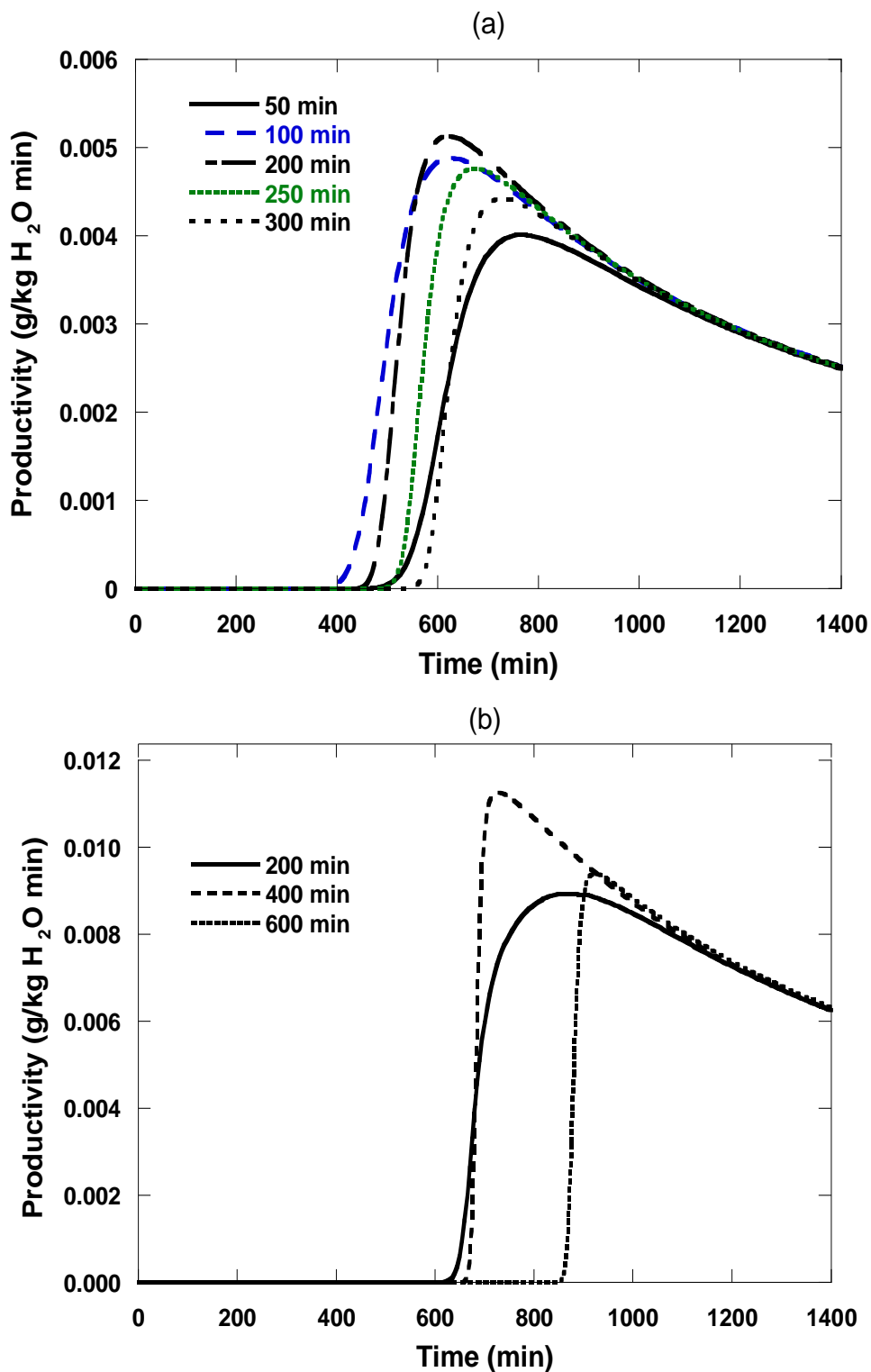
Figure 3.12: Productivity of enantiopure crystals under varying cooling protocols: (a) L-phenylalanine, (b) L-methionine

Finally, we considered the effect of cooling rates on the progress of the crystallization component of the process. We did this by choosing the two favored times for initiating cooling (200 minutes for phenylalanine and 400 minutes for methionine) and varied the constant rates of cooling from 0.1 °C/min to 0.4 °C/min. Figures 3.13(a) and 3.13(b) show the results for phenylalanine and methionine and illustrate that the productivity of phenylalanine crystals can be enhanced, without compromising crystal purity, by using a cooling rate of 0.2 °C/min but increasing the cooling rate for methionine led to a decrease in productivity, probably because lowered temperatures had an adverse effect on the rate of reaction.
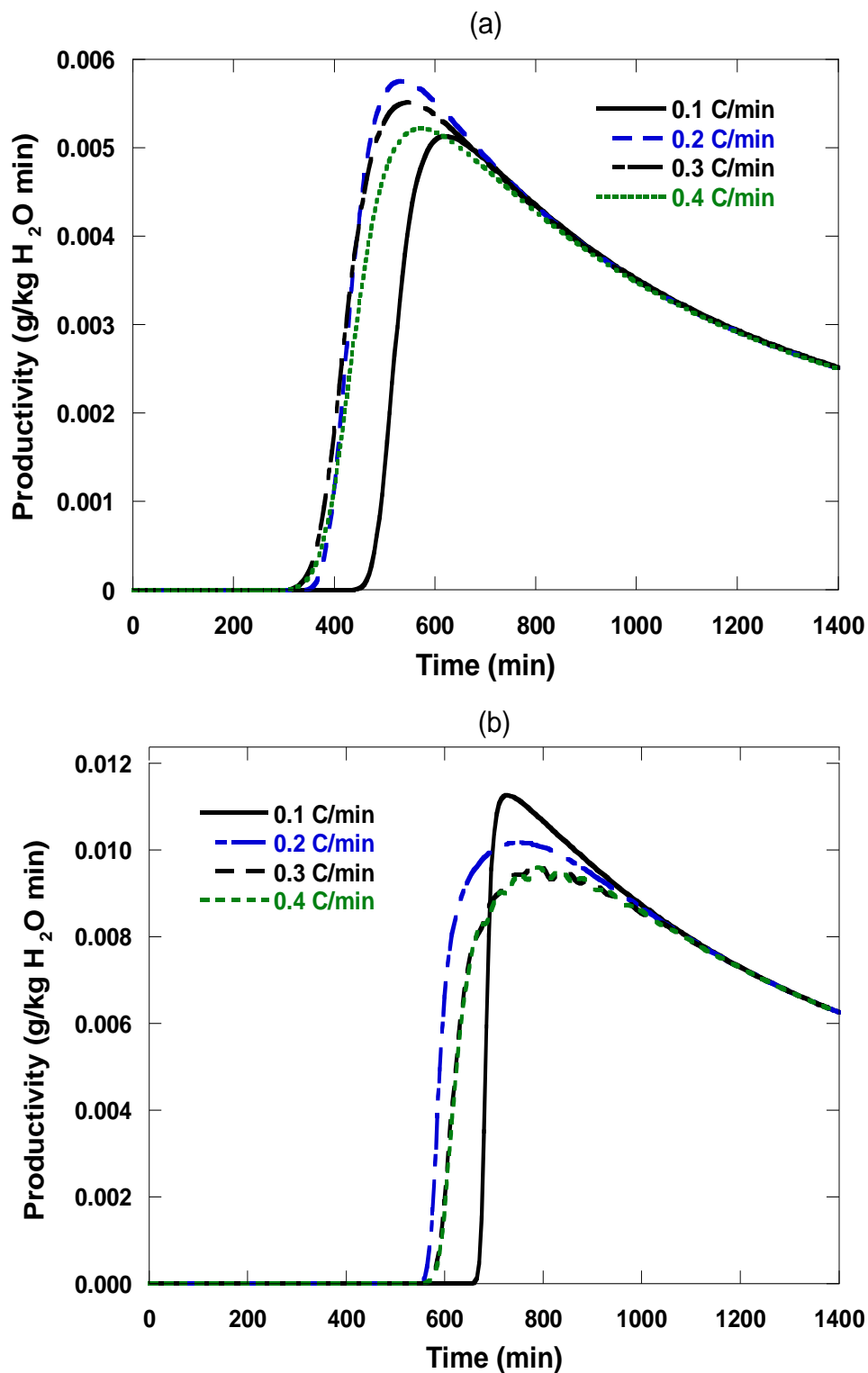
Figure 3.13: Effects of cooling rate on productivity of enantiopure crystalline products: (a) L-phenylalanine with cooling initiated at 200 minutes; (b) L-methionine with cooling initiated at 400 minutes.

The previous simulations show the potential advantages of performing parallel chemo-enzymatic reactive crystallization operations. The results demonstrated how different cooling profiles affect the productivity of crystals and their enantiomeric purity. It is expected that optimization of this reaction-crystallization process could further improve the productivity of the operation since the optimal temperature profile might not follow a linear profile and the cooling stage could start between any of the initial times tested in this set of simulations.

3.4 Conclusions

We link the conclusions drawn from our work to the objectives described in the Introduction. First and foremost we have formulated and demonstrated an effective strategy for producing enantiomerically pure species from racemic mixtures of racemate-forming amino acids. The strategy uses chemo-enzymatic stereoinversion to enrich the desired enantiomer in initially racemic solutions. Enrichment was shown to adjust the solution composition so that it was moved to a region of the phase diagram that ensured crystallization of the desired enantiomer.

Each element of the strategy was investigated experimentally; i.e. we successfully demonstrated that racemic mixtures of phenylalanine and methionine could be enriched in their respective L enantiomers using a reaction cycle that moved solution concentrations to zones where the L enantiomers could be crystallized without contamination by the DL racemate. The experiments included measuring or otherwise obtaining phase-equilibrium data for the two model systems, verifying that the enzyme critical to the stereoinversion could be used at the high solute concentrations essential to the success of the process, testing that crystallizations at process conditions resulted in high enantiomeric purity, and obtaining kinetic expressions for the chemo-enzymatic

56

stereo inversion and for crystallization that could be used in modeling the combined process.

Simulations based on the models developed from our experiments showed the potential advantages of coupling chemo-enzymatic reactions and crystallization to resolve racemic mixtures of amino acids. The results show that the key feature of this operation is the reduction of the total time of the operation, which enhances the productivity of the process.

Although the data and simulations were for phenylalanine and methionine, the strategy developed has broader potential and may be found useful in other high-value systems where enantiomeric impurity is important.

CHAPTER 4

Generic Dynamic Optimization for Reactive-Crystallization of Chiral Compounds

4.1 Introduction

Crystallization is a widely used for the separation and purification of specialty chemicals and pharmaceutical compounds. However, even though crystallization has been used in multiple industries during the past century, systematic approaches for the design of efficient crystallization-based operations has been discussed recently. For example, Wibowo et al. discussed the integration of crystallization in downstream processing (Wibowo et al., 2001). In their work, the effect of crystallization on other operations such as filtration, washing, dewatering, re-crystallization, and drying was studied. As expected, crystal size distribution (CSD) played an important role on the efficient integration of crystallization and these other operations. Schroer et al. and Berry et al. used a systematic approach to design reactive crystallization operations (Berry et al., 1997; Kelkar et al., 1999). In their work, information about reaction and crystallization kinetics is used for to design upstream-downstream operations.

In this work, a general scheme for the dynamic optimization of reactive-crystallizations is presented. The idea is to select an optimal temperature profile that benefits both upstream (reaction) and downstream (crystallization). As a result, the productivity of the operation can be enhanced. This is illustrated by performing an optimization of a reactive crystallization towards the production of enantiomerically pure compounds from racemic mixtures. Chiral compounds exhibit the same chemical and physical properties. Hence, most separation techniques fail on the resolution of enantiomers. Although these compounds exhibit multiple similarities, they can form independent solid phases. Therefore, crystallization can be used to recover

enantiomerically pure compounds (Schroer et al., 2001). In this chapter, we will use experimental information related to solubility, reaction kinetics, and crystallization kinetics to develop models that could be used to maximize different performance criteria.

4.2 Parameter Estimation

4.2.1 Solubility and Phase diagrams

The first step on the design of any crystallization-based separations is getting equilibrium data. Therefore, solubility data has been obtained for the racemic mixture, enantiopure compound, and the solubility at the eutectic point. For simplification purposes, we will assume that only the desired enantiomer is going to be crystallized, and its solubility will only depend on temperature. Equation 4.1 was used to model the solubility as a function of temperature, where the heat of melting (ΔH_M), difference in sensible heat between liquid and solid phase (ΔC_P), and melting temperature (T_M) were the parameters obtained fitted by an error minimization routine developed in MATLAB. Figure 4.1 shows the solubility data along with a fitting used to model solubility as a function of temperature.
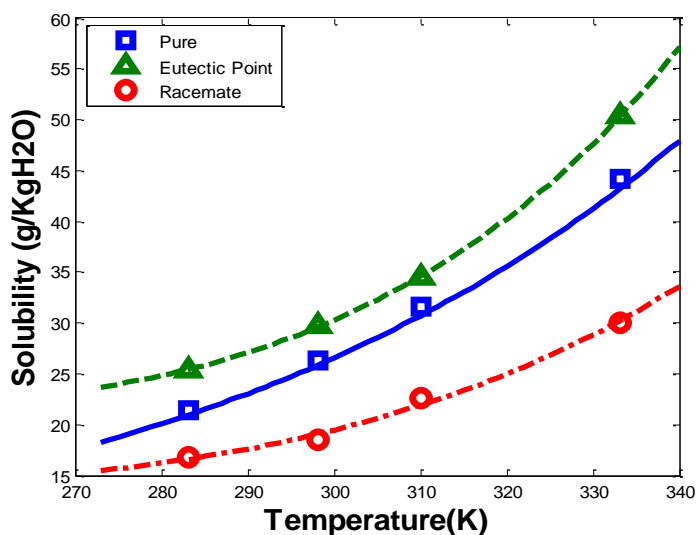
Figure 4.1: L-phenylalanine, DL-phenylalanine, and phenylalanine eutectic point solubility.

$$\ln x = -\frac{\Delta H_{\mathrm{m}}}{RT}\left(1 - \frac{T}{T_{\mathrm{m}}}\right) + \frac{\Delta C_{\mathrm{p}}}{R}\left(\frac{T}{T_{\mathrm{m}}} - 1\right) + \frac{\Delta C_{\mathrm{p}}}{R}\ln\frac{T}{T_{\mathrm{m}}} \tag{4.1}$$

Table 4.1: L-phenylalanine solubility constants.

	ΔH_{m} (J/mol)	ΔC_{p} (J/mol·K)	T_{m} (K)
L-phenylalanine	50327	93	728

Using the previous information, the solubility can be easily estimated if the temperature is known. In Section 4.2.4, temperature will be used to estimate the solubility, and therefore, the driving force of crystallization.

4.2.3   Reaction kinetics

Kinetic models for chemo-enzymatic stereoinversions have been studied before (Kroutil et al., 1998; Soda et al., 2001). This reaction proceeds through multiple oxidation-reduction steps, in which the undesired enantiomer is transformed into an achiral intermedia and then reduced to a racemic mixture of amino acids. However, since the first step is enantioselective, the overall "net" reaction is enantioselective. As shown in Figure 4.2, the net effect of the cyclic oxidation-reduction is the transformation of the undesired enantiomer to its counterpart. In this example we simplified the rate of reaction to first order kinetics, in which the undesired enantiomer is transformed to the desired one (i.e. ignoring intermediate steps). By assuming this reaction mechanism the observable reaction constant was determined from the slope of the concentration profile and its value was $10.6 \ \mathrm{mMs}^{-1}\mathrm{gEnzyme}^{-1}$.
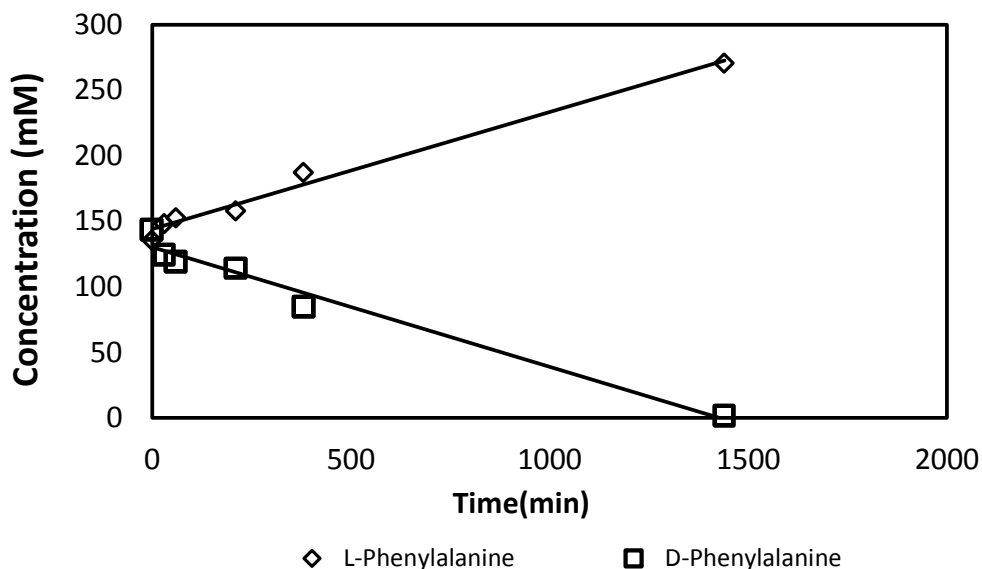
Figure 4.2: Chemo-Enzymatic Stereoinversion of phenylalanine at saturated conditions.

4.2.4   Crystallization kinetics

Crystallization kinetics was determined through the method of moments. The advantage of using this form is that the partial differential equation that represents the population balance is transformed to a system of ordinary differential equations. Equation 4.2 shows the definition of the moments of a population density function. The different indexes $i,$ represent the different moments of the population density. In this case, the zeroth, first, second, and third moments represent the total number of nuclei, length, area, and volume of crystals, respectively. The total volume of crystals is linked to the mass of crystals by assuming a certain particle density. Transforming volume to mass is useful since the mass concentration is easier to quantify than the volume of particles. Equations 4.3 and 4.4 represent the rate of change of each of moment, which were used to estimate the kinetic constants of nucleation and growth rate.

$$\mu_i = \int_0^\infty n(L,t)L^j dL \qquad (4.2)$$

$$\frac{d\mu_0}{dt} = B \qquad \text{where,} \qquad B = k_B \exp\left(\frac{-E_B}{RT}\right)S^b \qquad (4.3)$$

$$\frac{d\mu_i}{dt} = iG\mu_{i-1} \qquad \text{where} \qquad G = k_G \exp\left(\frac{-E_G}{RT}\right)S^g \qquad (4.4)$$

$$\text{and,} \qquad S = \left(C - C^{sat}\right)/C^{sat}$$

Finally, by assuming a certain particle density and shape factor we can obtain an expression for the rate of change of solution concentration.

$$\frac{dC}{dt} = -3\rho_c k_v hG\mu_2 \qquad (4.5)$$

This equation was used to estimate crystallization kinetics of L-phenylalanine whose values are reported in Table 4.2. Figure 4.3 shows a desupersaturation plot for L-phenylalanine. The green line on the graph represents a solubility cure, while the red (model) and blue (experimental) represent concentration profiles. The concentration was measured using an online monitoring system in which the solution was recirculated through a polarimeter and a refractometer, and solubility was estimated by measuring the temperature and using the model developed in Section 4.2.1 (Experimental set-up is not discussed in this chapter).

Table 4.2: Parameters of L-phenylalanine crystallization kinetics

k_B (#/(g/kg)^b·min)	b	k_G (m/(g/kg)^g·min)	g
$7.08 \times 10^5 \pm 2.32 \times 10^4$	7.56 ±0.14	$1.99 \times 10^{-7} \pm 6.07 \times 10^{-9}$	1.36 ± 0.03

L-Phenylalanine Crystallization
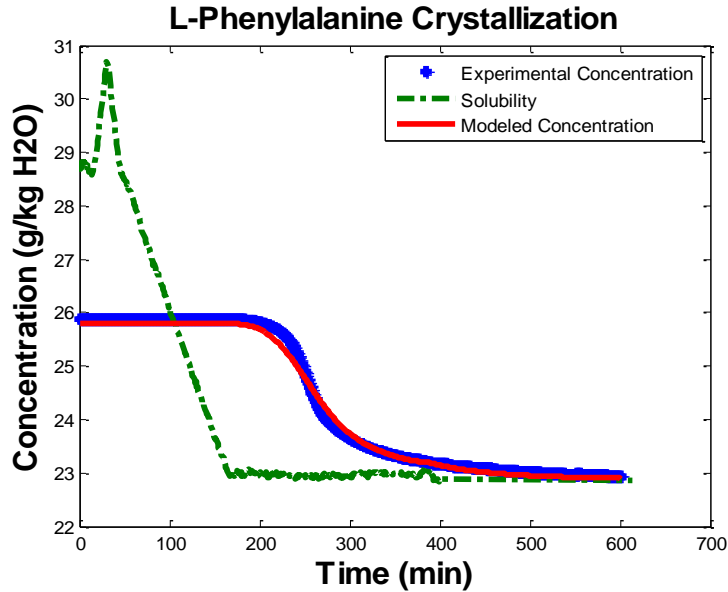
Figure 4.3: Cooling crystallization of L-phenylalanine.

4.3 Dynamic Optimization Models

4.3.1 Reaction and parallel nucleation and growth rate

The following model represents a reactive crystallization where the reactions is being modeled by a first order reaction and crystallization by primary nucleation and growth rate kinetics. The fundamental assumption of the model it is that when the solution becomes supersaturated, nucleation and growth are going to start simultaneously. Similar models had been used in the literature (Kelkar et al., 1999) to design crystallization processes. Equations 4.6-4.8 represent the mass balance of all the components. Notice, that all the differential equations depend on temperature.

$$\frac{d[D]}{dt} = k_R [E_o][D] \tag{4.6}$$

$$\frac{d[L]}{dt} = k_R [E_o][D] - k_B \exp\left(\frac{-E_B}{RT}\right)\left([L]-[L^*]\right)^b - k_G \exp\left(\frac{-E_G}{RT}\right)\left([L]-[L^*]\right)^g \quad (4.7)$$

$$\frac{d[L_{Solid}]}{dt} = k_B \exp\left(\frac{-E_B}{RT}\right)\left([L]-[L^*]\right)^b + k_G \exp\left(\frac{-E_G}{RT}\right)\left([L]-[L^*]\right)^g \quad (4.8)$$

$$k_R = k_{R,o} \exp\left(\frac{-E_R}{RT}\right) \quad (4.9)$$

The optimization criteria selected for this model was time minimization. The idea it is minimize the time required to meet a certain yield of the desired enantiomer in the solid phase.

$$\min_T \quad \phi_T = t_f \quad (4.10)$$

$$\text{s.t.} \quad \frac{dz(t)}{dt} = f\left(z(t),u(t)\right) \quad (4.11)$$

$$[L_{solid}](t_f) = yieldL_{solid} \quad (4.12)$$

Such a formulation will maximize the productivity of the operation since the time required to meet certain product specification it is minimized. In this minimization strategy the temperature was selected as the control vector (i.e. u(t)=T(t)) and used in the state equations z(t) (i.e. differential Equations 4.7 to 4.9). This simulation was performed with an initial temperature of 60 °C, an initial concentration of the racemic mixture of 60 g/kg solvent, and all the moments of the distribution were set to zero (i.e. μ_i (0)=0). The optimization was performed in MATLAB using the dynamic optimizer (*GPOPs*). Figure 4.4 (Left) shows the optimal temperature profile, while Figure 4.4 (Right) shows the results of the state variables (Concentration profiles).
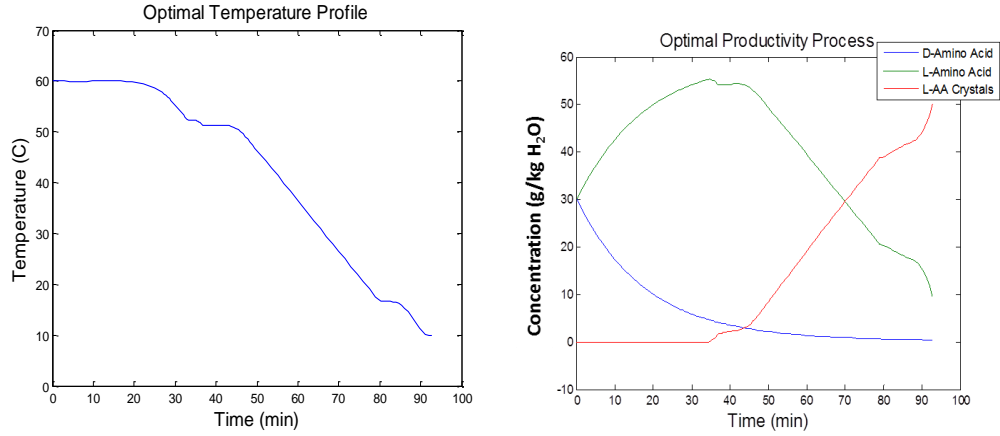
Figure 4.4: Left: Optimal temperature profile. Right: Concentration profiles.

The behavior of the optimal temperature profile makes sense because at the beginning we want

to maintain high temperatures to enhance the rate of production of the desired product, and then,

decrease the temperature to enhance the rate of crystallization. To verify the validity of the

optimization, a mass balance was used to verify mass conservation through time. The

verification of mass conservation it is important because crystallization is a very non-linear

process, and since a collocation method is being used, the polynomial approximation could yield

an inaccurate mas balance. Also, to verify optimality, the Hamiltonian was evaluated through

time. In time minimization problems, the Hamiltonian does not explicitly depend on time.

Therefore,

$$\frac{\partial H}{\partial t} = 0 \tag{4.13}$$

$$H = Constant \tag{4.14}$$

and since we are trying to minimize t_f, this constant must be zero. Figure 4.5 (Left) shows the

mass conservation profile, while Figure 4.5 (Right) shows the Hamiltonian profile. We can

notice that mass is roughly conserved, but at the end of the problem the Hamiltonian deviates

65

even more from zero. Most likely, this is due the high non-linearity of the problem, which can make quick changes to either the states or the costates.
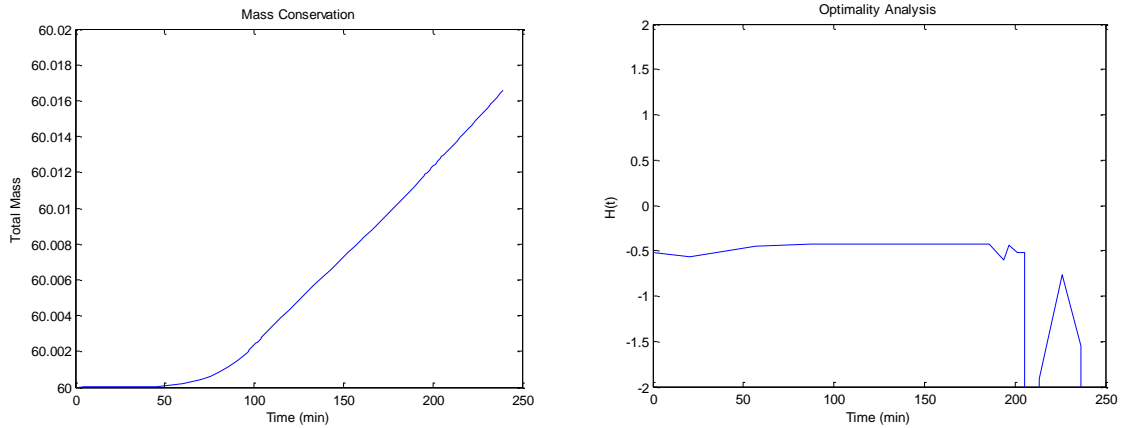
Figure 4.5: Left: Mass conservation. Right: Hamiltonian evaluation.

To finalize the analysis of this model, sensitivity on the parameters of the rate of crystallization was performed. This is important since during the parameter estimation of the crystallization kinetics, multiple solutions (or local minima) were found. Figure 4.6 shows the optimal temperature profile for two different values on the rate of nucleation constant k_B. We can notice, that the behavior of these plots is relatively similar.
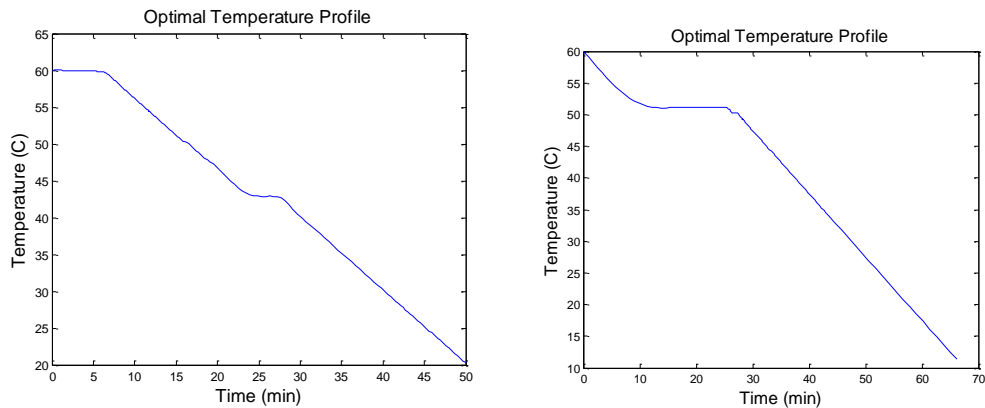
Figure 4.6: Temperature profile for $k_B = 1x10^9 \#/min$ (Left) and $k_B = 1x10^7 \#/min$ (Right).

However, when the nucleation exponent was varied (Figure 4.**7**), the behavior of the optimal temperature profile was completely different. Therefore, if the number of estimated parameter

must be reduced, the nucleation exponent should be fixed. This would increase the robustness of

the model and the optimization.
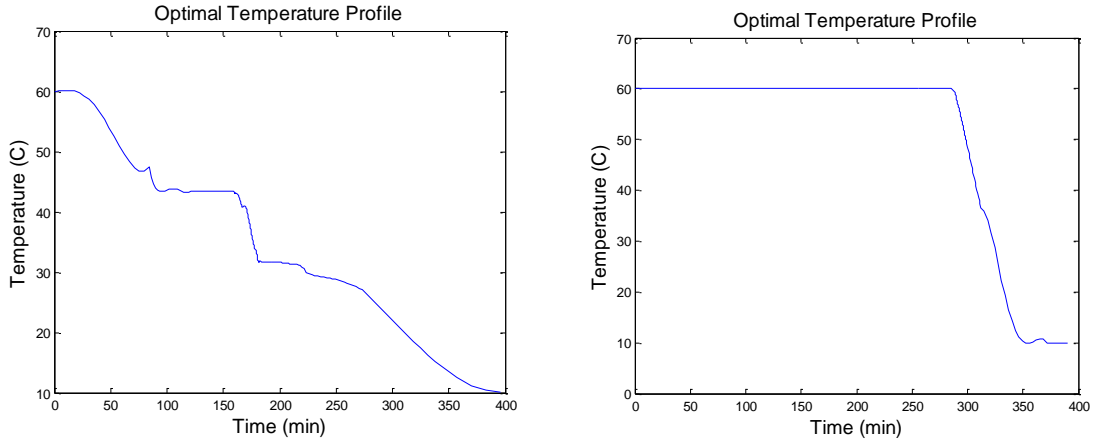
Figure 4.**7**: Temperature profile for b = 4 (Left) and b = 5 (Right).

4.3.2 *Reaction and method of moments*

An alternative model was developed based on the method of moments. In this case, a

reaction term was included into the mass-based third moment. By doing such a manipulation, a

model in which nucleation and growth do not start simultaneously can be developed.

$$\frac{dL}{dt} = k_R [E_o][D] - 3\rho_c k_v G \mu_2 \tag{4.15}$$

Using this model, we can capture other information about the process such as crystal size

distribution since average properties of the population are being capture. For example, we can

calculate the mean size or size variance.

$$L_{avg} = \mu_1 / \mu_0 \tag{4.16}$$

$$Variance = \mu_2 / \mu_0 - \mu_1 / \mu_0^{\ 2} \tag{4.17}$$

In this model, we consider maximizing the yield of the product and its final mean size. Equation 4.18 shows the objective function used for this optimization. A weight constant was used to give more importance to one objective vs. the other.

$$\phi = -w\left[L_s\right]\left(t_f\right) - \left(1-w\right)\mu_1/\mu_0\left(t_f\right) \tag{4.18}$$

If maximizing the yield was heavily weighted, the problem is analogous to the time minimization problem. However, in this case, the time is fixed and the yield is maximized. Nevertheless, both problem formulations maximize the productivity of the operation. Figure 4.8 shows the optimal temperature profile (Left) and the respective mass accumulation profile (Right) using the same initial conditions as the problem stated in the previous section. As expected, the temperature is maintained high at the beginning and then it is decreased to enhance the rate of crystallization.
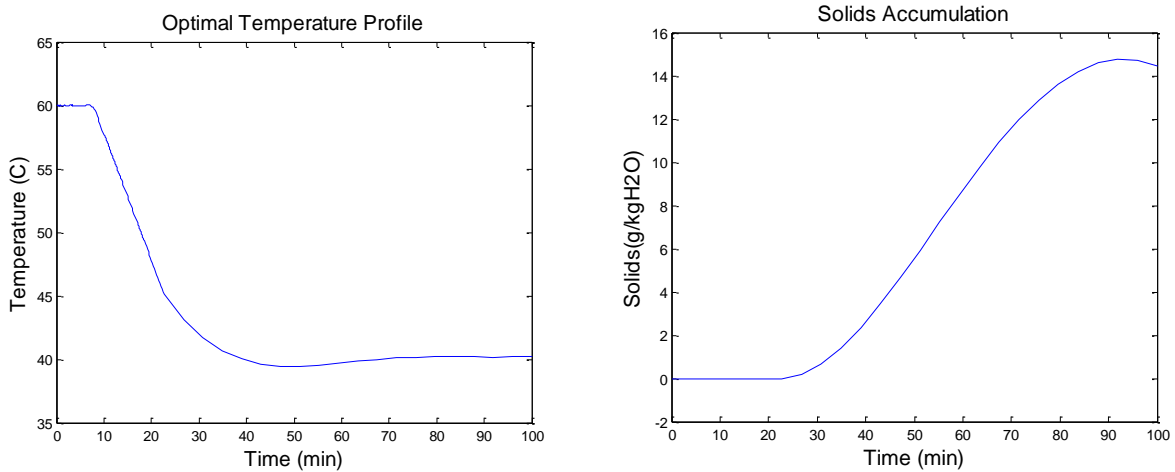
Figure 4.8: Optimal temperature profile (Left) and crystals accumulation profile (Right) for the yield maximization problem.

Now we consider reducing the value of *w*; hence, the problem becomes a multiobjective optimization. In this case, we want to maximize both the yield and mean size. Figure 4.9 shows the temperature profile (Left) and crystals accumulation (Right). The behavior of this optimal temperature profile is not obvious; at the beginning, instead of maintaining the temperature

constant, the temperature is reduced. Probably, by reducing the temperature, the rate of reaction is reduced, which reduces the rate of supersaturation build-up. It is well known, that a high supersaturation leads to high nucleation rates. Therefore, since we want to maximize the size of the crystals, we want to suppress nucleation and enhance crystal growth rate.

As expected, the amount of crystals recovered from this operation is lesser than the one in which only the yield was considered. However, the crystals of this operation would have a bigger mean size, which is desirable in downstream processing of solids (i.e. filtration, washing, and recrystallizing). Therefore, on each specific example, the importance of size distribution vs. productivity must be weighted. In some operations such as recovery of bulk chemicals productivity would be a predominant factor, but for pharmaceutical compounds, crystal size distribution is a major factor.
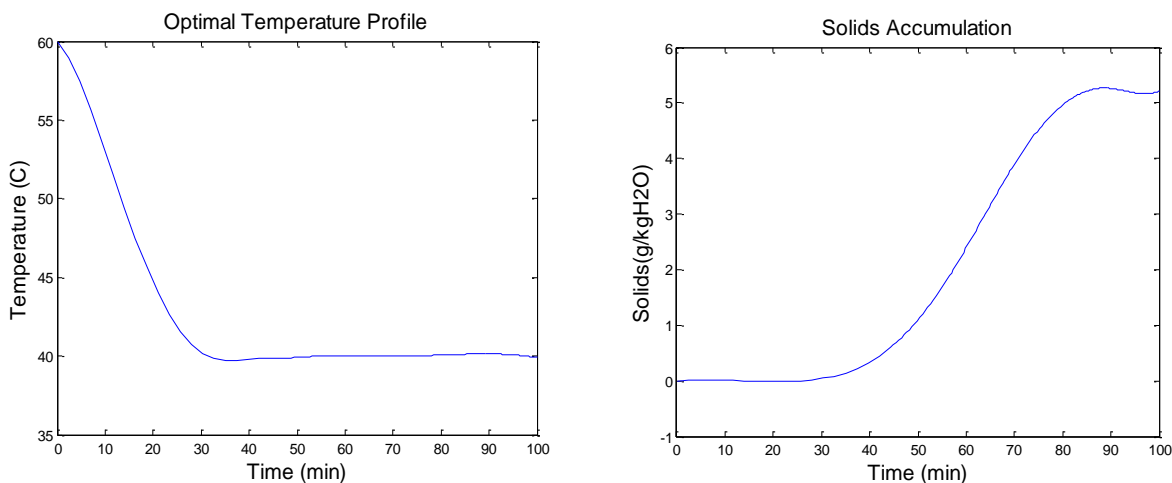
Figure 4.9: Optimal temperature profile (Left) and crystals accumulation profile (Right) for the multiobjective maximization of yield and mean size.

4.4 Conclusions

` In this work, the framework for a dynamic optimization of a reactive-crystallization of enantiomerically pure compounds was developed. The results show the possibility of enhancing

the productivity of reactive-crystallization operations by selecting an optimal temperature profile. One of the key and still unclear issues it is the parameters used in the model. During the crystallization kinetics parameter estimation routine, multiple set of parameters were able to fit the experimental concentration profile. Nevertheless, if the only focus is maximizing the productivity (maximize yield or reduce time) of the operations, any set of parameters might be enough (We do not care about distinguishing between nucleation and growth). However, the second model was developed using a reactive-method-of-moments. In this case, we wanted to maximize the yield and mean size. Therefore, since the mean size is defined using the moments (and the respective nucleation and growth parameters), inaccurate prediction on the crystallization kinetics will produce an inaccurate temperature profile. Another key point noticed was that collocation methods gave inaccurate integrations on some critical points. During the onset of nucleation the concentration profiles becomes extremely non-linear and polynomial approximations will fail on predicting the concentration. A possible strategy can be adding more collocation points around that region to obtain a better integration.

CHAPTER 5

QUANTIFICATION OF THE EFFECT OF PH AND CONCENTRATION ON PGA REACTION KINETICS

5.1 Introduction

β-lactam antibiotics are the class of antibiotics that contain a β-lactam ring within their structure. This group includes a broad range of penicillin derivatives such as ampicillin and amoxicillin, and cephalosporins, monobactams, and carbapenems. These antibiotics span approximately 65% of the world market of antibiotics, with sales greater than $15 billion (Elander, 2003; Giordano et al., 2006). Commercial manufacturing of β-lactams antibiotics usually is achieved through conventional organic synthesis where low temperatures, organochloride solvents, and protection/deprotection groups are employed (Ospina et al., 1996). As a result, significant amount of waste is generated through the process.

An alternative route for the manufacture of β-lactam antibiotics is the enzymatic synthesis by penincillin G acylase (PGA). This enzyme can catalyze the acyl transfer from an activated side chain donor to the nucleophilic β-lactam forming the desired antibiotic. For example, the enzymatic synthesis of ampicillin can be achieved by reacting 6-aminopenicillanic (6-APA) acid and D-phenylglycine methyl ester (D-PGME) in the presence of PGA. Similarly, other β-lactam products can be synthesized by simply changing the initial reactants.

The overall reaction scheme is presented in Figure 5.1. As it can be seen in the figure, PGA does not only catalyze the synthesis of ampicillin but it also catalyzes the hydrolysis of D-PGME to D-phenylglycine and the hydrolysis of ampicillin to D-phenylglycine and 6-APA. In fact, the production of 6-APA can be achieved through hydrolysis of penicillin G by PGA(Abian et al., 2003).
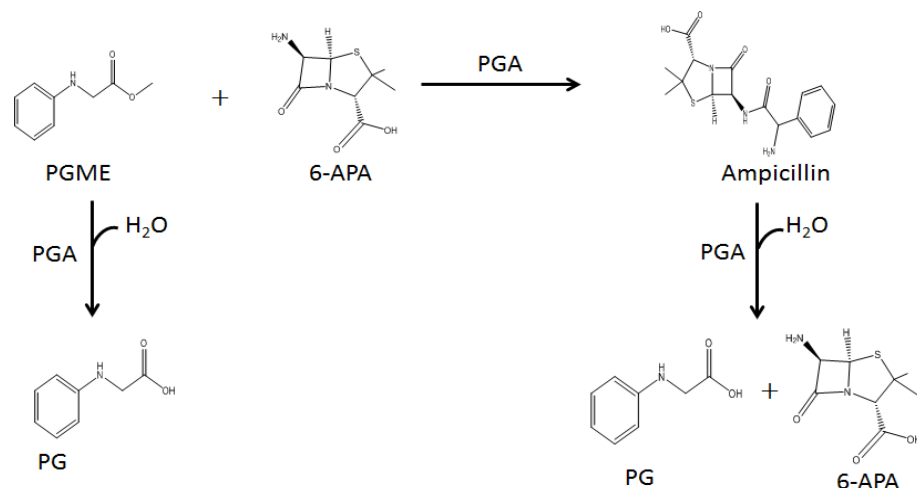
Figure5.1: Enzymatic synthesis of ampicillin by PGA.

As it can be observed in the figure, this system is a kinetically controlled reaction, where ampicillin is an intermediate within the network. Multiple reaction engineering strategies had been used to improve the yield of 6-APA towards ampicillin. These strategies can be classified into thermodynamically controlled reactions or kinetically controlled reactions. The first one relies on medium optimization to shift the microscopic reversibility of the enzymatic reaction towards the synthesis reaction. Based on the fact that the undesired reaction is a hydrolysis reaction, organic co-solvents have been used to shift equilibrium towards synthesis (Abian et al., 2003; Illanes et al., 2002; Kim et al., 1996). This approached demonstrated to improve the equilibrium constants but the kinetics of reaction can be drastically reduced.

In the other hand, optimization of this system is possible by acquiring information about the three main reactions: (1) synthesis, (2) primary hydrolysis, and (3) secondary hydrolysis. Significant work has been performed in this area including building kinetic models, pH and temperature optimization, heterogeneous reactions, and complex reactor design (Ferreira, 2007; Youshko, Chilov, et al., 2002; Youshko & Svedas, 2000; Youshko, van Langen, et al., 2002). In this work we are quantitatively examining the effect of pH on these reactions (synthesis, 1°

hydrolysis, and 2° hydrolysis) to understand the predominant factors that influence the selectivity and absolute rate of these reactions. Each reaction was carried out in the pH range of 6.0 to 8.0 at multiple concentrations to verify their optimal operation.

5.2 Materials and Methods

5.2.1   Chemicals

D-Phenylglycine methyl ester (PGME), 6-aminopenicillaninc acid (6-APA), phenylglycine (PG), and ampicillin (Amp) were purchased from Sigma Aldrich USA (St. Louis, MO). Potassium phosphates monobasic and dibasic were purchased from VWR USA (Radnor, PA). Penicillin G acylase was kindly donated by DSM-Sinochem (The Netherlands). The enzymatic solution had a concentration of 17 mg/mL and its purity was verified using a gel showing no indication of other proteins. All the chemicals and enzyme were used without further purification.

5.2.2   Enzymatic Reaction

The enzymatic synthesis of ampicillin was performed in 10mL test tubes with a working volume of 2 mL. The temperature was maintained at 25 °C using a water-bath shaker at 125 RPM. The reactants were added to the 10 mL test tubes and dissolved using 250mM buffered solutions at the desired pH value and adjusting any deviation using hydrochloric acid or ammonia. Reactions were started by adding 25 µL of the enzymatic solution. Samples were withdrawn as a function of time to construct concentration profiles.

5.2.3   Synthesis vs. Hydrolysis Reaction

The initial rates of reaction of synthesis of ampicillin and D-PGME hydrolysis were measured at a pH value of 6.00, 6.500, 7.00, and 7.50. The rates of reaction were estimated by measuring the concentration of ampicillin and D-phenylglycine during the first 30 minutes of the

reaction. The reactions were carried starting with an initial concentration of D-PGME of 50 mM and 100mM, while the initial concentration of 6-APA was varied in the range of 10 mM to 300 mM.

5.2.4   Primary Hydrolysis Reaction

The initial rates of reaction of D-PGME hydrolysis were measured at a pH value of 6.00, 6.50, 7.00, 7.50, and 8.00. The rates of reaction were estimated by measuring the concentration of D-phenylglycine during the first 30 minutes of the reaction. The reactions were carried starting with an initial concentration of D-PGME in the range of 10 mM to 300 mM.

5.2.5   Secondary Hydrolysis Reaction

The initial rates of reaction of ampicillin hydrolysis were measured at a pH of 6.0, 6.50, 7.0, 7.5, and 8.0. The rates of reaction were estimated by measuring the concentration of ampicillin during the first 30 minutes of the reaction. The reactions were carried starting with an initial concentration of ampicillin in the range of 5 mM to 50 mM. However, the initial concentration of D-PGME for reactions performed at a pH of 6.00, 6.50, or 7.00 was in the range of 5-25 mM because the low solubility of ampicillin at these pH values.

5.2.6   Analytical Methods

Solution concentrations were analyzed using a Shimazdu (Kyoto, Japan) high-pressure liquid chromatography (HPLC) system using an isocratic method at 0.75 ml/min and a wavelength of 215 nm. Aliquots of 50 µL where withdrawn using a micropipette and diluted in 1mL of HPLC solution with 1%v HCl 2M quench the reaction. The HPLC solution consisted of an aqueous solution of 0.68g/L KH_2PO_4, 0.68g/L SDS at a pH of 3.0 and acetonitrile (70%v aqueous/30%v organic). A C18 Kinetix column (4.6 µm I.D. x 150 mm) from Phenomenex (Torrance, CA).

Calibration curves were performed at a pH of 6.00 and 7.00. This was done to ensure that the absorbance of the components was independent of pH value. It was noticed that some peaks split when the pH of solution was changed as charged species had a different retention time than zwitterions. However, charged and neutral species exhibit the same UV absorbance as a function of concentration.

5.3 Results and Discussion

5.3.1 Synthesis vs. Hydrolysis Reaction

To investigate the effect of concentration and pH value on the selectivity of the reaction, an experimental design consisting of 6 different concentrations at 5 pH values was investigated. The accumulation of ampicillin and D-phenylglycine was tracked and used to estimate the initial rates of synthesis and primary hydrolysis. Figure 5.2 shows the accumulation of ampicillin and D-phenylglycine at 6 different concentrations of 6-APA while maintaining D-PGME concentration constant and the pH value at 6.00. As expected, we can notice that the accumulation rate of ampicillin increases as the initial concentration of 6-APA increases. On the other hand, accumulation rates of D-phenylglycine decreased as the concentration of 6-APA was increased. This demonstrates an increase on selectivity towards synthesis as 6-APA concentration increases. Hence, these results suggest maintaining high 6-APA to D-PGME ratios to enhance selectivity towards ampicillin.

(a)

(b)
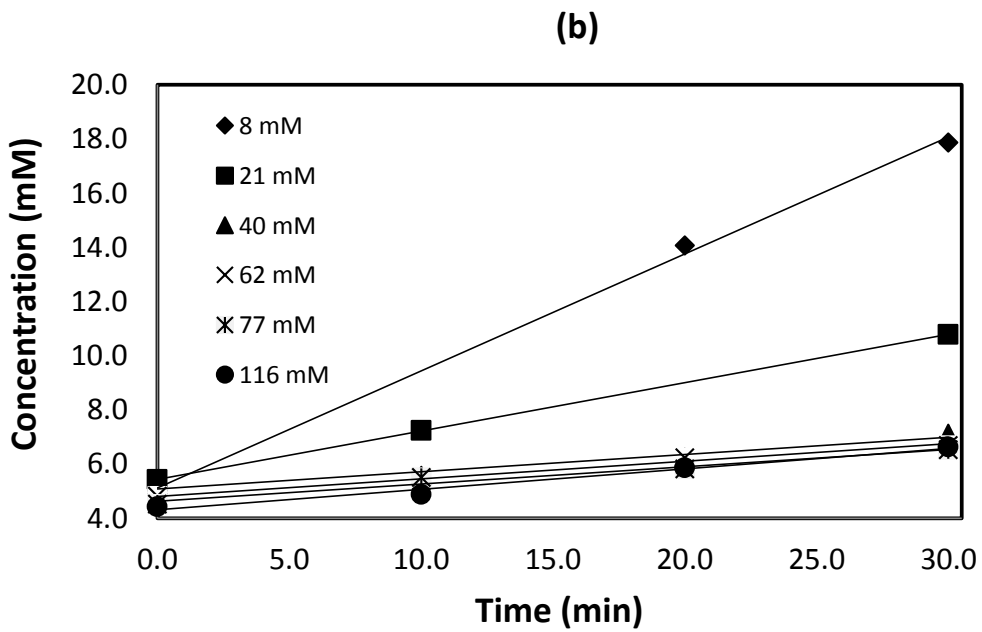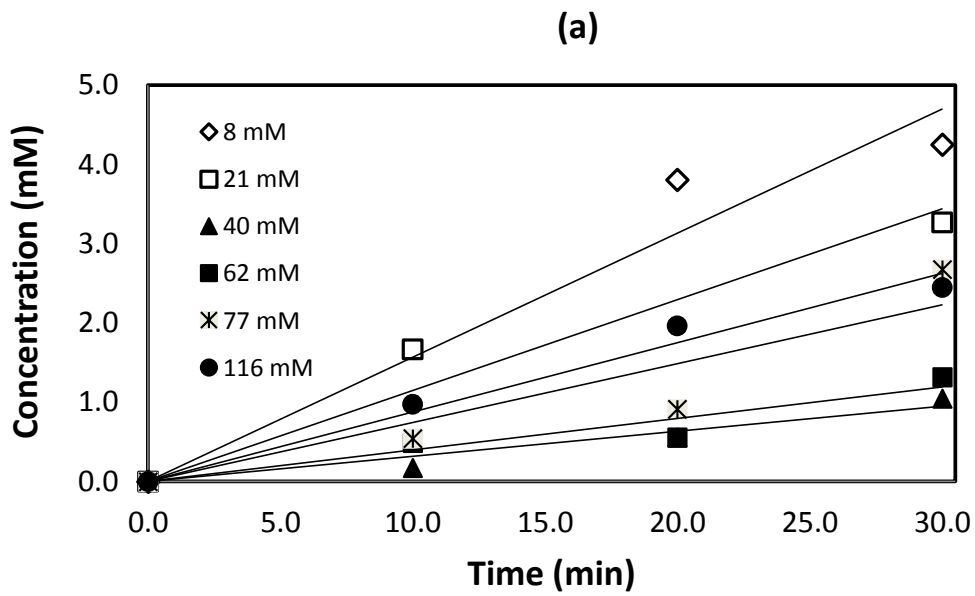
Figure 5.2: Initial accumulation of (a) ampicillin and (b) D-phenylglycine at a pH value of

6.50 and 298 K.

This behavior can be explained using the minimum kinetic scheme (equations 5.1-5.4) developed by Youshko et. al.(Youshko, Chilov, et al., 2002) in which the production of ampicillin is a function of the concentration of D-PGME and 6-APA. Since the accumulation it is based on initial rate experiments, the effect of secondary hydrolysis is negligible as the concentration of ampicillin is low.

$$\frac{d[\text{Amp}]}{dt} = E_o \frac{k_2}{K_s} \frac{\beta_o[APA][PGME] - \alpha[\text{Amp}](1 + \beta_o\gamma[APA])}{1 + \beta_o[APA] + \beta_o\gamma[APA]} \qquad (5.1)$$

$$\frac{d[PG]}{dt} = E_o \frac{k_2}{K_s} \frac{(1 + \beta_o\gamma[APA])([PGME] + \alpha[\text{Amp}])}{1 + \beta_o[APA] + \beta_o\gamma[APA]} \qquad (5.2)$$

$$[\text{PGME}] = [PGME]_0 - [AMP] - [PG] \qquad (5.3)$$

$$[APA] = [APA]_o - [AMP] \qquad (5.4)$$

Following the same procedure, the reaction was carried at multiple pH values. Figure 5.3 shows a summary of the effect of concentration and pH value to the initial rate of synthesis vs. hydrolysis. Figure 5.3 shows that increasing the ratio of 6-APA to D-PGME increase synthesis vs. hydrolysis ratios. Such behavior can be modeled by saturation-type kinetics in which the selectivity of the reaction is related to 6-APA concentration using Equation 5.5. However, in contrast to what was reported in other articles (Youshko, van Langen, et al., 2002), we did not find that pH value had a significant effect on the selectivity of the reaction.

$$\left(\frac{v_{Amp}}{v_{PG}}\right)_o = \frac{\beta_o[APA]}{1 + \beta_o\gamma[APA]} \qquad (5.5)$$

In Figure 5.3, the effect of substrate ratios to the selectivity of the reaction was fitted at each pH value using liner regressions. The slope of these regressions was used to construct Figure 5.4, which shows the effect of pH value on the synthesis vs hydrolysis as a function of substrate ratio.

A comparison of the slope of Figure 5.4 with the slopes of Figure 5.3 indicates that that the effect

of substrate ratio is approximately 5 times greater than the effect of pH value.
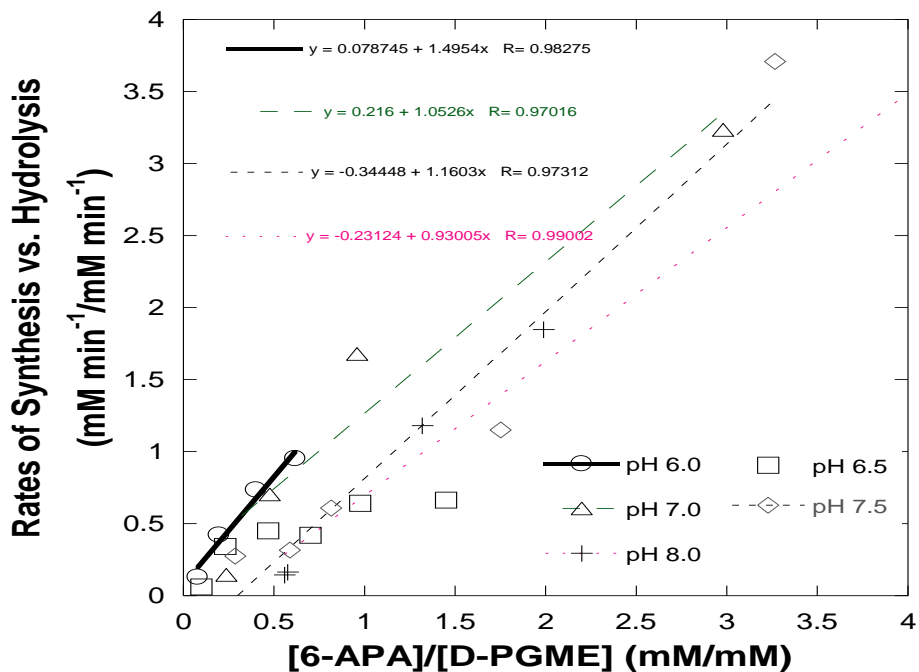
Figure 5.3: Effect of substrate ratio and pH value to the initial synthesis vs. hydrolysis ratios

for a varying concentration of 6-APA and a constant D-PGME initial concentration of 100 mM.
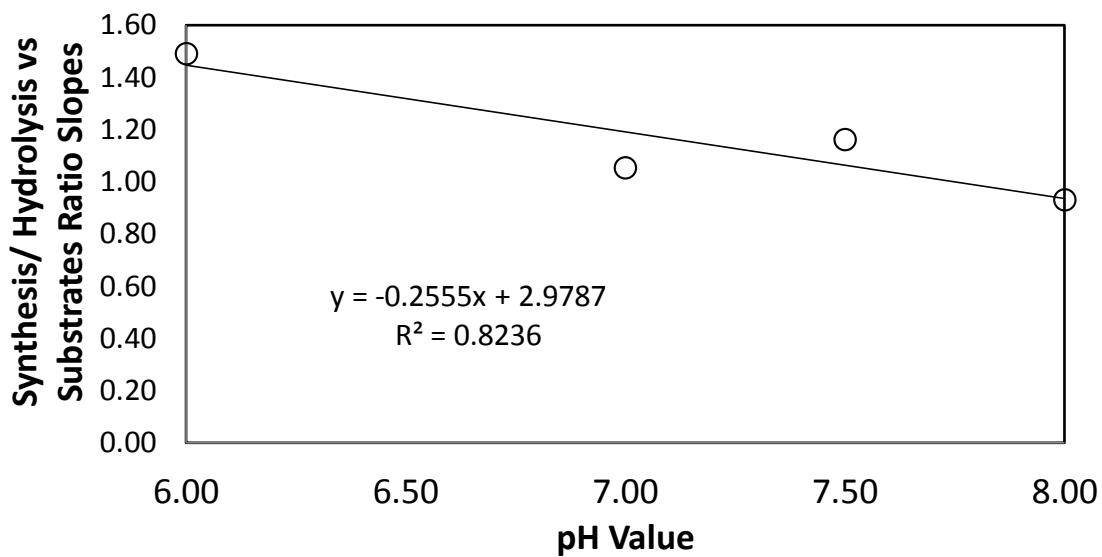
Figure 5.4: Slopes of the effect of substrate ratio at different pH values.

5.3.2 *Primary Hydrolysis Reaction*

In order to investigate the effect of concentration and pH value on the rate of primary hydrolysis, an experimental design consisting of 6 different concentrations at 5 pH values was investigated. The consumption of D-phenylglcyne methyl ester was tracked and used to estimate the initial rate of primary hydrolysis. Figure 5.4 shows an example of the hydrolysis reactions, in this case D-phenylglycine methyl ester concentration was monitored during the 30 minutes at multiple concentrations at a pH value of 7.00 and 298 K. As expected, higher concentrations enhances the rate of reaction.
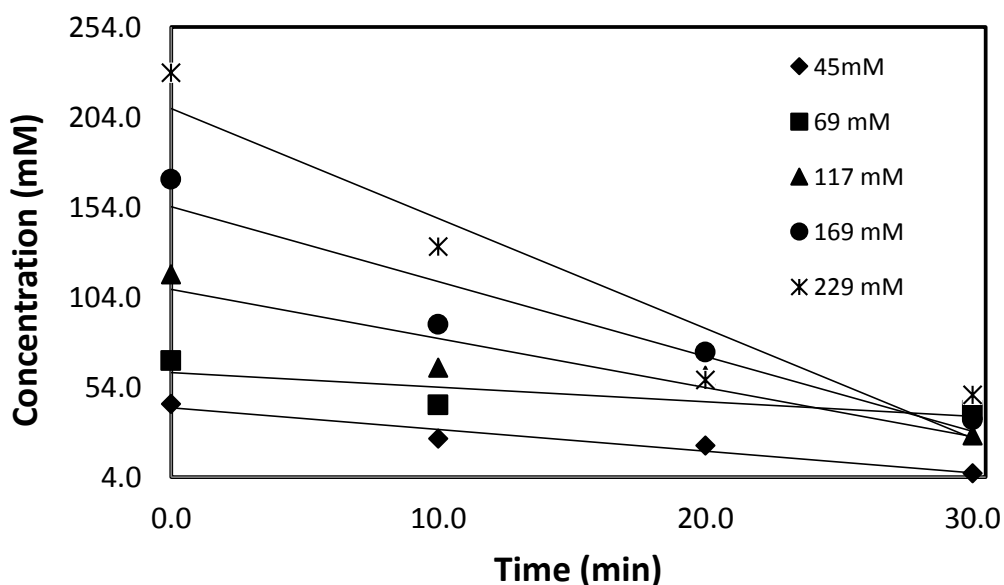
Figure 5.5: Hydrolysis of D-PGME at different initial concentration at a pH value of 7 and 298K.

Following a similar procedure, the initial rate of reaction was estimated at 4 additional pH value values and the results reported in Table 5.1. The results indicate that the rate of reaction has a maximum at a pH value of 7.00.

Table 5.1: Initial rate of primary hydrolysis v_0 (mM min^{-1}) at multiple concentrations (mM) and pH values.

[PGME]	v_0	[PGME]	v_0	[PGME]	v_0	[PGME]	v_0	[PGME]	v_0
pH 6.0		pH 6.5		pH 7.0		pH 7.5		pH 8.0	
28.73	-0.32	21.34	-0.37	42.63	-1.19	28.1	-1.11	39.32	-1.50
50.42	-0.19	46.12	-0.24	62.33	-0.81	54.49	-1.55	45.38	-0.54
76.55	-0.22	67.89	-1.58	108.37	-2.73	80.72	-1.59	75.00	-1.34
100.12	-0.46	93.39	-1.89	154.41	-4.16	108.41	-2.73	106.21	-2.36
146.51	-0.51	142.73	-2.02	208.89	-6.11	158.96	-3.98	151.88	-2.94
304.14	-1.59	292.46	-4.27	373.32	-8.29	312.61	-6.78	269.51	-3.59

5.3.3 Secondary hydrolysis reaction

As in the previous sections, the effect of pH value and concentration on the rate of secondary hydrolysis was investigated. Figure 5.5 shows the consumption of ampicillin at multiple concentrations and a pH value of 7.00. As expected, the rate of reaction increases as the concentration of ampicillin increases. Following a similar procedure, the rate of reaction was estimated at multiple pH value and their values reported in Table 5.2. Although there is some scattering in the data, we can see that the rate of secondary hydrolysis increases as the pH value increases. However, the rates of hydrolysis at a pH value of 7.50 and 8.00 are not significantly different. At these pH values most of the ampicillin it is negatively charged (anionic state); hence, it is possible that these negatively charged molecules have better affinity with the enzyme binding site; thus, their rate of reaction is relatively faster than its neutral state. Considering that the pKa of ampicillin is at 7.31, we could expect a huge increment on the rate of reaction at any value above that.
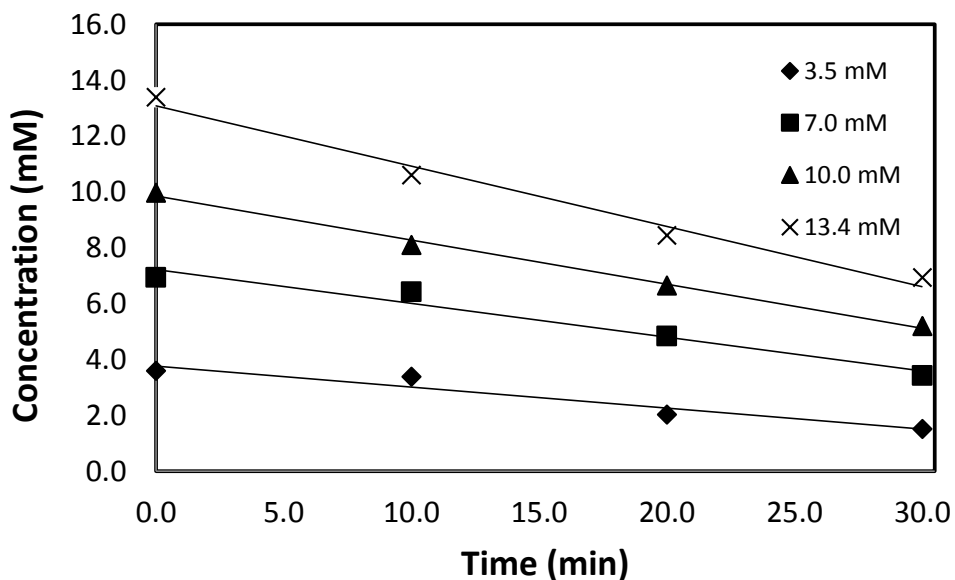
Figure 5.6: Hydrolysis of ampicillin at different initial concentration at a pH value of 7.00 and 298K.

Table 5.2: Initial rate of secondary hydrolysis v_0 (mM min^{-1}) at multiple concentrations (mM) and pH values.

[PGME]	v_0	[PGME]	v_0	[PGME]	v_0	[PGME]	v_0	[PGME]	v_0
pH 6.0		**pH 6.5**		**pH 7.0**		**pH 7.5**		**pH 8.0**	
3.77	-0.08	3.14	-0.41	2.75	-0.26	2.5	-0.25	3.08	-0.18
7.23	-0.12	7.02	-0.18	5.63	-0.5	5.63	-0.5	6.26	-0.05
9.86	-0.16	10.83	-0.25	8.2	-0.69	5.08	-0.44	9.21	-0.15
13.09	-0.22	14.61	-0.41	11.08	-0.7	10.3	-1.02	12.52	-1.22
-	-	-	-	-		20.75	-1.77	21.79	-0.61
-	-	-	-	-		27.99	-2.11	31.07	-2.15

5.4 Conclusions

In this work the effect and concentration on the synthesis of ampicillin by PGA was investigated. The reaction scheme was decouple into three different reactions: (1) synthesis vs. hydrolysis, (2) primary hydrolysis, and (3) secondary hydrolysis. The results demonstrated that the rate of each reaction increased as the pH value was raised. However, we did not see a significant effect on the selectivity of the reaction as both synthesis and hydrolysis reaction

exhibited similar pH value dependence. Therefore, we can conclude that the main variable to control in the process it is the ratio of the reactants. If 6-APA it is maintained in excess, synthesis of ampicillin will be favored over hydrolysis of D-phenylglycine methyl ester. However, such an approach will limit the conversion of 6-APA towards ampicillin. In order to deal with this issue reaction configurations should be transformed from batch to semi-batch. This reactor design will allow control on the ratio of the substrates and total conversion of each towards the desired product.

CHAPTER 6

Crystallization kinetics of ampicillin using online monitoring tools and robust parameter estimation routine

6.1 Introduction

As previously discussed, an alternative route for the manufacture of β-lactam antibiotics is the enzymatic synthesis by pencillin G acylase. This enzyme can catalyze the reaction of phenylglycine methyl ester (D-PGME) and 6-aminopenicillanic acid (6-APA) to form ampicillin. However, as shown in Figure 6.1, it also catalyzes the hydrolysis of D-PGME (primary hydrolysis) into phenylglycine (D-PG) and the hydrolysis of ampicillin into 6-APA and D-PG (secondary hydrolysis).
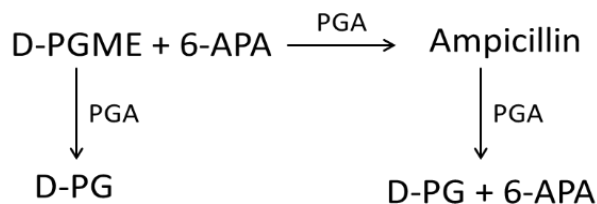
Figure 6.1: Enzymatic synthesis of ampicillin by penicillin G acylase.

As shown in Figure 6.1, the reaction network is a classic example of kinetically-controlled synthesis where ampicillin must be removed from the system before it is consumed by secondary hydrolysis. Developing a means to accomplish this is the focus of the present work, which is aimed at developing a robust model for separation of ampicillin from the reaction medium by crystallization. Because such an operation would have to be integrated with the required enzyme-catalyzed reaction, the model must be applicable to a variety of crystallization conditions. Previous work (Ottens et al., 2001, 2004) reported crystallization kinetics of ampicillin and the effects of reactants and by-products on the induction time for nucleation of

ampicillin. The objective of our work is expanding the range of conditions for which the model and associated parameters are applicable. This requires investigating multiple crystallization variables such as both pH value and rate of change of pH value, initial supersaturation, and of the use of seed crystals. All were explored in a pH range that is suitable for an enzymatic reactive system (i.e., the crystallization kinetics were obtained over a pH range of 6.00 to7.50). Additionally, most of the work was done using online monitoring tools, which has become common in model development and control of crystallization processes (Fujiwara et al., 2005; Nagy et al., 2013). Typically, online process analytical technologies provide larger data sets that can be used in the design of more robust models.

To accomplish these objectives the following strategy was developed. First, as described in Section 3.2, the necessary equilibrium data have been obtained from the literature and fit with a thermodynamic model that allows estimation of the solubility as a function of pH value. Second, in Section 3.3 results of induction time experiments are used to relate initial supersaturation with primary nucleation. This information was used to estimate the exponential primary nucleation constant. Third, in Section 3.4 a combination of seeded and unseeded crystallization experiments were used to obtain further information about both primary and secondary nucleation kinetics, and crystal growth kinetics. Finally, these sets of experiments were combined and a single set of parameters was obtained in Section 3.5. In Section 6.3.6, the parameters were used in the model to estimate the final crystal mean size of each run and compare it to the experimental one.

6.2 Materials and Methods

6.2.1 Chemicals

Anhydrous ampicillin was purchased from Alfa Alsear (Ward Hill, MA) and used without further purification. Ammonia was purchased in a 30% solution from Ricca Chemical Co. (Arlington, TX) and 5M hydrochloric acid was purchased from Sigma Aldrich (St. Louis, MO).

6.2.2 Equipment

Experiments to determine crystallization kinetics were performed in a 1 L OptiMax Synthesis Station from Mettler Toledo (Columbus, OH). A dosing unit was used to add 2 M HCl (diluted HCl 5M solution solution) to the reactor, and a pH probe unit from Mettler Toledo was used to monitor the pH in solution with a precision of ± 0.001 pH units. Solution concentration was monitored using a MCP 500 polarimeter and an Abbemat 500 refractometer from Anton Paar by using signal-concentration calibrations shown in Appendix A.1.2. As shown in Figure 6.2, solution was withdrawn from the reactor using a peristaltic pump and circulated through the refractometer and polarimeter. Chord length distribution of crystals was monitored using a Focus Beam Reflective Measurement (FBRM) apparatus from Mettler Toledo. Further details on this unit can be found elsewhere (Shi et al., 2003).
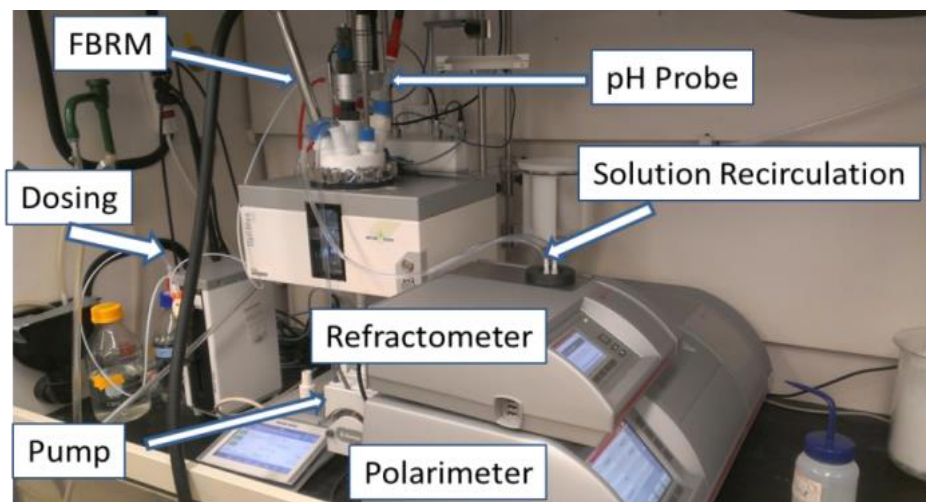
Figure 6.2: Crystallization system.

6.2.3 *Crystallization Experiments*

The initial solutions in all crystallization experiments were obtained by charging the 1-L vessel with 500 g of DI-water and adding 2M NH_3 solution until the pH was approximately 7.75(exact pH were used to estimate the solubility). Then, the desired amount of ampicillin was added to the vessel and stirred at 300 RPM until all the particles were dissolved. The FBRM was used to monitor the appearance of new crystals and the evolution of the chord length distribution throughout the length of the run. In order to compare experiments, counts were normalized by the total counts in each run to take into account variations in the signal from run to run.

Induction-time experiments were begun by abruptly changing the pH in the system in the range 7.85 to 6.00 by adding by adding 1 M HCl solution (exact pH were used to estimate the solubility). The time at which the FBRM had a rapid increase in chord counts was defined as the induction time.

Unseeded crystallization runs were initiated by gradually changing the pH in the system in the range 7.85 to 6.00 by adding 1M HCL at a predetermined rate (specific conditions reported later). The solute concentration was measured by recirculating a small portion of the solution through the polarimeter and refractometer as described in Section 6.2.2, and the evolution of the chord length distribution was monitored using the FBRM. At the end of each run (after stabilization of polarimetric signal), crystals were filtered, dried, and examined by light microscopy. The aspect ratio of crystals was approximated by measuring the width and length of multiple crystals using the scales of pictures taken with a light microscope.

Seeded crystallization runs were initiated by adding 1M HCl to reduce the pH in the system in the range 7.85 to 6.00 by adding (exact pH were used to estimate the solubility). Different seed loads in the range 20 to 250 μm were added into the crystallizer and the pH was

gradually changed to 6 at a rate of predetermined rate using the acid dosing unit (specific

conditions reported later). The solution concentration, evolution of the chord length distribution,

and the recovery and analysis of crystals were accomplished as described in the preceding

paragraph.

6.3 Results and Discussion

6.3.1 Crystallization kinetics

Crystallization kinetics can be used to describe the evolution of crystal size distribution in

a crystallizer. Equations 6.1 through 6.3 show a population balance along with initial and

boundary conditions for a batch system in which agglomeration and breakage are neglected.

$$\frac{\partial n(t,L)}{\partial t} = -\frac{\partial [n(t,L)G(t)]}{\partial L} \tag{6.1}$$

$$n(t,0) = \frac{J(t)}{G(t)} \tag{6.2}$$

$$n(0,L) = n_0 \tag{6.3}$$

Alternatively, crystallization kinetics can be described by using the method of moments where

instead of using a partial differential equation, an ordinary differential equation is employed to

describe the dynamics. First, the moments of the distribution are defined using the following

equation.

$$\mu_i = \int_0^\infty n(t,L)L^i dL \tag{6.4}$$

Differentiation of the moments leads to expressions that contain nucleation and growth kinetics:

$$\frac{d\mu_0}{dt} = J \tag{6.5}$$

$$\frac{d\mu_i}{dt} = iG\mu_{i-1} \tag{6.6}$$

In this work the following constitutive equations are used to model the rates of primary and secondary nucleation and crystal growth rate where [Amp] is the concentration of ampicillin, [Amp*] is the corresponding concentration at equilibrium, and S is the system supersaturation (S=[Amp]/[Amp*]).

$$B_1 = k_{B1} \exp\left(\frac{-B_o}{\ln(S)^2}\right) \tag{6.7}$$

$$B_2 = k_{B2} M^{b_M} (S-1)^s \tag{6.8}$$

$$J = B_1 + B_2 \tag{6.9}$$

$$G = k_G (S-1)^g \tag{6.10}$$

Additionally, the rate of change of the moments of the distribution is related to the change in solution concentration through a mass balance. This equation will be used in Section 6.3.5 to model ampicillin concentration and compare it with the experimental one.

$$\frac{d[\text{Amp}]}{dt} = -\rho_c k_v \frac{d\mu_3}{dt} = -3\rho_c k_v G\mu_2 \tag{6.11}$$

6.3.2 Solubility

All the crystallization protocols in this work are based on pH-induced supersaturation. Ampicillin is an ionizable compound that can exist in solution in three different forms (anion, cation, zwitterion), where the ratio of these form will depend on the pH in solution. The distribution among the charged species can be related with the concentration at the isoelectric point using equilibrium constants.

$$K_{A1} = \frac{[\text{Amp}^-][\text{H}^+]}{[\text{Amp}^\pm]} \tag{6.12}$$

88

$$K_{A2} = \frac{[Amp^{\pm}][H^+]}{[Amp^+]}$$
(6.13)

The distribution among the species at any pH can be obtained through the Henderson-Hasselbach

$$pK_A = pH + \log \frac{[Amp^{\pm}]}{[Amp^-]}$$
(6.14)

where $pK_A = -\log K_A$.

Assuming that the solubility of the zwitterion $[Amp^{\pm}]$ is constant throughout the pH range

of interest, the solubility of ampicillin ($[Amp] = [Amp^{\pm}] + [Amp^-]$) can be estimated using the

Henderson-Hasselbach equation. Non-idealities in solutions can be included by using the

extended Pitzer model (Pessoa et al., 2008) for electrolyte systems. This approach was used by

Franco et al. (Franco et al., 2013) where they model the solubility of multiple ionizable

compounds as a function of pH and temperature. However, in the present case we will focus on

the pH dependence as the primary contributor to the solubility of ampicillin. Using this approach

Equation 6.15 was used to fit solubility data, where parameters A_{ij} and B_{ij} were used as

adjustable parameters within the model. These parameters take into account non-idealities in

solution, and are representative of the interactions in solution. Note that regardless the

complexities of the equation only two parameters are used to correlate pH with solubility.

$$\log \frac{[Amp^*](pH)}{[Amp^*](pI)} = pI\text{-}pH + \log\left[\frac{1+10^{pH-pK_{A1}}}{1+10^{pI-pK_{A1}}}\right]$$
$$+ \log\left[\frac{1+10^{pH-pK_{A2}}}{1+10^{pI-pK_{A2}}}\right] + \frac{2}{\ln 10}\lambda_{ij}\left([Amp^*](pI)\text{-}[Amp^*](pH)\right)$$
(6.15)

$$\lambda_{ij} = \frac{2\pi\sigma^3 N_A \rho}{3}\left(1 - \frac{\varepsilon}{k_B T}\right)$$
(6.16)

$$A_{ij} = \frac{2\pi N_A \rho \sigma^3}{3}$$
(6.17)

$$B_{ij} = -A_{ij} \frac{\varepsilon}{k_B} \tag{6.18}$$

The solubility of ampicillin as a function of pH was obtained from the literature (Rudolph et al., 2001; Santana et al., 2010). Although there are differences between the two sources, our crystallization experiments tend to equilibrate at near-average values of their data.

Figure 6.3 shows experimental and modeled values for the solubility of ampicillin as a function of pH, while Table 6.1 shows the parameters obtained by fitting experimental data. During the parameter fitting either the adjustable Pitzer parameters A_{ij} and B_{ij} or the thermodynamic parameters σ and ε/k_B can be used to fit the data as they are related by Equations 6.17 and 6.18. As seen from the figure, when the pH is close to the isolectric point there is little difference between ideal and non-ideal solution behavior. As the pH increases, however, the solubility of associated with non-ideal solution behavior becomes greater than ideal behavior. This deviation from ideality is controlled by ε/k_B, where a value greater than the experimental temperature makes the interaction parameters negative. Therefore, the solubility exhibits a negative deviation from ideality and its activity coefficient will be less than unity (i.e. solubility greater than the one of an ideal solution). This is expected as charged species should exhibit greater interactions with a polar solvent than their zwitterion counterparts.
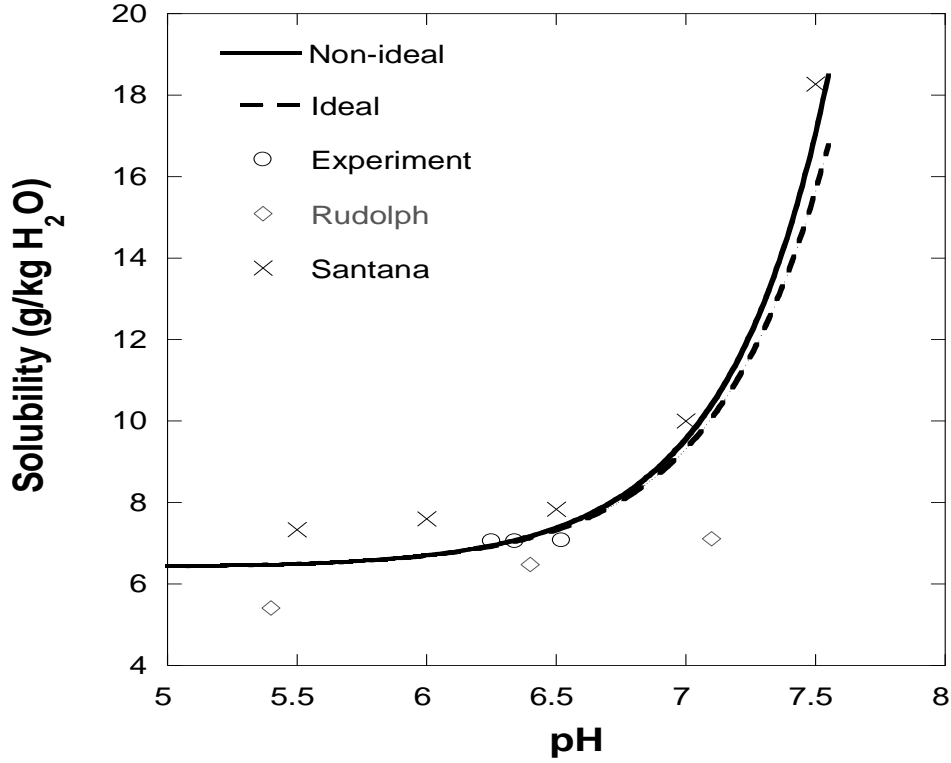
Figure 6.3: Modeled and experimental solubility of ampicillin at different pH.

Table 6.1: Extended Pitzer model parameters for ampicillin at 298 K.

A_{ij}	B_{ij}	σ	ε/k_B	λ_{ij}
11.05	-3.71×10^3	5.42×10^{-10}	336.18	-1.42

6.3.3 Nucleation Rate and Induction Time

Primary nucleation rate can be related to induction time, which is the time between a solution becoming supersaturated and detection of crystals (Sohnel et al., 1988). Hence, induction time can be considered as the combination of the time required to create a nucleus and growing it to a detectable size:

$$t_{ind} = t_N + t_G \tag{6.19}$$

Assuming that nucleation is the limiting step (i.e. $t_N \gg t_G$), the induction period can be related to the rate of nucleation J as

$$t_{ind} = J^{-1} \tag{6.20}$$

where

$$J = B_1 \tag{6.21}$$

and B_1 is the rate of primary nucleation. Finally, by substituting Equation 6.7 into 6.20 and rearranging, the induction time can be related to supersaturation by

$$t_{ind} = k_{B1} \exp\left[\frac{-B_0}{\left(\ln S_0\right)^2}\right] \tag{6.22}$$

or

$$\ln t_{ind} = \frac{B_0}{\left(\ln S_0\right)^2} - \ln k_{B1} \tag{6.23}$$

Figure 6.4 shows the total counts in the range of 0-10 μm for an induction time experiment at conditions reported in the figure. In this experiment, as mentioned in Section 6.2.3, instantaneous supersaturation was induced by addition of hydrochloric acid into the crystallizer and particles in solution were monitored using an FBRM. It can be observed in the figure that the number or particles in the range of 0-10 μm spikes after 8 minutes. Hence, 8 minutes is the corresponding induction time for an initial supersaturation of 3.02 C_0/C_0*.
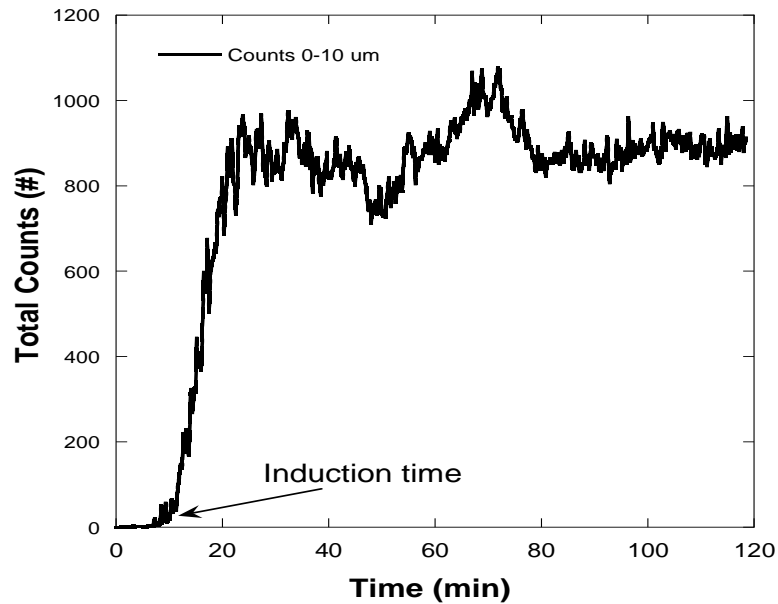
Figure 6.4: Detection of induction time from FBRM data for induction time experiment of an initial supersaturation of 3.02 (C_0/C_0^*) at 298 K.

Following the procedure just described, induction periods at multiple initial supersaturations were obtained and fitted using Equation 6.23, as shown in Figure 6.5. The slope of the regression represents the exponential primary nucleation constant B_0, which in this case was 1.27. Finally, using this value, Figure 6.6 was constructed. These results show that an initial supersaturation of at least 1.75 is necessary to achieve nucleation within a practical time range. Further details on the physical meaning of induction periods can be found elsewhere (Sohnel et al., 1988).
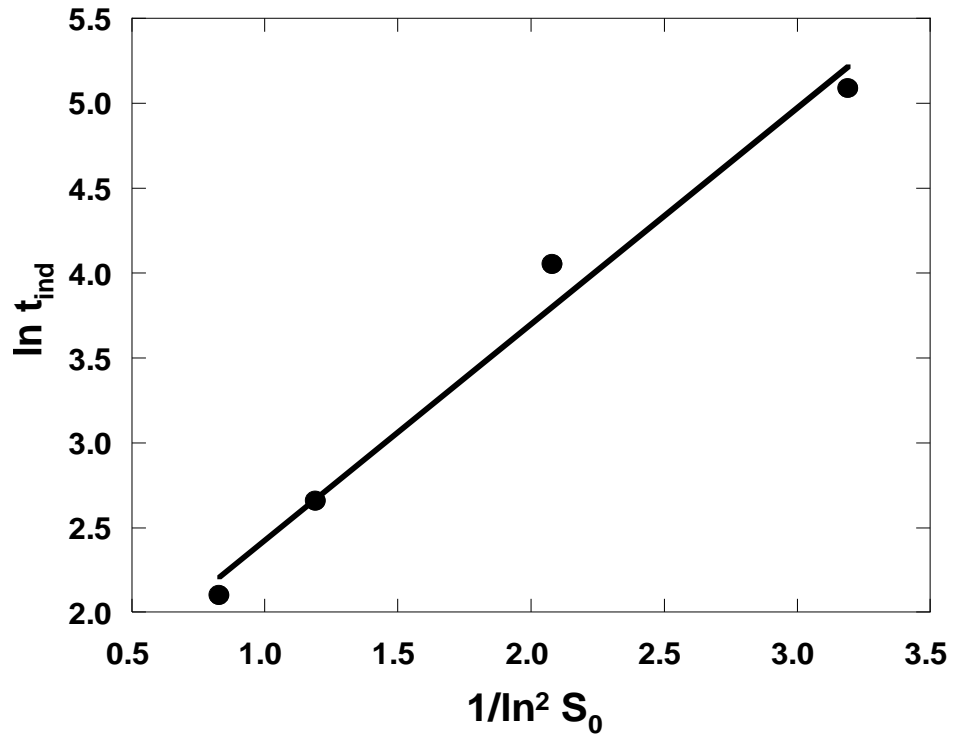
Figure 6.5: Logarithmic of induction time vs. logarithmic square of inverse initial supersaturation.
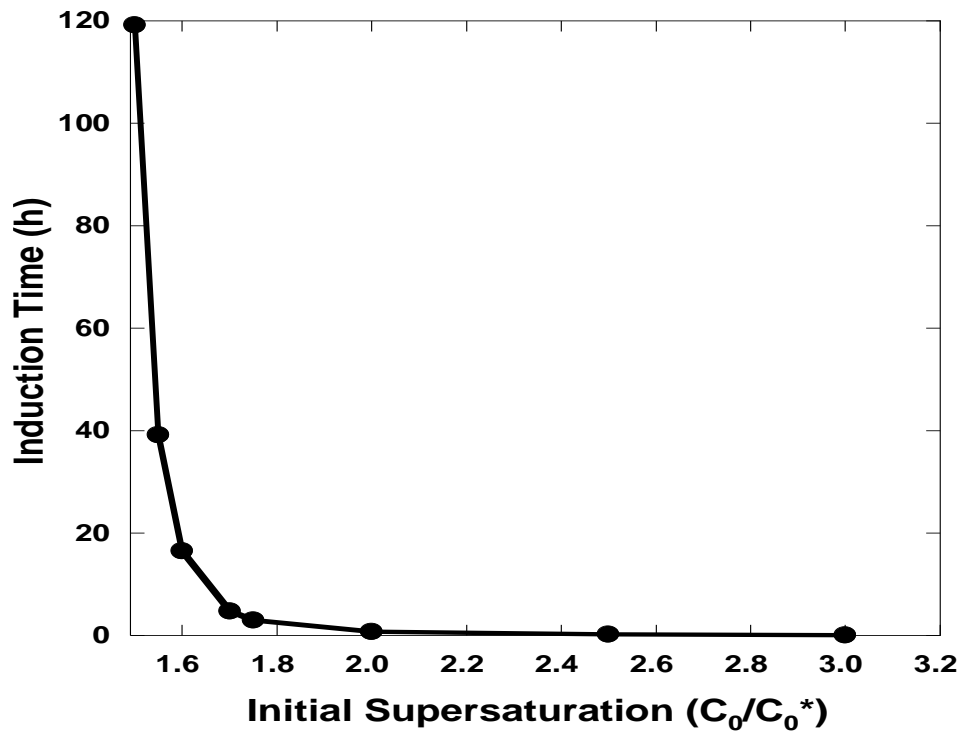
Figure 6.6: Induction time vs initial supersaturation.

6.3.4 Crystallization experiments

In the previous section induction time experiments were used to estimate the exponential

primary nucleation constant B_0. However, as can be seen in Equations 6.7 through 6.10 there are

still 6 parameters to be determined in order to have a full description of the batch crystallization

process. In order to determine these parameters, a set of experiments consisting of seeded and

unseeded crystallization runs were performed. In these experiments, multiple conditions such as

initial concentration, rate of change of pH, initial mass of seed crystals (wt. %=mass of seed

crystals/expected mass of product crystals), and initial supersaturation were changed from run to

run accordingly to Table 6.2. The idea of this is to train the model with multiple conditions such

that it can be used to predict system behavior under multiple crystallization protocols.

Table 6.2: Crystallization runs experimental conditions

Run	Seed (wt. %)	C_0	S_0	pH/h	pH_0	pH_F
a	0	15.94	0.98	1.0	7.47	5.97
b	0	17.93	0.47	3.1	7.85	6.41
c	0	18.09	0.54	6.0	7.84	6.45
d	1.8	11.30	1.07	1.5	7.09	6.25
e	3.0	11.36	1.18	1.4	7.01	6.34
f	15.0	14.00	1.64	0.6	7.06	6.51

Figure 6.7 shows concentration profiles of unseeded ampicillin crystallization

experiments at three different rates of pH change and initial concentrations. The data were

obtained by transforming signals from the polarimeter to concentration as described in Section

6.2.2. As seen in the figures, more rapid changes in pH led to steeper desupersaturation curves,

which is characteristic of a system undergoing extensive nucleation followed by rapid growth of

the resulting crystals. In such cases, the signal occassionally became unstable for a few minutes

since nucleation often occurred in the sampling loop. Nevertheless, the signal was stabilized

when crystals in the sampling loop were flushed back into the crystallizer.

(a)

(b)

(c)
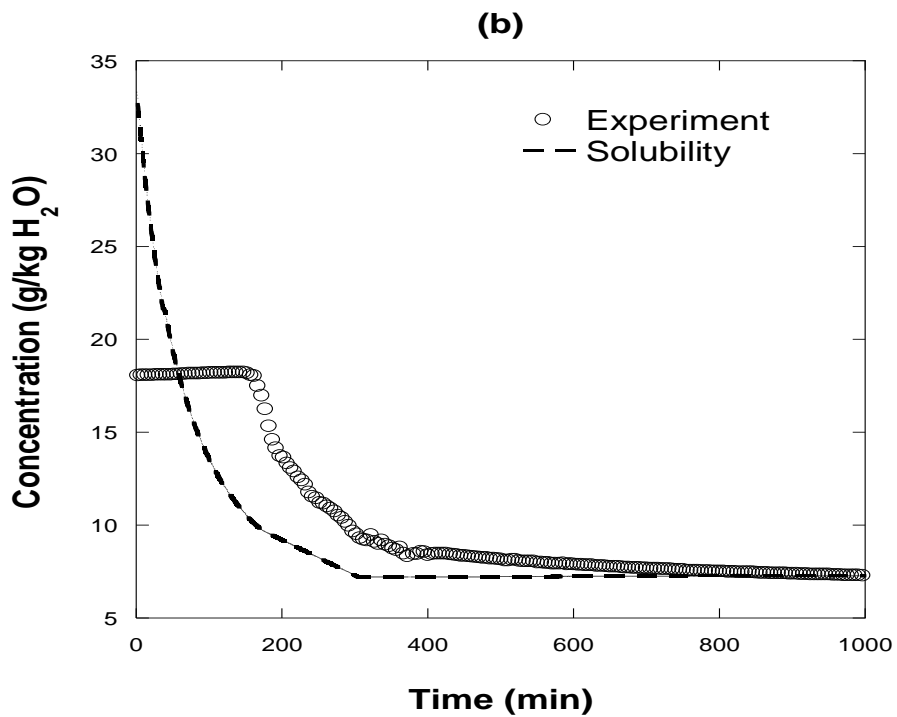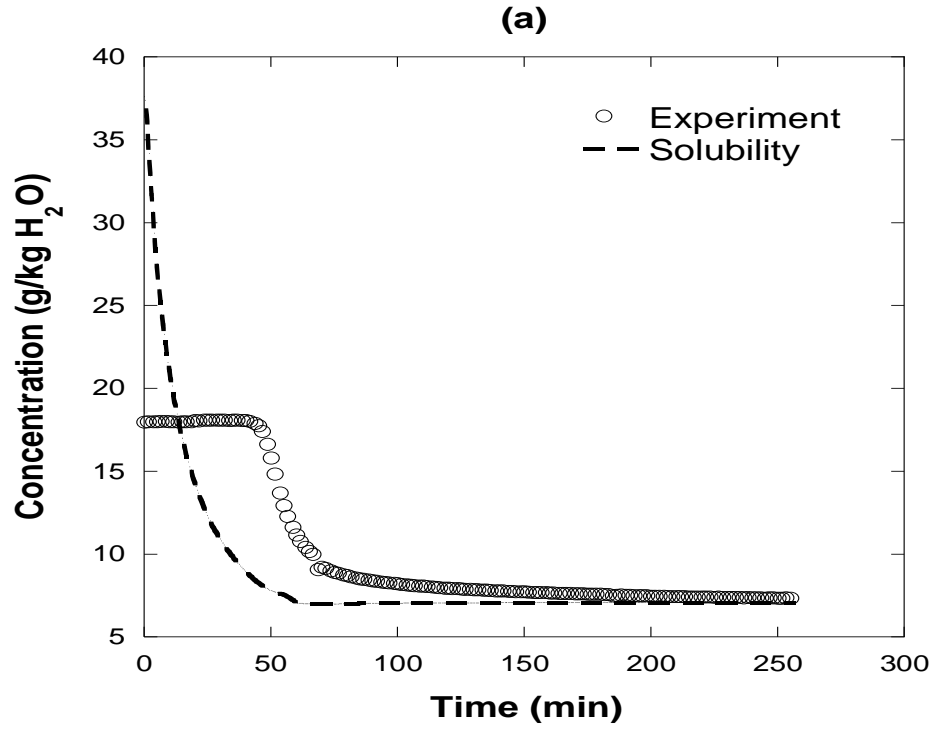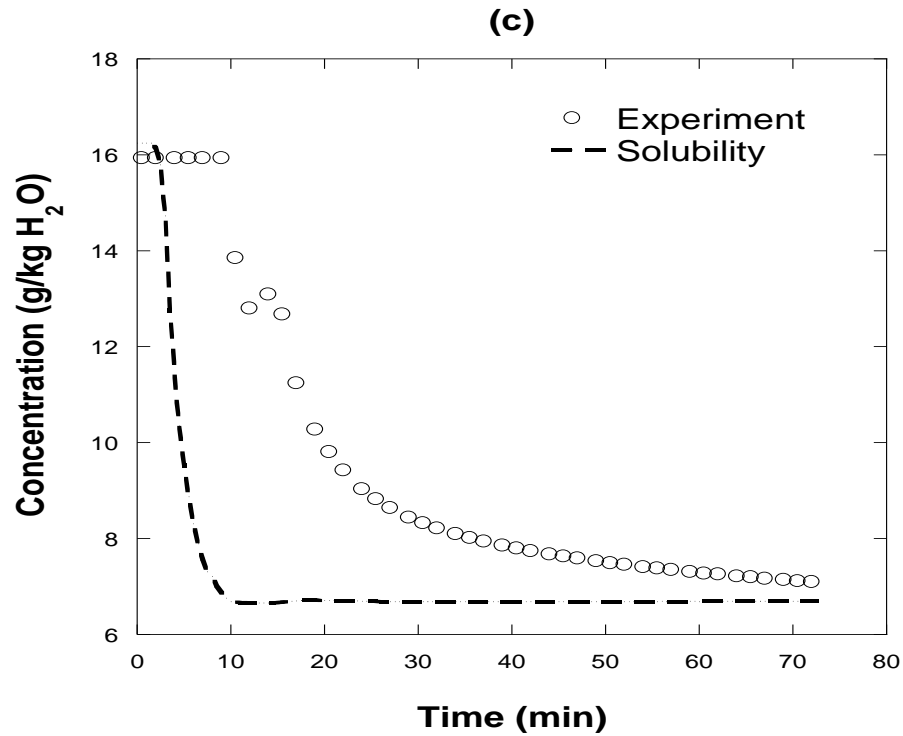
Figure 6.7: Unseeded crystallization for a rate of change of pH (a) 1.00 pH units/ h, (b) 3.10 pH units/h, and (c) 6.00 pH units/h.

The effect of the rate of change of pH on crystal size distribution was determined by measuring the chord length distribution (CLD) of these runs. Figure 6.8, shows the final CLD for the runs in Figure 6.7. Note there is only a slight deviation between the final CLDs, and only Run c looks significantly different from the other two. It was expected that this run would have a smaller mean size as it was subjected to steeper changes in supersaturation.
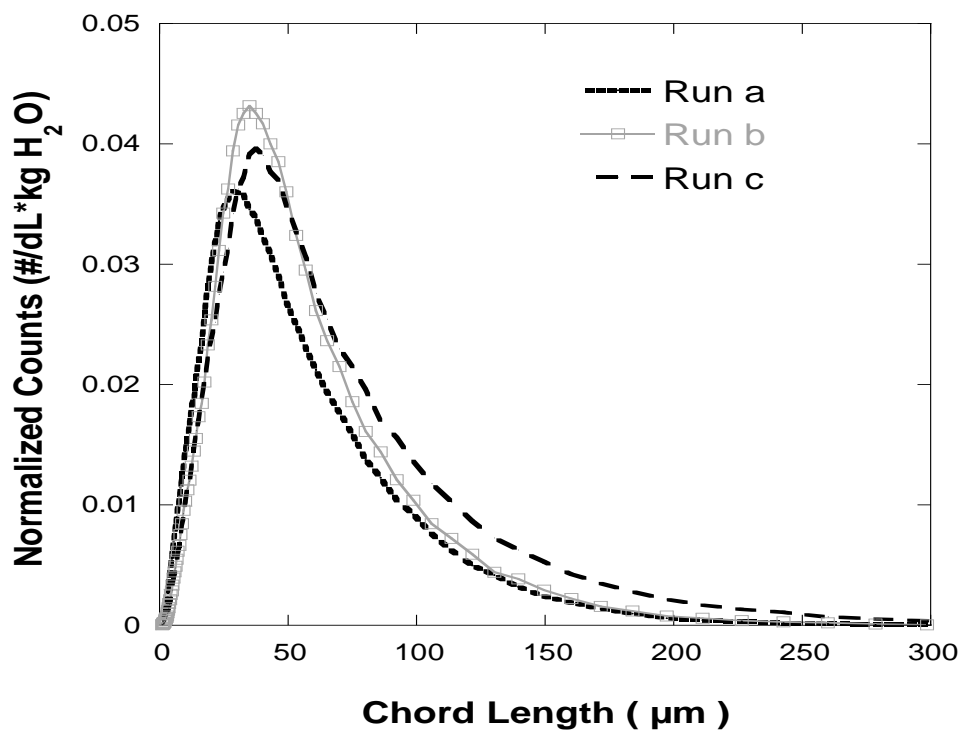
Figure 6.8: Final chord length distribution of each run.

As mentioned before, seeded and unseeded crystallization experiments were considered for the quantification of ampicillin crystallization kinetics. Hence, characterization of the seed crystals was necessary to define the initial conditions. Figure 6.9 shows crystal size distribution and chord length distribution of the seed crystals used in seeded crystallization experiments. The crystal size distribution was determined from sieve analysis, while chord length distributions were determined from FBRM data by adding seed crystals into a saturated solution and recording the resulting initial CLD. Additionally, Figure 6.10 was used to determine the area and volume shape factors of the seed crystals used. This ratio along with crystal size distribution was used to determine the properties of the seed crystals shown in Table 6.3. The mean crystal size was based on a mass arithmetic average as shown in Equation 6.24, where m_i is the mass on sieve i, L_i

is the sieve mid-size, and m_{Total} is the total mass. The average crystal density was obtained from

the literature (Ottens et al., 2001).

$$\bar{L}_{CSD} = \sum_{i=1}^{n} m_i L_i / m_{Total} \qquad (6.24)$$

(a)

(b)
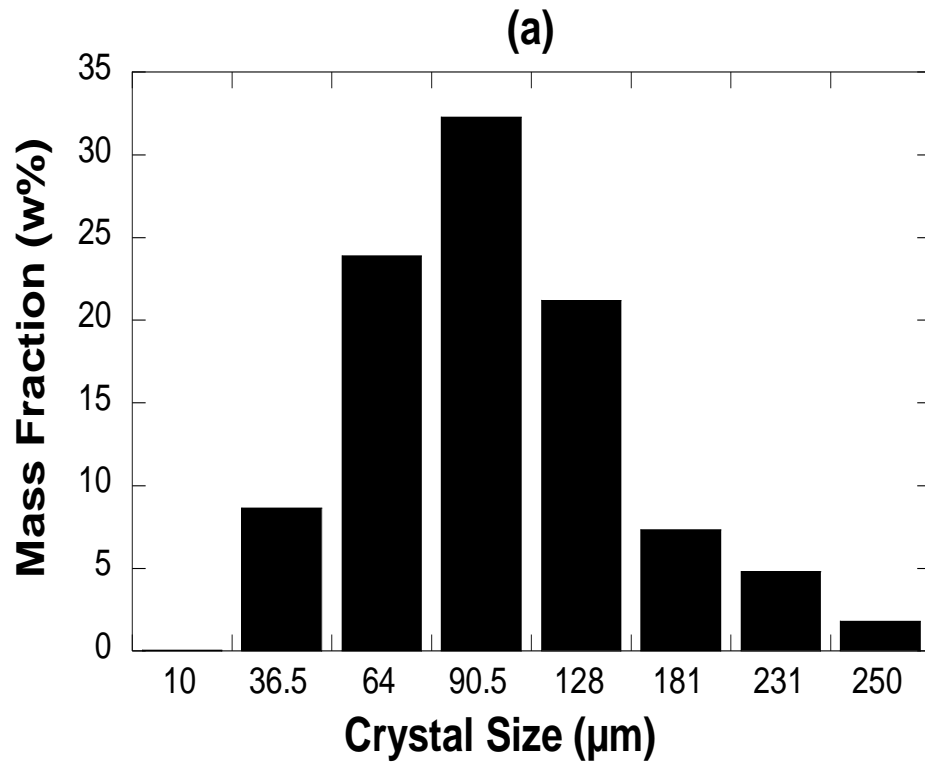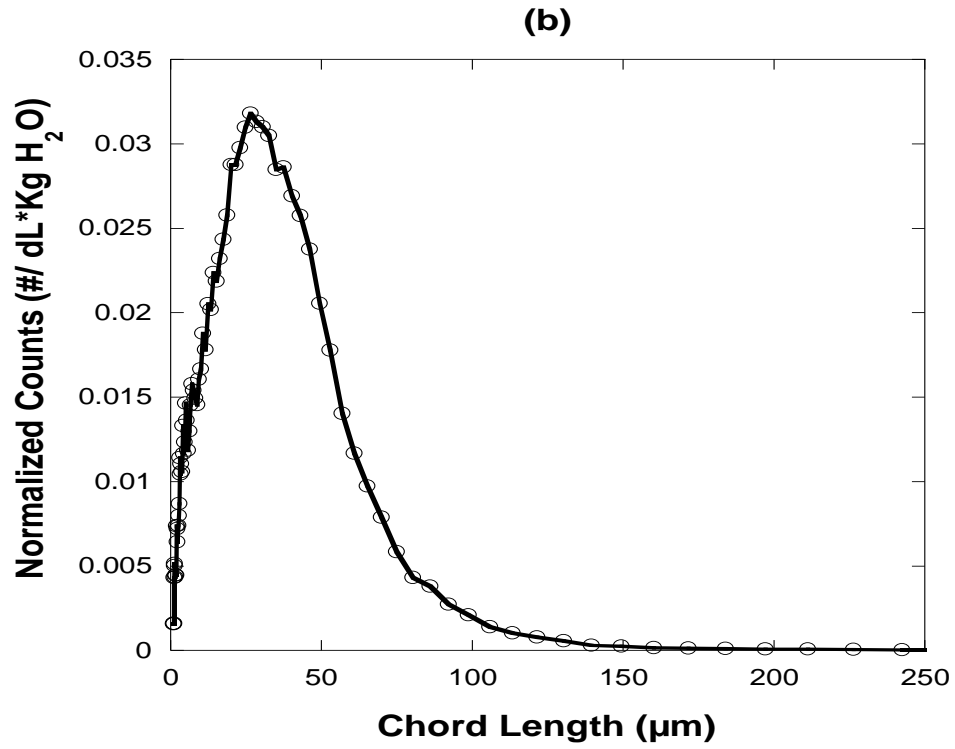
Figure 6.9: (a) Ampicillin sieved seed crystal size distribution and (b) seeds chord length distribution.
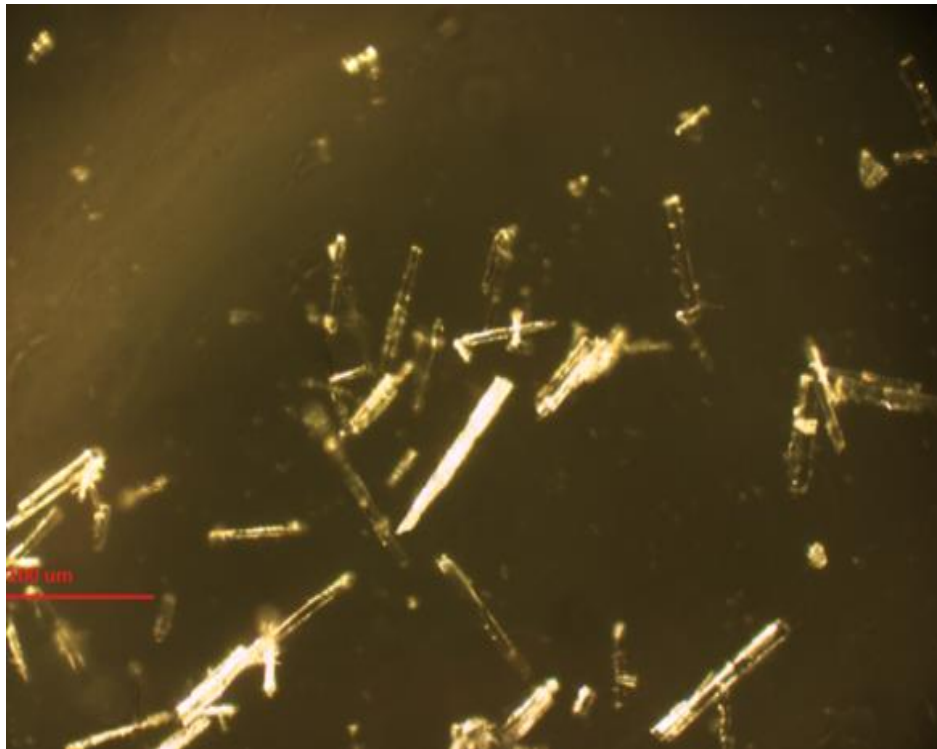
Figure 6.10: Light microscopy picture of ampicillin seeds.

Table 6.3: Properties of ampicillin seed crystals.

$\bar{L}_{seed}$ (μm)	ρ_c (kg/m³)	k_a	k_v
104	1500	0.09	0.03

Figure 6.11 shows concentration profiles for seeded crystallization experiments of ampicillin using different masses of seed crystals, initial concentrations, and rates of change of pH. The same plots show the solubility curves for each case, where the solubility of ampicillin was maintained below the concentration at any given time. Initial supersaturations were design such that the system supersaturation was within its metastable limit. The data in Figure 10(f) show that significant amounts of seed crystals were necessary to induce fast desupersaturations. This is in agreement with the crystallization parameters that will be presented later since the exponent of mass of crystals is relatively small. It is expected that this behavior would not only depend on the mass of seed crystals, but on their size distribution. Hence, keeping the total mass constant and using seed crystals with a smaller mean size would reduce the necessary mass needed to promote secondary nucleation as the total surface area increases. Details on how to approximate such a critical mass for different sizes can be found elsewhere (Doki et al., 2002; Tseng et al., 2014). Additionally, final CLDs of runs d and f are shown in Figure 6.12 (Run e was not included because high level of noise).

(d)

(e)

(f)
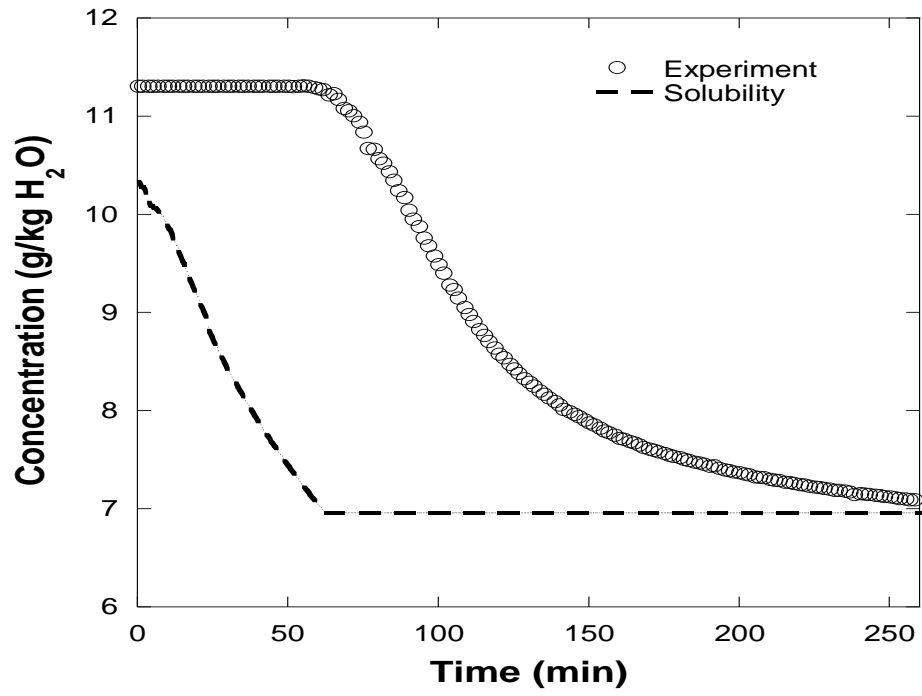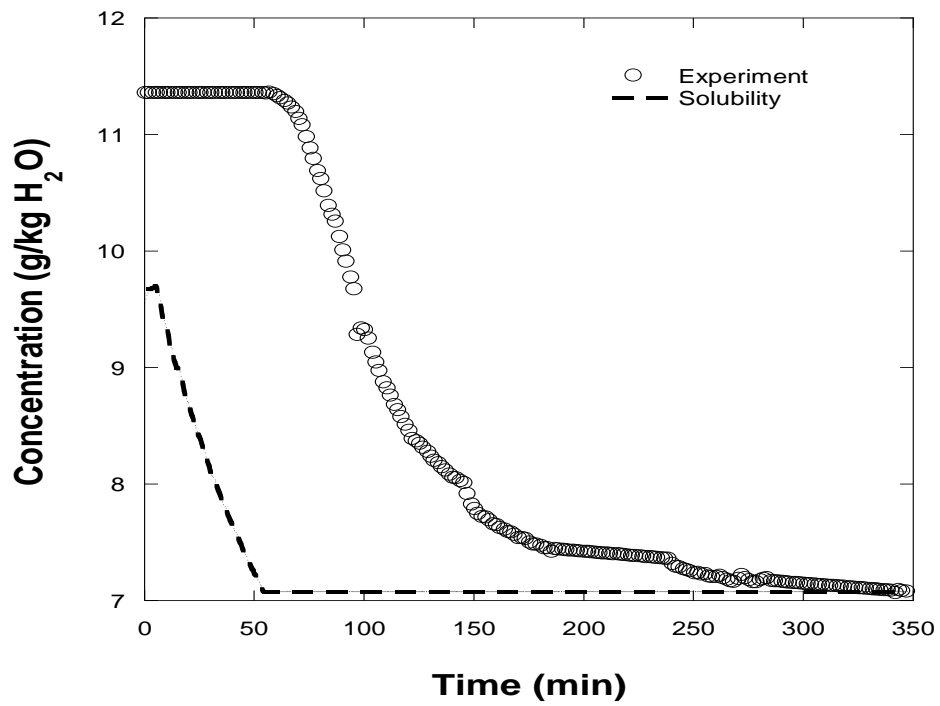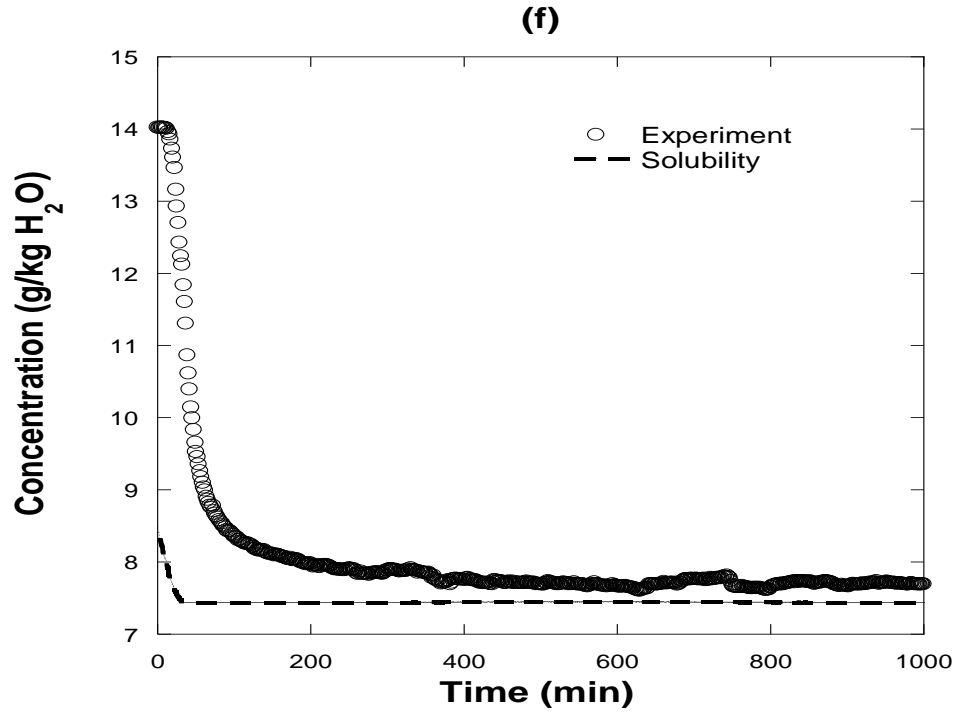
Figure 6.11: Crystallization of ampicillin using seed loads (d) 1.8 % wt., (e) 3.0% wt. and (f) 15.0 % wt. of final crystals mass.
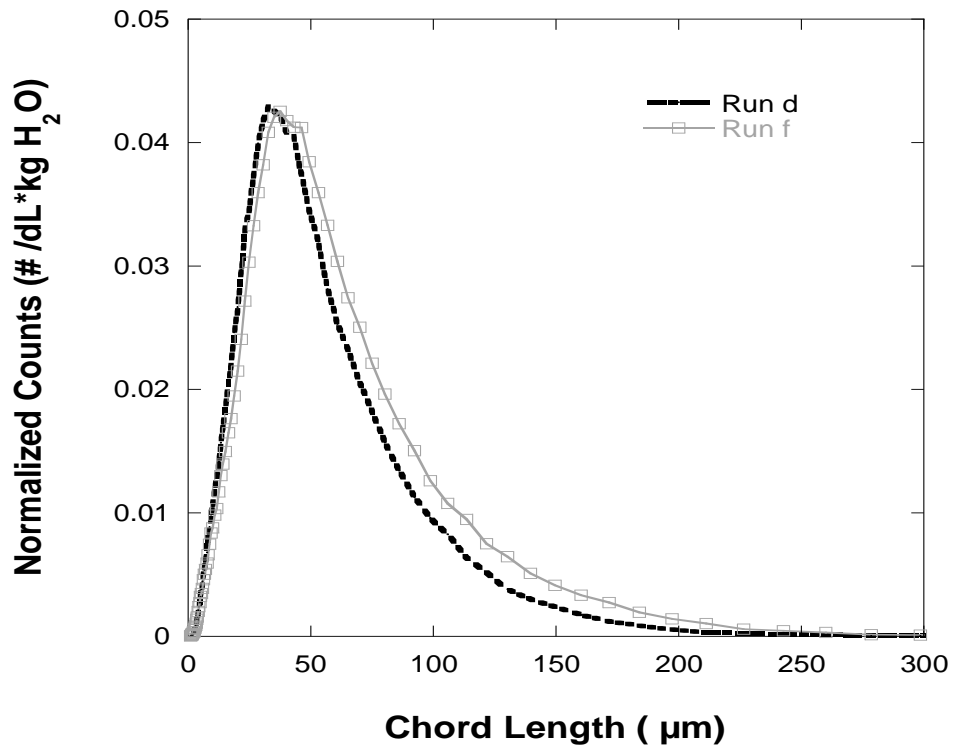
Figure 6.12: Final chord length distribution of seeded runs.

6.3.5 Crystallization Kinetics Parameter estimation

In the previous sections the data necessary to obtain crystallization kinetics was determined from seeded and unseeded crystallization experiments. In this section, Equations 6.4-6.11 will be used to fit the experimental data where primary nucleation, secondary nucleation, and crystal growth rate parameters will be determined. The exponential factor B_0 was the only parameter fixed prior to the parameter-estimation routines, as it was determined from the work described in Section 6.3.3. Equation 6.11 represents the rate of change of the concentration of ampicillin in solution, which was related to the moments using a mass balance. This mass-based moment was compared to the experimental concentration, and their difference was minimized in the parameter estimation routine. Initial conditions were based on initial concentration and the mass of seed crystals and their average length and aspect ratio.

Estimation of parameters in the kinetic expressions was performed using the following objective function:

$$\min_{p} E = \sum_{j=1}^{N\exp} \sum_{i=1}^{Nx} ([Amp]_{i(t,p)} - [Amp]_{i(t)}^{\exp})^2 \tag{6.25}$$

where $[Amp]_{i(t,p)}$ represents the modeled concentration at some set of parameters $p = [k_{B1}\ k_{B2}\ b\ s\ k_g\ g]$, $[Amp]_{i(t)}^{\exp}$ represents the set of concentrations determined experimentally, N_x is the number of data points, and $N_{\exp}$ the number of experiments ($N_{\exp} = 6$) . Usually, estimation of crystallization kinetic parameters leads to multiple solutions (combinations of parameters) that provide good equally good fits of the experimental data. Therefore, to minimize the probability of being trapped in a local minima two consecutive minimizations of Equation 6.25 were performed. First, a stochastic minimization (*MATLAB simulannealbnd*) was used to identify the best set of parameters among a wide range. This minimization is specially a good idea when there is not a good idea about the initial guess. Then, parameters estimated from the stochastic

minimization were used as the starting point of a deterministic minimization (*MATLAB fminsearch*) which refines the parameters and further reduce the error. The utilization of a large data set, where multiple operational conditions were included allowed us to obtain a single set of parameters that have predictability capabilities over a wide range of conditions. Even though the fitting of a single experiment is more accurate for that specific experiment, its parameters could not provide a good fitting when the conditions were changed. The results of the multi-experimental approach are shown in Figure 6.13, and as it can be seen the model is capable of fitting all the conditions tested.

In order to address the robustness of the parameters, confidence intervals were evaluated using a parameter perturbation method as reported by Nagy et al.(Nagy, 2008) and Rawlings et al. (Miller et al., 1994). Additional information on the effect of parameter uncertainty and how to minimize its effect was reported by Ma et al.(Ma et al., 1999) and Nagy et al. (Nagy et al., 2004). In this case, let S_p represent a measurements matrix that contains the sensitivities matrixes ($S_p^{y_i}$), P the precision matrix, and V the covariance matrix.

$$S_p = [S_p^1 ... S_p^{N\exp}]^T \tag{6.26}$$

$$S_p^{y_i} = \frac{dy_i}{dp} \tag{6.27}$$

$$P = (S_p^T S_p)^{-1} \tag{6.28}$$

$$V = s_R^2 P \tag{6.29}$$

Using the previous equation confidence intervals can be calculated; in this case, a *t*-test evaluation for a 95% confidence was used to estimate the intervals.

$$p = p* \pm t_\alpha \sqrt{diag(V)} \tag{6.30}$$

Table 6.4 shows the results of the parameter estimation routing along the respective absolute values of the confidence intervals for one experiment, unseeded experiments, and for all the

experiments. As it can be seen in the table when a single experiment is used for the calculation of confidence intervals, the respective intervals are very broad. In some cases even bigger than the actual parameter, which would not have any physical meaning (i.e. negative nucleation rates). In contrast, as the number of experiments is increased, the confidence interval gets so narrow that it appears that the calculated set is very close to the true set. It is obvious that this analysis does not provide any proof that the obtained set is a global minima. However, it certainly demonstrates that the multi-experimental parameter estimation routine provides superior estimates than these of single experiment routines. In other words, the greater the number of experiments, the less of possible solutions that can reduce the error. In this case, 6 experiments were sufficient to constraint the number of possible solutions of the parameter estimation problem.
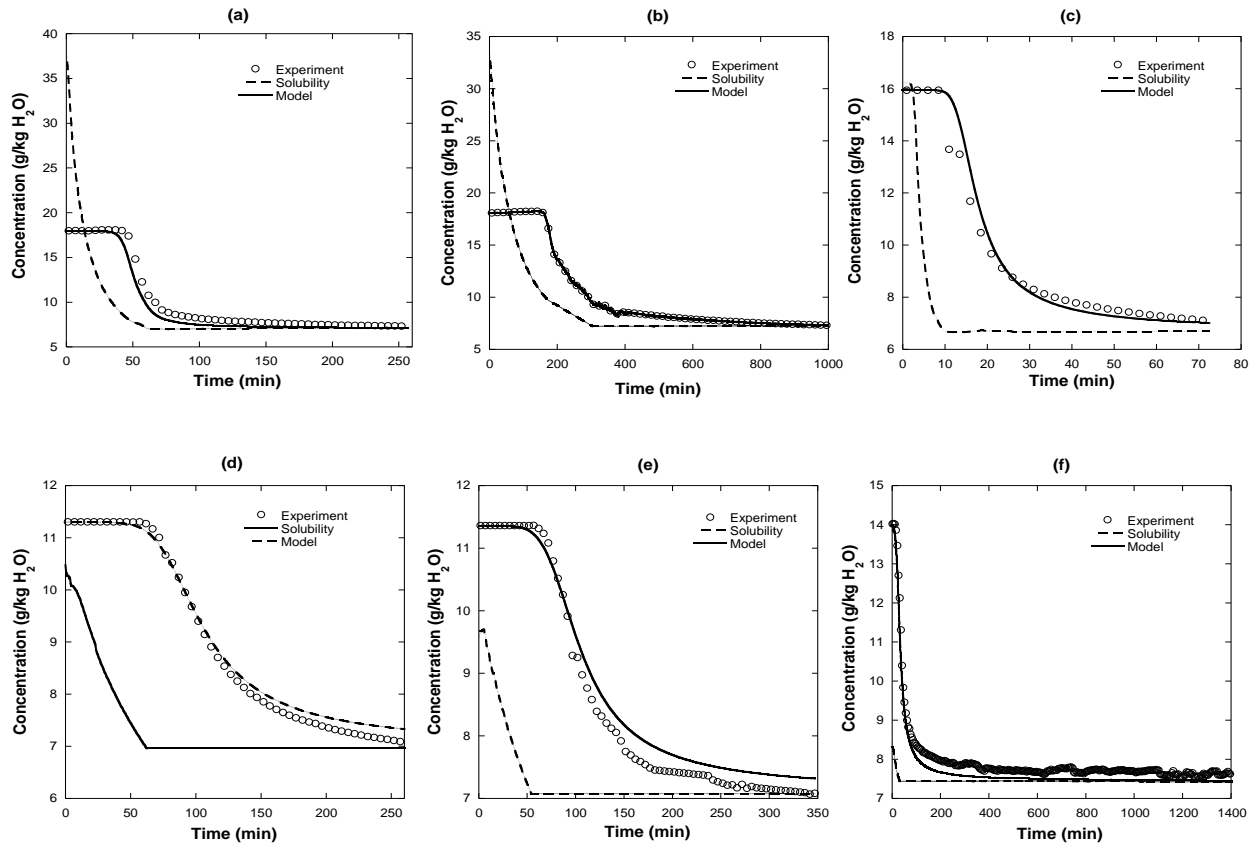
Figure 6.13: Fitting of seeded and unseeded crystallization experiments.

Table 6.4: Parameters obtained from multi-experimental parameter fitting routine.

	k_{B1} m($\#$/(g/kg) min)	B_0	k_{B2} ($\#$/(g/kg) min)	b	s	k_G (m/min)	g
θ	5.24×10^{10}	1.27	6.63×10^8	0.34	1.37	1.07×10^{-5}	1.87
$\pm$ (Run d)	6.38×10^{10}	-	2.24×10^{10}	1.23	77.66	4.51×10^{-6}	0.38
$\pm$ (Runs d-f)	2.43×10^{10}	-	2.10×10^8	0.03	0.11	1.75×10^{-6}	0.08
$\pm$(All runs)	2.77×10^9	-	3.06×10^7	0.0	0.04	1.93×10^{-7}	0.02

6.3.7 Approximations on crystal mean siz

The utility of the kinetic parameters was tested by assessing predictions of crystal size distribution. First, we recognize that the crystallization kinetic expressions were obtained from concentration data; therefore, the model should predict the desupersaturation behavior but not necessarily the corresponding crystal size distribution. To see if the model has any capabilities of predicting CSD, the final number-based chord length average was calculated.

$$\bar{L}_{CLD} = \sum_{i=1}^{n} n_i L_i / n_{Total} \qquad (6.31)$$

It is expected that this mean size will be significantly lower than the mean size of the CSD. This is because it is very improbable that the laser will cross all the crystals through their characteristic length. Instead, just the fraction of crystal that is aligned with the laser beam will be identified as the length of the crystal. In order to factor this in, we compared the mean size of the CSD of the seed crystals with the mean size of their CLD. A ratio these means was calculated and called k (i.e. $k = \bar{L}_{CSD} / \bar{L}_{CLD}$). This constant was used to transform the mean of the CLD into a CSD mean as shown in Equation 6.32. Finally, to assess the validity of the model, the moments at the end of each run were used to estimate the mean crystal size by using Equation 6.33.

$$\bar{L}_{CSD} = k\bar{L}_{CLD} \tag{6.32}$$

$$\bar{L}_{Model} = \mu_{1,end} / \mu_{0,end} \tag{6.33}$$

The second column in Table 6.5 shows the mean size of the final CSD for each run obtained by using Equation 6.32, while the third and fourth columns show the mean size obtained from the moments of the distribution (Equation 6.33). The third column represents the estimated mean using the parameters obtained from a multi-experimental, while the fourth column represents the estimated mean when only Run f was used in the parameter estimation routine. Note that when the parameters obtained using all the experiments were used, the modeled mean size is relatively close to the experimental one. In contrast, when a single experiment is used, the mean size greatly deviates from the estimated experimental values. Therefore, we can conclude that by employing such a multi-experimental parameter estimation routine we can obtain a set of parameters from concentration data that provide relatively good estimates on the average size of crystals. This observation can be quantified by determining the error between experimental and modeled means, obtaining an error of 6% for the multi-experimental approach vs. 38% for the single-experiment approach. This methodology can be useful as in many cases transformation from CLD to CSD can be time consuming. This is especially true when crystals have very small aspect ratios as in the case of needles, where CLD data is best used as a qualitative indicator of the direction of the process (Leyssens et al., 2011). In a more robust approach the characteristic chord length at each crystal size is obtained and the relation is used to estimate crystal size distributions throughout the process (Li et al., 2014).

Table 6.5: Final mean crystals size obtained from modelling and fitting of CLDs.

Run	Experiment (μm)	Model $_{All}$ (μm)	Model $_{Run\,f}$ (μm)
a	99	103	63
b	103	102	56
c	113	113	38
d	115	123	51
f	90	112	87

6.4 Conclusions

In this work crystallization kinetics of ampicillin were determined from a large set of data obtained from an online monitoring system. This system allows us to follow the system concentration and chord length distribution. The data from all the experiments were combined and, using stochastic and deterministic minimizations, crystallization kinetics were determined. Since the data span multiple rates of pH change, supersaturations, and amounts of seed crystals, the parameters should be more useful than parameters obtained at a fixed condition. This was demonstrated by doing a confidence interval analysis for different numbers of experiments, which showed that the confidence interval gets narrower as the number of experiments is increased. Such an analysis provides information about the minimum number of experiments required to obtain a robust set of parameters. Additionally, the utilization of a wide range of conditions allowed us to obtain parameters that not only predict concentration profiles, but also provide good estimates on the average size of the particles.

CHAPTER 7

Reactive crystallization of β-lactam antibiotics: Strategies to enhance productivity and purity of ampicillin

7.1 Introduction

β-lactam antibiotics are among the top in the list of most used pharmaceutical compounds worldwide. In fact, antibiotics span 5% of the global pharmaceutical market with sales greater than $42 billion in the United States(Hamad, 2010). These compounds have been of great utility during the past decades because of their effectiveness in treating bacterial infections. For this reason β-lactams are listed by the World Health Organization (WHO) as an essential medicine in any country. Conventional production of β-lactam antibiotics includes several chemical processes in which sub-zero temperatures, organochloride solvents, protection and deptrotection groups, and additional raw materials are required during the process (Ospina et al., 1996). As many pharmaceutical processes, these processes have a high E-factor (35 kg of raw material/kg of product).

An alternative route for the manufacture of β-lactam antibiotics is the enzymatic synthesis by penincillin G acylase (PGA). This enzyme can catalyze the acyl transfer from an activated side chain donor to the nucleophilic β-lactam forming the desired antibiotic. As for example, enzymatic synthesis of ampicillin can be achieved by reacting 6-aminopenicillanic (6-APA) acid with D-phenylglycine methyl ester (D-PGME) in the presence of PGA. Similarly, other β-lactam products can be synthesized by simply changing the initial reactants.

The overall reaction scheme is presented in Figure 7.1. As can be seen, PGA catalyzes the synthesis of ampicillin and, unfortunately, it also catalyzes the hydrolysis of D-PGME to D-phenylglycine and the hydrolysis of ampicillin to D-phenylglycine and 6-APA. In fact, 6-APA production can be achieved through hydrolysis of penicillin G by PGA (Abian et al., 2003).
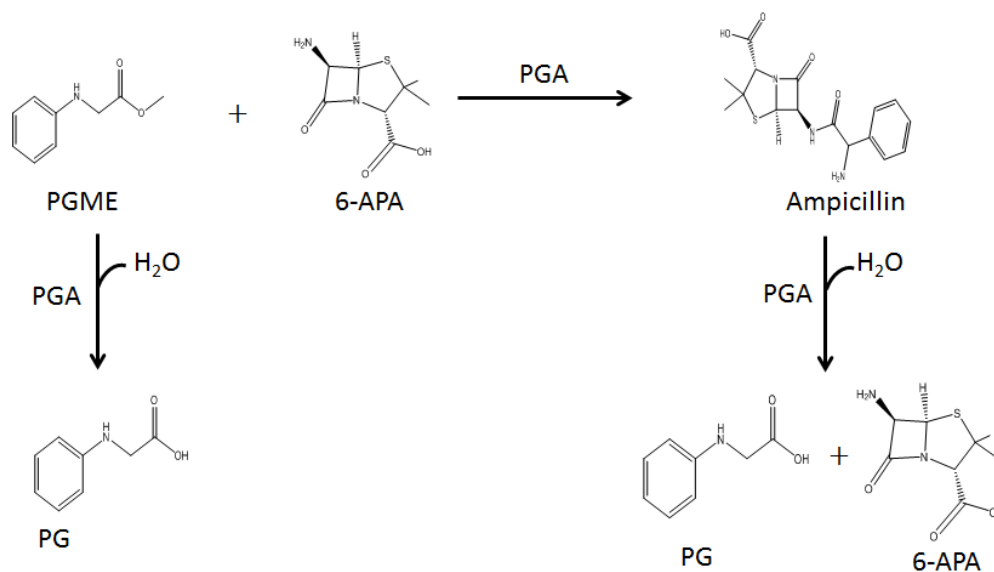
Figure 7.1: Enzymatic synthesis of ampicillin by PGA.

The synthesis of ampicillin illustrated in Figure 7.1is kinetically controlled, meaning the ampicillin is an intermediate within the reaction network. Multiple reaction-engineering strategies have been used to improve the conversion of 6-APA to ampicillin. These strategies can be classified into thermodynamically controlled reactions or kinetically controlled reactions. The first relies on optimization of the reaction medium to shift the microscopic reversibility of the enzymatic reaction towards the synthesis reaction. Based on the fact that the undesired reaction is an hydrolysis reaction, organic co-solvents have been used to shift equilibrium towards synthesis (Abian et al., 2003; Illanes et al., 2002; Kim et al., 1996). This approach was

demonstrated to improve the equilibrium constants but the kinetics of reaction can be drastically reduced.

Reaction optimization is possible by acquiring information about the three main reactions: (1) synthesis, (2) primary hydrolysis, and (3) secondary hydrolysis. Significant work has been done in this area, including building kinetic models, optimization of pH and temperature of the reaction, heterogeneous reactions, and complex reactor design (Ferreira, 2007; Youshko, Chilov, et al., 2002; Youshko & Svedas, 2000; Youshko, van Langen, et al., 2002). Among these, reaction with product precipitation seems like a promising alternative due the advantage of obtaining high concentrations of product and recovering it in the solid phase. Several authors have reported the possibility of precipitating ampicillin while is being produced in solution (Ferreira, 2007; Youshko, van Langen, et al., 2000). However, as far as we know, ampicillin precipitation was accompanied by precipitation of D-phenylglycine. This has some potential downstream disadvantages, as it will be necessary to design a strategy for separation of the two crystallized species. Unfortunately, as far as we known there is only a single publication that discusses the separation of ampicillin from D-phenylglycine (Hoeben et al., 2009).

In the present work we have developed a reaction-crystallization protocol in which ampicillin is the only product crystallized. In order to achieve this goal, we have used information about solution thermodynamics, and reaction and crystallization kinetics. The experimental results indicated that the best protocol to ensure high product recovery and purity is a reactive seeded crystallization. In the following sections we demonstrate the process by showing reaction data, and the effect on the concentration profile of adding seed crystals to the system.

7.2 Materials and Methods

7.2.1   Chemicals

D-Phenylglycine methyl ester (PGME) was purchased from Sigma Aldrich USA (St. Louis, MO), 6-aminopenicillaninc acid (6-APA), phenylglycine (PG) and ampicillin (Amp) were purchased from VWR USA (Radnor, PA). Penicillin G acylase from *E. Coli* was kindly donated by DSM-Sinochem (The Netherlands). The enzymatic solution had a concentration of 17 mg/mL of protein its purity was verified using a SDS-PAGE gel showing no indication of other proteins. All the chemicals and enzyme were used without further purification.

7.2.2 Enzymatic Reaction

The enzymatic synthesis of ampicillin was performed in 10-mL test tubes with a working volume of 5 mL. The temperature was maintained at 25 °C using a water-bath shaker operated at 150 rpm. The reactants were added to the 10-mL test tubes and dissolved using deionized water and adjusted to the desired pH using 5N ammonia. Reactions were started by addition of 50 µL of the enzymatic solution. Samples were withdrawn as a function of time to construct concentration profiles by removing 50 µL aliquots from solution. If product precipitation was evident approximately 0.5 mL of the slurry were filtered and the clean solution was used to obtain the used to obtain the 50 µL aliquots.

7.2.3 Scale-up and particle tracking

Reaction crystallization experiments were scaled up from 5 mL to 250 mL using the 1-L OptiMax Synthesis Station from Mettler Toledo (Columbus, OH) shown in Figure 7.2. Reaction mixtures were prepared by dissolving the desired amount of 6-APA and D-PGME and adjusting the pH using 5N ammonia. Solution temperature was maintained at 25 °C and a stirrer speed of 300 rpm. Samples were withdrawn using a syringe. Whenever two phases were present, the

solution was withdrawn with a syringe and a 0.45-µm filter was used to remove particles from the solution. Chord length distribution of crystals was monitored using a Focus Beam Reflectance Measurement (FBRM) apparatus from Mettler Toledo. Further details on this probe can be found elsewhere (Shi et al., 2003).

Figure 7.2: 250 mL reactive crystallization set up.

7.2.4Analytical Methods

Solution concentration was analyzed using a Shimazdu (Kyoto, Japan) high-pressure liquid chromatography (HPLC) system. Aliquots of 50 µL where withdrawn using a micropipette and diluted in 1mL of HPLC solution with 1 vol%2M HCl to quench the reaction. If particles were present in solution, approximately 0.5 mL of slurry was withdrawn with a syringe and filtered prior taking the 50 µL aliquot. HPLC solution consisted of an aqueous solution of 0.68g/L KH_2PO_4, 0.68g/L SDS at a pH of 3.0 and acetonitrile (70 vol% aqueous/30 vol% organic). A C18 Kinetix column from Phenomenex (Torrance, CA) was used.

Calibration curves were obtained at a pH of 6.00 and 7.00 to ensure that the absorbance of the components was independent of pH value. It was noticed that some peaks split when the

pH of solution was changed as charged species had a different retention time than zwitterions. However, charged and neutral species exhibit the same UV absorbance as a function of concentration.

7.3 Results and Discussion

7.3.1 Solubility

Since the goal of this work is to design a reactive crystallization scheme that facilitates recovery of high-purity ampicillin, it is necessary to obtain information about the solubility of all components in the system. Figure 7.3 shows the solubilities of ampicillin, D-phenylglycine, and 6-APA as a function of pH (Santana et al., 2010). Data on D-PGME was not considered as its solubility is significantly higher than that of other components in the system. As shown in the figure the solubilities of ampicillin and D-phenylglycine are significantly lower than that of 6-APA. These results indicate the feasibility of designing a reactive crystallization scheme since the concentration of ampicillin reaches its solubility with only partial conversion of 6-APA. Additionally, we see that the solubility of ampicillin and 6-APA exhibit a strong dependence on pH in contrast to D-phenylglycine. This behavior can be attributed to the difference in the pKa of each molecule (Franco et al., 2013; Pessoa et al., 2008). Ampicillin and 6-APA have smaller pKa values, meaning that their fractions of negatively charged species will be higher, and, typically, charged molecules exhibit a higher solubility in water than their zwitterion counterparts.
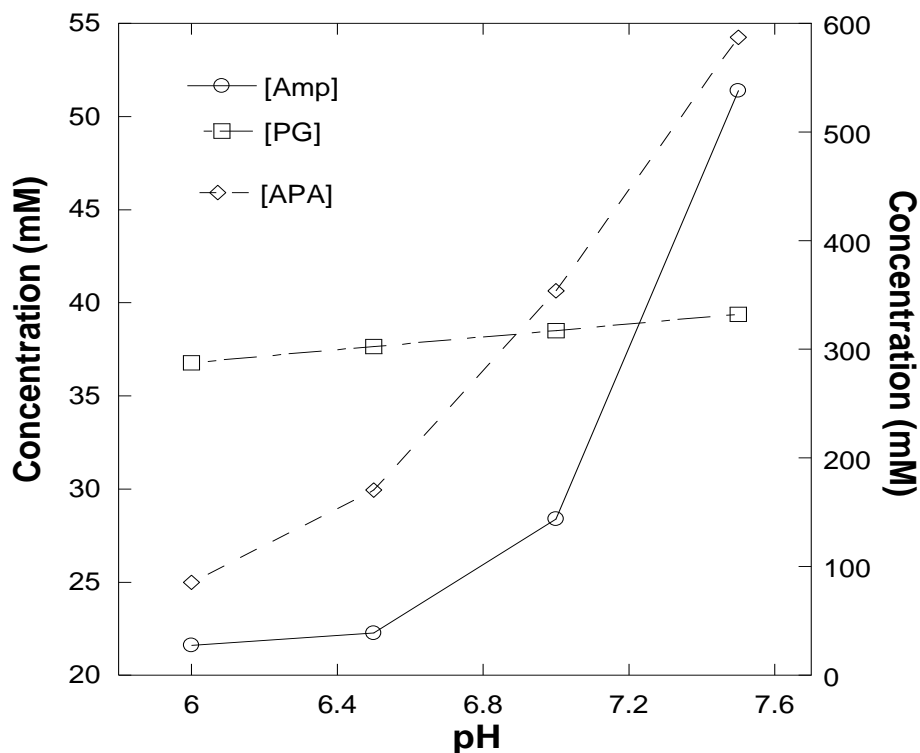
Figure 7.3: Solubility of ampicillin, D-phenylglycine, and 6-APA (right axis) as a function of pH at 298 K. Data from Santana et al. 2010.

7.3.2 Reaction at highly concentrated conditions

In the previous section the solubility of ampicillin, D-phenylglycine, and 6-APA was presented. According to these data, the solubility of ampicillin should be easily reached during its synthesis when using relatively high concentrations of substrate. Hence, we tested reactions at conditions in which ampicillin crystallization should be possible ($[6\text{-APA}]_0 = 200mM$); at these conditions, only ~15% conversion is necessary to reach the solubility of ampicillin. Figure 7.4 shows the concentration of ampicillin as a function of time at multiple initial concentrations of D-PGME. The data show that the rate of synthesis was enhanced when the concentration of D-PGME was increased. However, Figure 7.5 shows that such conditions also enhanced the rate of production of D-phenylglycine, which decreased the selectivity of the reaction.
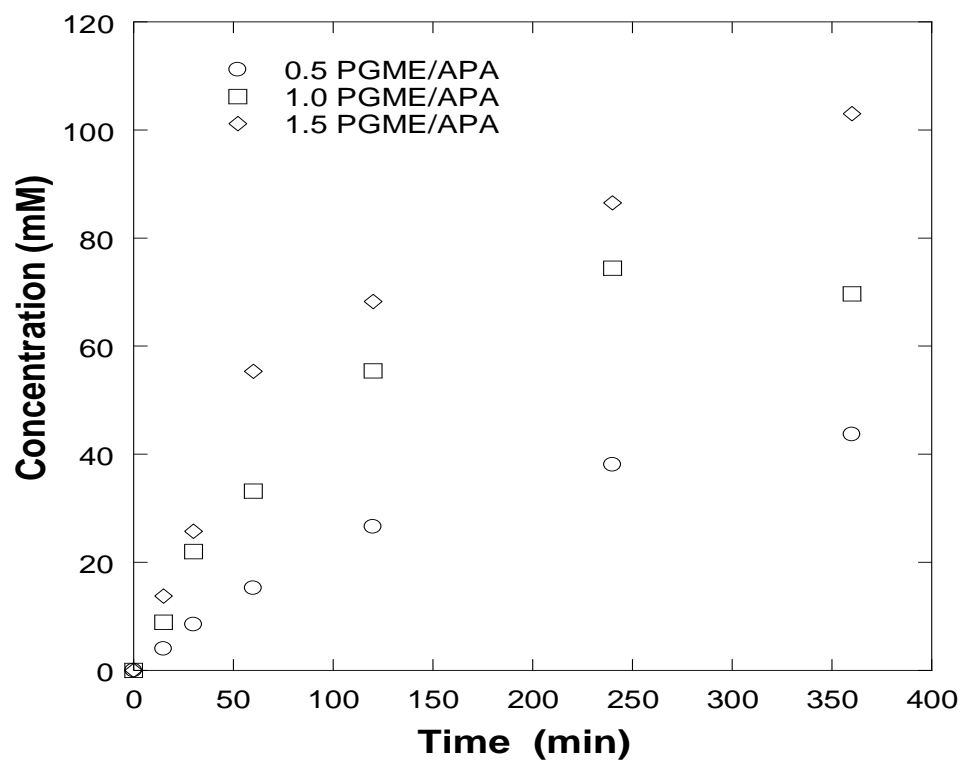
Figure 7.4: Synthesis of ampicillin at 25°C and pH of 7. Initial concentration of 0.20 M 6-APA and 0.10-0.30 M D-PGME.
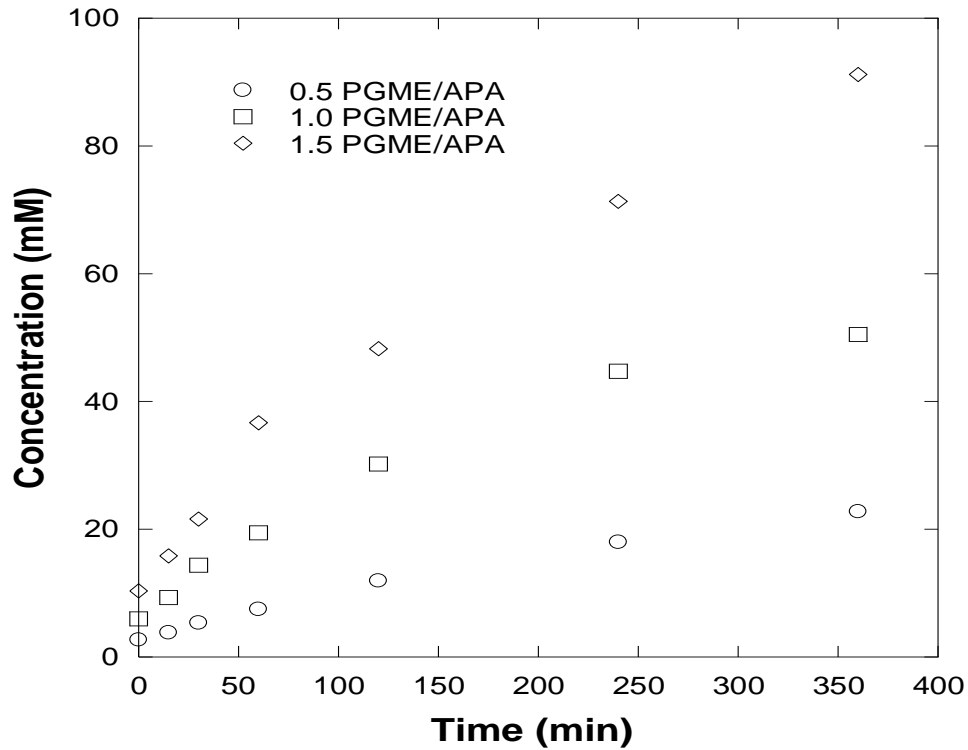
Figure 7.5: Accumulation of D-phenylglycine at 25°C and pH of 7. Initial concentration of 0.2 M 6-APA and D-PGME 100-300.

Yousho et al. (2002) developed a model that predicts reaction kinetics for this complex reaction (Youshko, Chilov, et al., 2002). The results of this model are show in Equation 7.1, which indicates that an increase in D-PGME concentration will decrease the selectivity of the reaction because a significant amount of substrate is lost through primary hydrolysis.

$$\frac{d[\text{Amp}]}{d[PG]} = \frac{\beta_o[APA][PGME] - \alpha[\text{Amp}](1 + \beta_o\gamma[APA])}{(1 + \beta_o\gamma[APA])([PGME] + \alpha[\text{Amp}])} \tag{7.1}$$

As observed in Figure 7.4, the concentration of ampicillin did not decrease at any point throughout the runs. This indicates that no crystallization occurred during the process even though very high supersaturations were reached, even though the maximum supersaturation ($S =$ [Amp]/[Amp*]) in the reactions was in the range of 2 to 5.

Since no product crystallization was occurred in any of the previous examples, the initial concentration of 6-APA was raised to 0.50 M and D-PGME to 0.75 M. Concentration profiles of ampicillin and D-phenylglycine for such reaction are shown in Figures 7.6 and 7.7, which show the concentration of ampicillin reached 0.30 M before showing a slight decrease in its concentration. On the other hand, D-phenylglycine concentration started to decrease after 100 mM. Crystals were observed in the system after 100 minutes, meaning that D-phenylglycine precipitation was taking place. Analysis of the solid phase indicated a purity of only 4.85 wt% ampicillin. Hence, we attribute a significant portion of the decay in ampicillin concentration to secondary hydrolysis because high concentrations of ampicillin favor that reaction. In the next section, we will discuss why ampicillin crystallization was not possible at considerable levels of supersaturation.
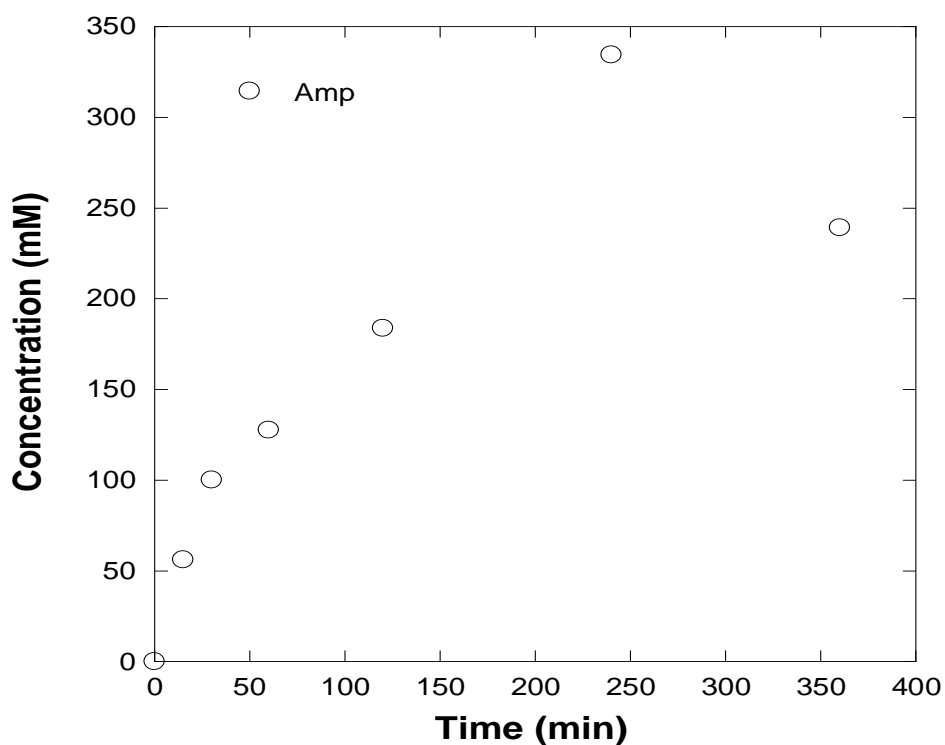
Figure 7.6: Ampicillin concentration profile of reaction starting with 0.50 M 6-APA and 0.75 M D-PGME.
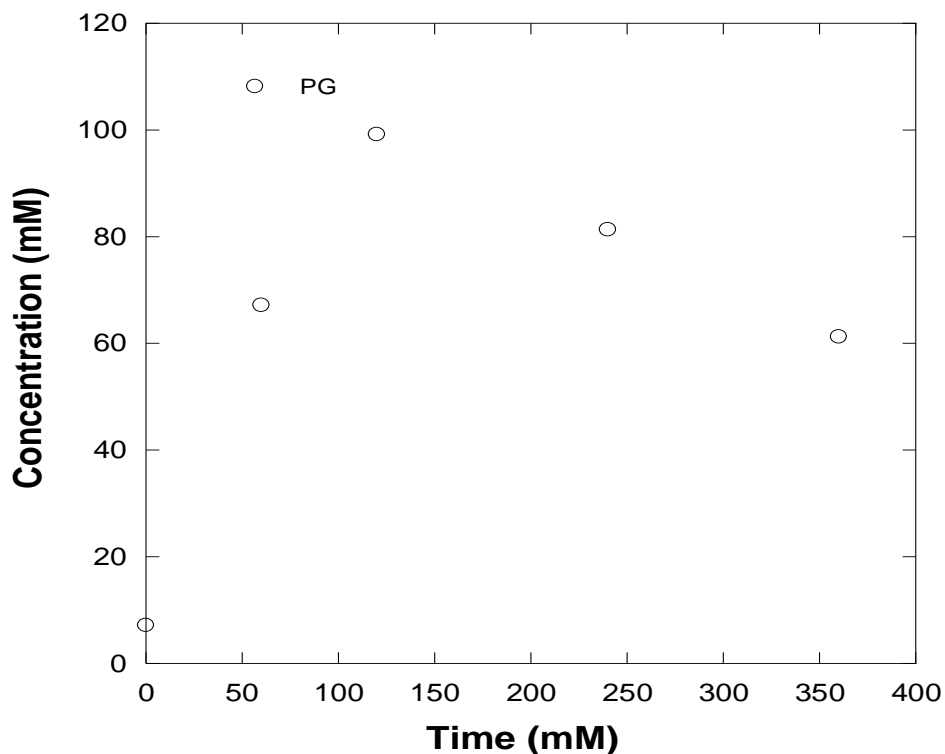
Figure 7.7: D-phenylglycine concentration profile of reaction starting with 0.50 M 6-APA and 0.75M D-PGM.

7.3.3 Ampicillin nucleation and crystallization

When a homogeneous supersaturated solution reaches sufficiently high supersaturation, a new crystalline solid phase forms and the mechanism of its formation is referred to as primary nucleation. As described in Chapter 6, it is possible to relate primary nucleation kinetics to induction time, which is the time that elapses between a solution becoming supersaturated and when crystals of a detectable size are observed in solution (Sohnel et al., 1988). To reach such a detectable size, a nucleus of an indistinguishable size must be created and grown to the micron range. Therefore, the total time of this process can be divided into the time required to create a nucleus and the time required to grow it to a detectable size.

$$t_{ind} = t_N + t_G \qquad (7.2)$$

In most cases it is acceptable to assume that nucleation is the limiting step (i.e. $t_N \gg t_G$); hence, induction periods can be related to the rate of primary nucleation.

$$t_{ind} = B_1^{-1} \tag{7.3}$$

where:

$$B_1 = k_{B1} \exp\left(\frac{-B_0}{\ln(S)^2}\right) \tag{7.4}$$

Substitution of Equation 7.4 into 7.3 leads to an expression that can be used to relate induction time to primary nucleation.

$$t_{ind} = \left[k_{B1} \exp\left(\frac{-B_0}{\ln(S_0)^2}\right)\right]^{-1} \tag{7.5}$$

Linearization of Equation 7.5 yields an expression whose slope represents the exponential primary nucleation constant. This constant controls the onset of primary nucleation and can be used to obtain relationships between supersaturation and induction periods. More details on induction periods and the physical meaning embodied in the constants can be found elsewhere (Sohnel et al., 1988).

$$\ln t_{ind} = \frac{B_0}{\ln(S_0)^2} - \ln k_{B1} \tag{7.6}$$

Ottens et al. (2001) reported on induction-time experiments that were performed to estimate the primary nucleation rate constant B_0 (Ottens et al., 2001). In a later work by the same group Ottens et al. (2004), the effect of multiple impurities on ampicillin crystallization was reported. According to their results, reaction substrates and by-products inhibit ampicillin crystallization. This behavior is illustrated for three different initial concentrations of 6-APA in Figure 7.8, which shows induction periods as a function of initial supersaturation based on the functional form of Equation 7.6. Clearly, as 6-APA concentration increases the slope of the

121

semi-logarithmic plot also increase, meaning that a higher supersaturation was necessary to induce nucleation.
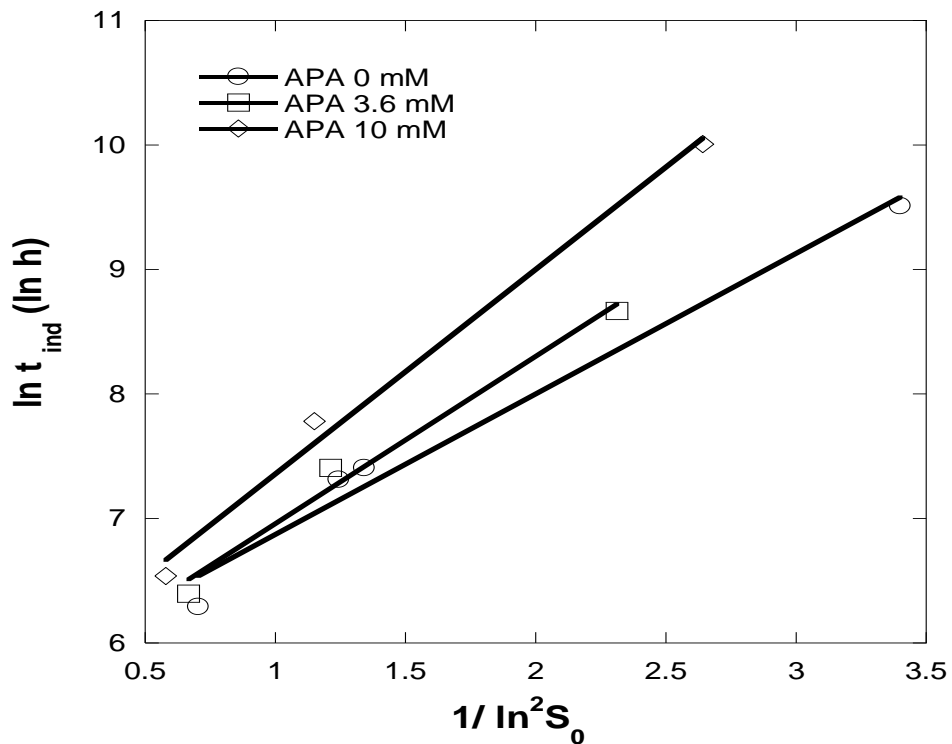
Figure 7.8: Log of induction time against log of inverse of initial squared. Data obtained from Ottens et al., 2004.

The slope of each plots represents the primary nucleation constant B_0 for the given 6-APA concentration. As shown in Figure 7.9, the slopes follow a linear relationship over the experimental range of 6-APA concentrations.

.
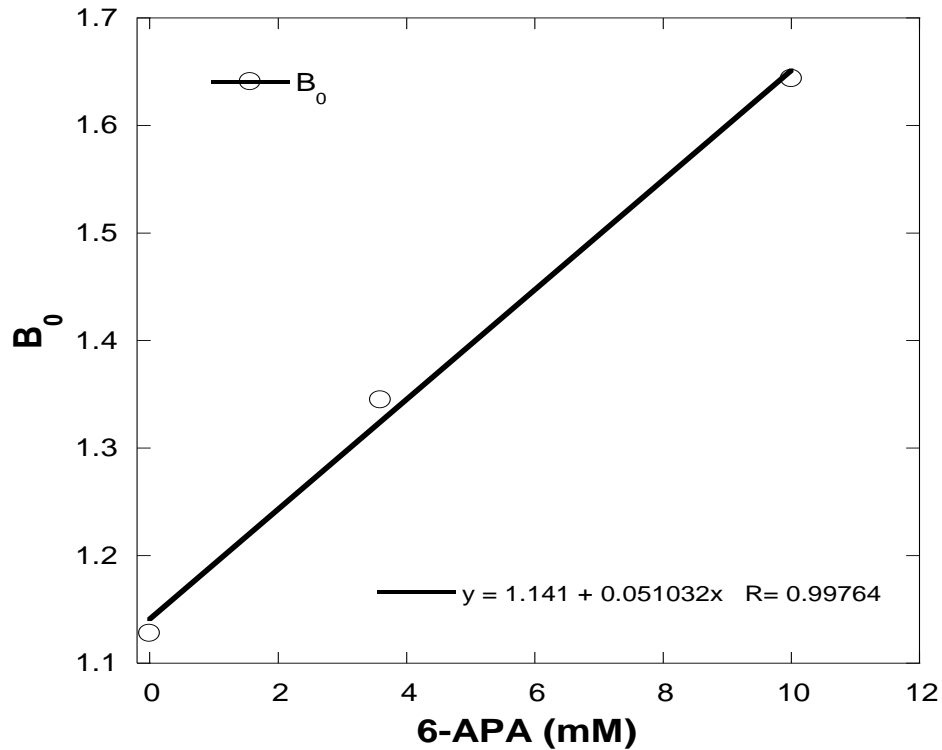
Figure 7.9: Nucleation rate constant B_o as a function of 6-APA concentration. Data obtained from Ottens et al., 2004.

Finally, just for qualitative purposes we have performed an extrapolation of the

nucleation rate constant to higher concentrations of 6-APA (up to 150 mM) by using the slope

calculated in Figure 7.9. Using these nucleation rate constants, we predicted the required

induction time as a function of the concentration of 6-APA at multiple initial supersaturations.

As seen in Figure 7.10, 6-APA concentration strongly affects induction periods, which may

explain why ampicillin crystallization was not possible at a supersaturation as high as 5. In fact,

at such conditions a supersaturation of approximately 10 is predicted to be necessary for primary

nucleation.
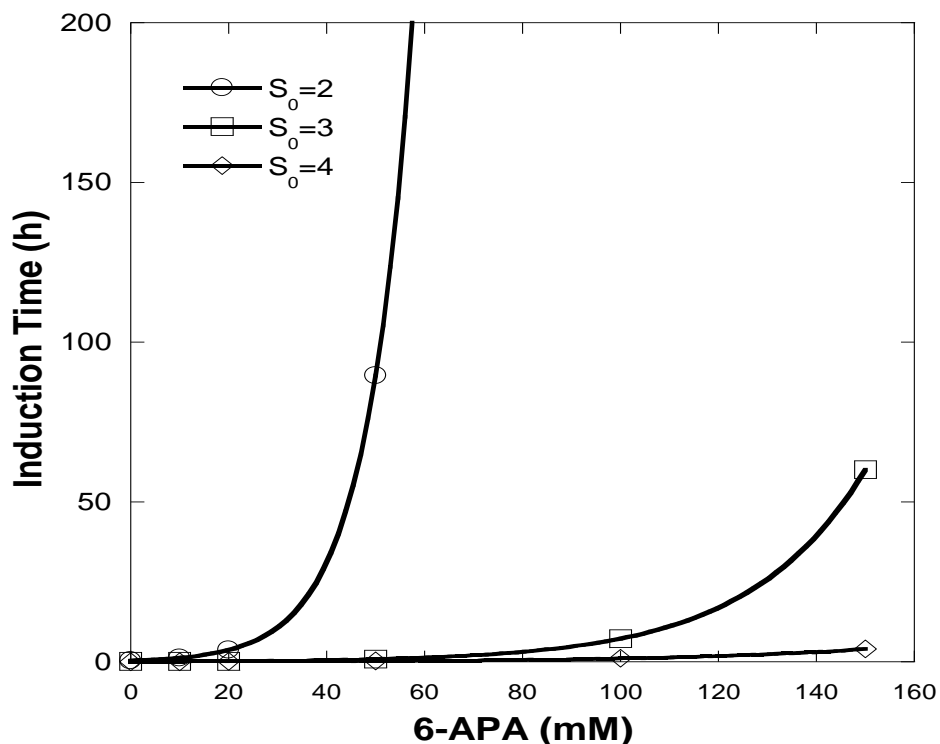
Figure 7.10: Extrapolation of induction time against 6-APA concentration at multiple supersaturation levels.

Usually, extremely high supersaturations are undesirable in crystallization processes. These typically induce uncontrolled nucleation leading to small crystals and incorporation of impurities. Additionally, as mentioned in the previous section, increasing the concentration of the substrates led to D-phenylglycine precipitation (<5% wt. ampicillin). Hence, in order to reduce the required initial supersaturation for crystallization and improve solid-phase purity, addition of seed crystals are explored in the next section.

7.3.4 Seeded reactive crystallization

As discussed in the previous section, unseeded experiments did not lead to crystallization unless the concentration of substrates was raised to very high concentrations. In this section seeded crystallization is explored since secondary nucleation can promote crystal formation at significantly lower supersaturations than primary nucleation. Figures 7.11 and 7.12 show the

124

results of seeded reactive crystallizations at conditions described in the figures. In these experiments the solution was seeded with 0.05 g of ampicillin crystals after 2 hours of starting the reaction. The time for seeding the solution was seeded was based on the concentration profiles of unseeded reactions. As seen in Figure 7.4, after 2 hours the concentration of ampicillin was higher than its solubility at the conditions of the reaction. Hence, solutions were seeded after two hours and it can be observed that the concentration starts to decrease after 4 hours. This was not observed during unseeded reactions at the same conditions where ampicillin concentration continuously increased.
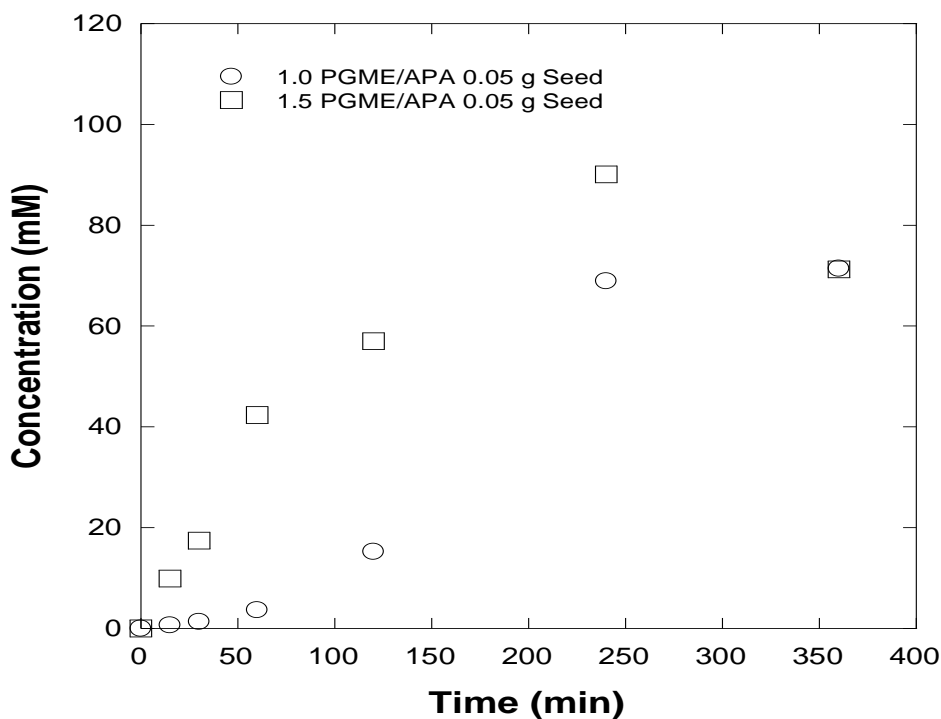
Figure 7.11: Accumulation of ampicillin at 25°C and pH of 7.00. Initial concentration of 0.20 M 6-APA and D-PGME 0.20 M to 0.30 M and seed loads of 0.05g.

Figure 7.12 shows that the D-phenylglycine concentration profiles for the same experiments continuously increased, which is evidence that crystallization of D-phenylglycine did not occur during the process. The data demonstrate one of the potential advantages of seeded reactive crystallization: i.e. the desired product is selectively recovered in the solid phase as it is synthesized and, therefore, subsequent product recovery and purification is not necessary.
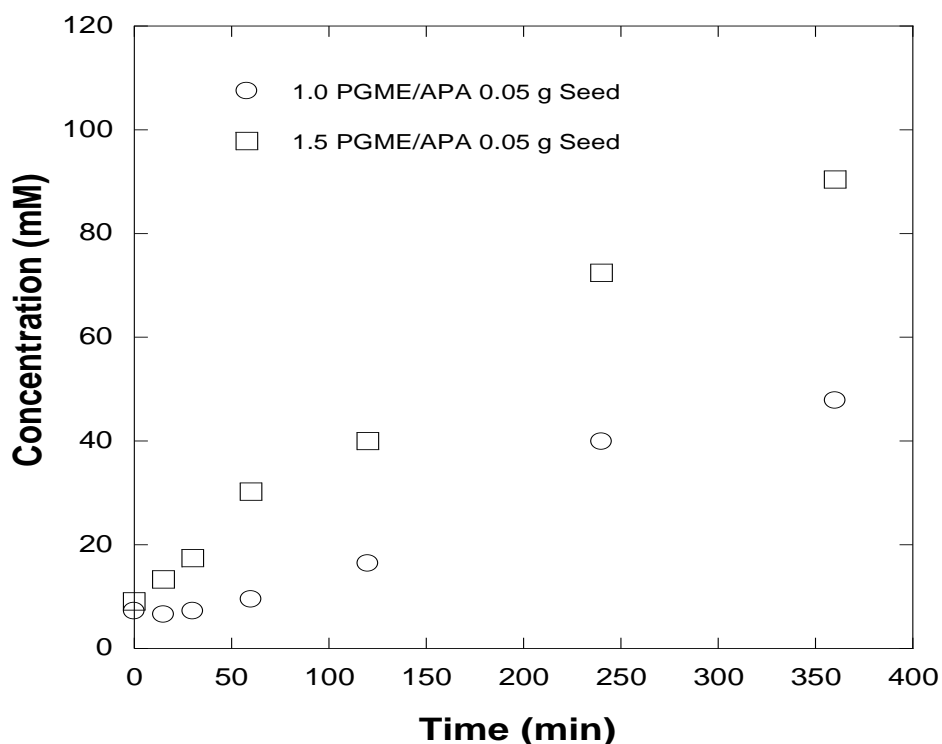
Figure 7.12: Accumulation of D-phenylglycine at 25°C and pH of 7.00. Initial concentration of 0.20 M 6-APA and D-PGME 0.20 M to 0.30 M and seed load of 0.05g.

The effect of the specific time at which the seed crystals were added was determined by maintaining the amount of seed crystals constant and varying the time at which they were added to the system. Figures 7.13 and 7.14 show the concentration profiles of ampicillin and D-phenylglycine when the seed crystals were added at 30 min, 60 min, and 120 min. As seen from Figure 7.13, adding seed crystals at 30 min maintained lower ampicillin concentration as ampicillin crystallization is promoted earlier in the process. Figure 7.14 shows the effect of

seeding at different times on the concentration profiles of D-phenylglycine; again, there was an insignificant effect on the concentration of D-phenylglycine, providing further evidence that the seed crystals promoted only secondary nucleation of ampicillin.
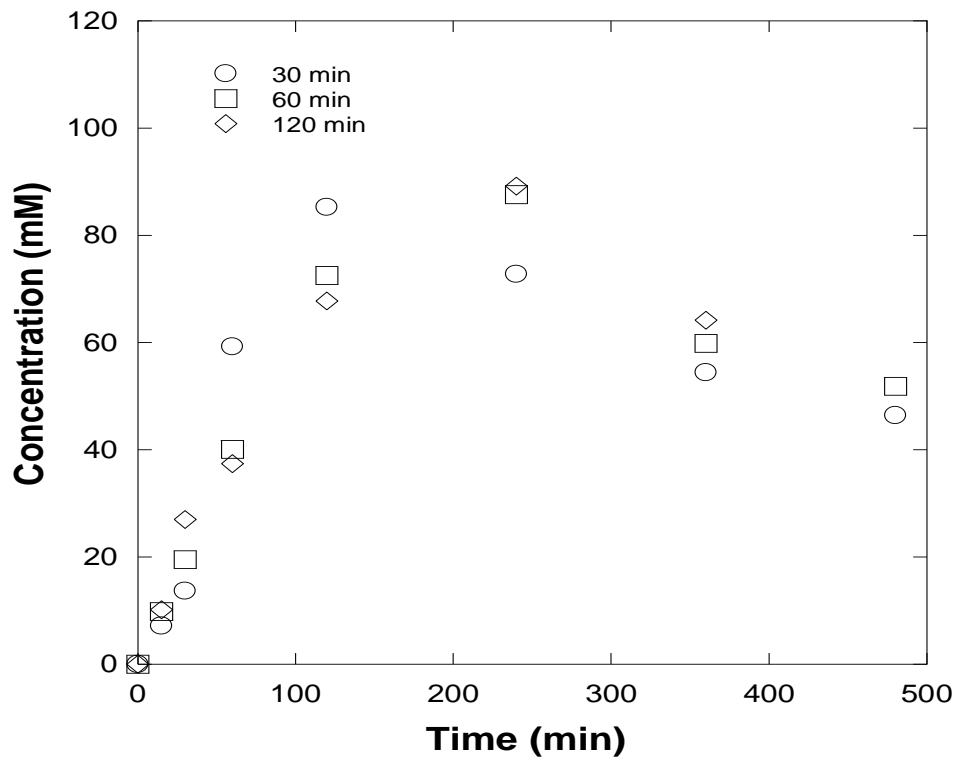
Figure 7.13: Effect of seed time on ampicillin concentration profiles.
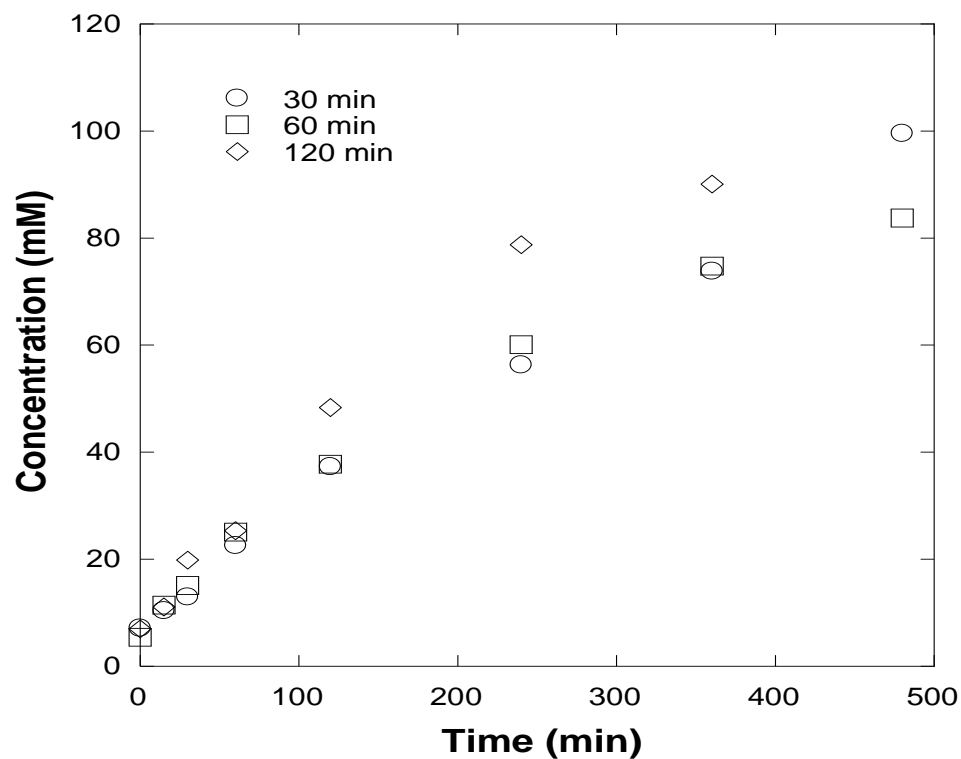
Figure 7.14: Effect of seed time on D-phenylglycine concentration profiles.

To investigate the effect of the mass of seed crystals on product concentration profiles, three different seed-crystal loads were added to the reaction system after 2 hours. Figure 7.15 shows the concentration profiles of ampicillin using seed-crystal loads of 0.01g, 0. 05 g, and 0.10g. As expected, higher loads enhanced crystallization rates and maintained lower concentrations of ampicillin in solution, but there was a negligible effect on D-phenylglycine concentration profiles.
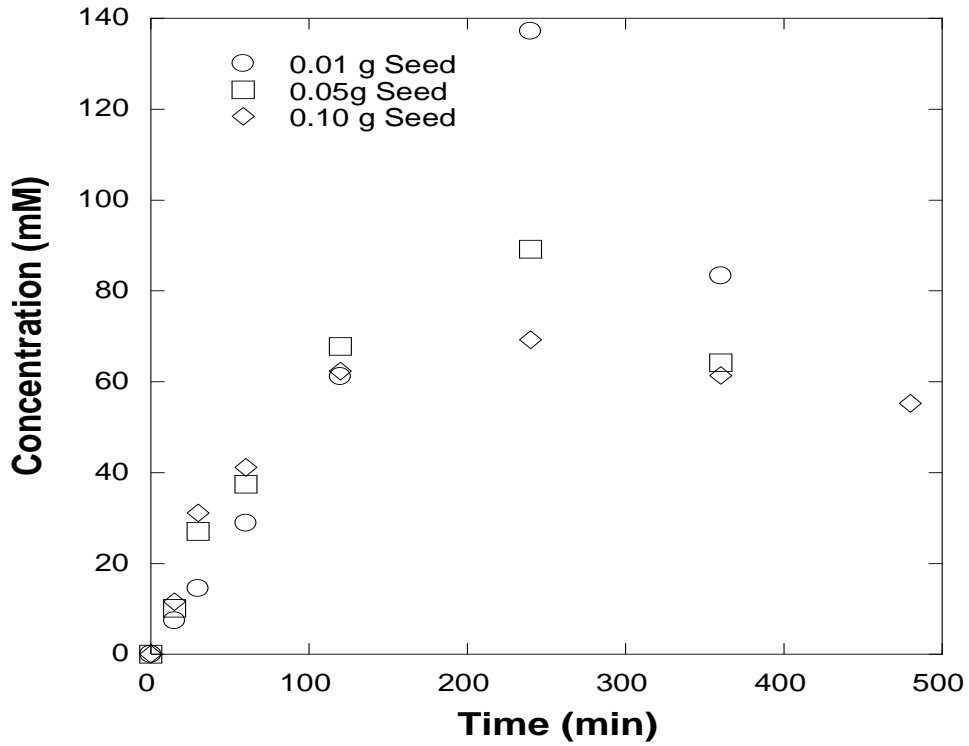
Figure 7.15: Accumulation of ampicillin at 25°C and pH value of 7.00. Initial concentration of 0.200 M 6-APA and 0.30 M D-PGME using seed loads of 0.01g, 0.05g, and 0.10g.
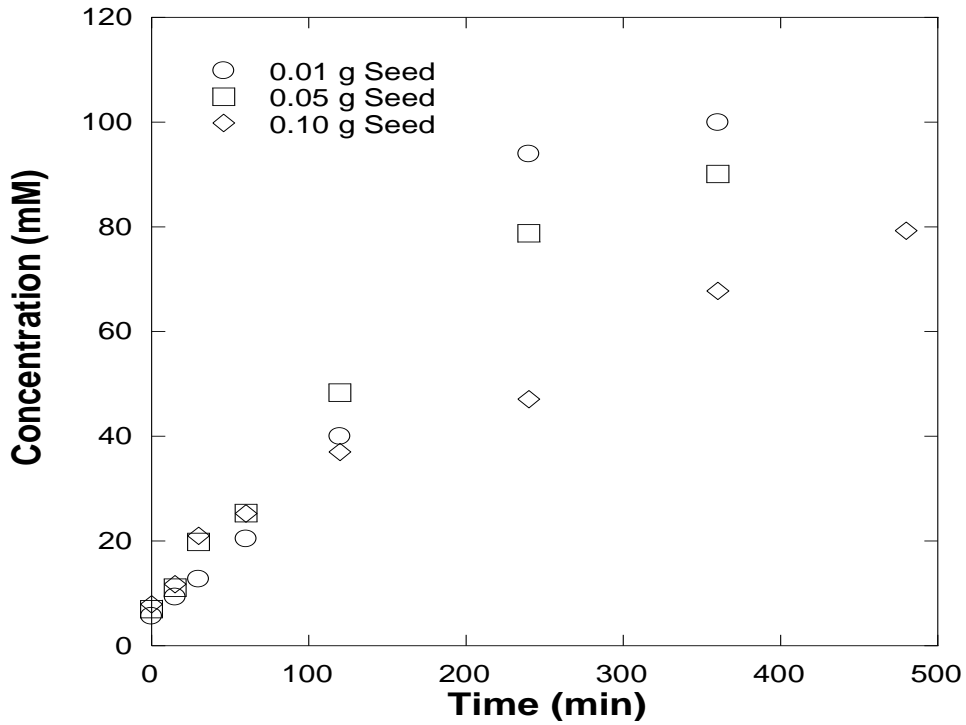

Figure 7.16: Accumulation of D-phenylglycine at 25°C and pH value of 7.00. Initial concentration of 0.20 M 6-APA and 0.30 M D-PGME using seed loads of 0.01g and 0.05g.

In order to determine the purity of the recovered crystals, solutions were filtered after 6 hours, dried at room temperature, and the solid phase was analyzed through HPLC. The results in Table 1 show that high purity resulted in all the runs in which seed crystals were used. In fact, the mole fractions of D-phenylglycine in the solid phase were similar to those of 6-APA and D-PGME, which implies that the impurities in the solid phase resulted from entrapment or adherence of the filtered solution. It is worth noting that the recovered crystals were not washed, as they would be in an industrial setting. Moreover, ampicillin crystallizes with a needle-like morphology, which limits the efficiency of washing and filtration.

Table 1: Crystal purity for different reactive-crystallization protocols.

Run	$[\text{6-APA}]_0$ (M)	$[\text{D-PGME}]_0$ (mM)	Seed load (mg)	Seeding time (min)	Crystals Purity (wt. %)
1	0.20	0.30	0.00	-	-
2	0.20	0.30	50.0	30	98.36
3	0.20	0.30	50.0	60	99.08
4	0.20	0.30	10.0	120	99.36
5	0.20	0.30	50.0	120	95.17
6	0.20	0.30	100.0	120	92.26
7	0.20	0.20	50.0	120	99.75
8	0.50	0.75	0.00	-	4.85

The previous experiments were performed with a total volume of 5 mL. Additionally, during the experiments aliquots of approximately 0.5 mL were withdrawn every time a sample was prepared, meaning roughly 60% of the material was lost through sampling. This does not consider all the material lost during transferring and filtration; thus, the total material recovered is certainly less than the one produced by the process. Hence, the total amount of crystals produced was approximated from the following equation.

$$\text{Crystal Mass} = ([\text{Amp}]_{\text{Run1}} - [\text{Amp}]) \cdot V \cdot MW_{\text{Amp}} \qquad (7.7)$$

First, it is assumed that in the absence of crystallization the concentration should follow a trend similar to that of run 1 in Table1. This run was used as a baseline for reactive crystallization experiments at the same initial conditions (i.e. initial concentration of substrates). Then, we attribute the difference in concentration between those to crystallization. Finally, using Equation 7.7 we have estimated the accumulated mass of crystals after 6 hours for different crystallization protocols.

Table 7.2: Comparison of mass of crystals produced after 6 hours for selected runs (Calculated using Equation 7.7).

Run	$[6\text{-APA}]_0$ (mM)	$[D\text{-PGME}]_0$ (mM)	Crystals Mass (mg)
1	0.20	0.30	0.0
2	0.20	0.30	84.7
3	0.20	0.30	75.3
4	0.20	0.30	34.3
5	0.20	0.30	67.7
6	0.20	0.30	72.73

For qualitative purposes, pictures of the reactive crystallization through the length of the reaction are shown in Figure 7.17. There is a clear progression from a clear solution to a cloudy slurry after addition of seed crystals, to a slurry nearly white from the presence of crystals in the slurry.

Figure 7.17: Picture of reactive-crystallization Run 4 and 5 when reaction started (left), after seeding (center), and after 6 hours (right).

7.3.5 Scale-up and CLD evolution

In order to have better understanding of the process, the reaction was scaled up from 5 mL to 250 mL. At this scale an FBRM probe can be used to monitor particles the chord length distribution in the slurry. Additionally, the final mass of crystals can be measured as losses during the experiment are insignificant in comparison with the mass of crystals recovered. Figure 7.18 shows the concentration profile for such a run in which 2.5 g of ampicillin seed crystals were added after 1 hour of reaction time. The concentration profile looks very similar to those obtained using the 5-mL vessels in which a decay in concentration was observed when the concentration reached approximately 80 to 100 mM.
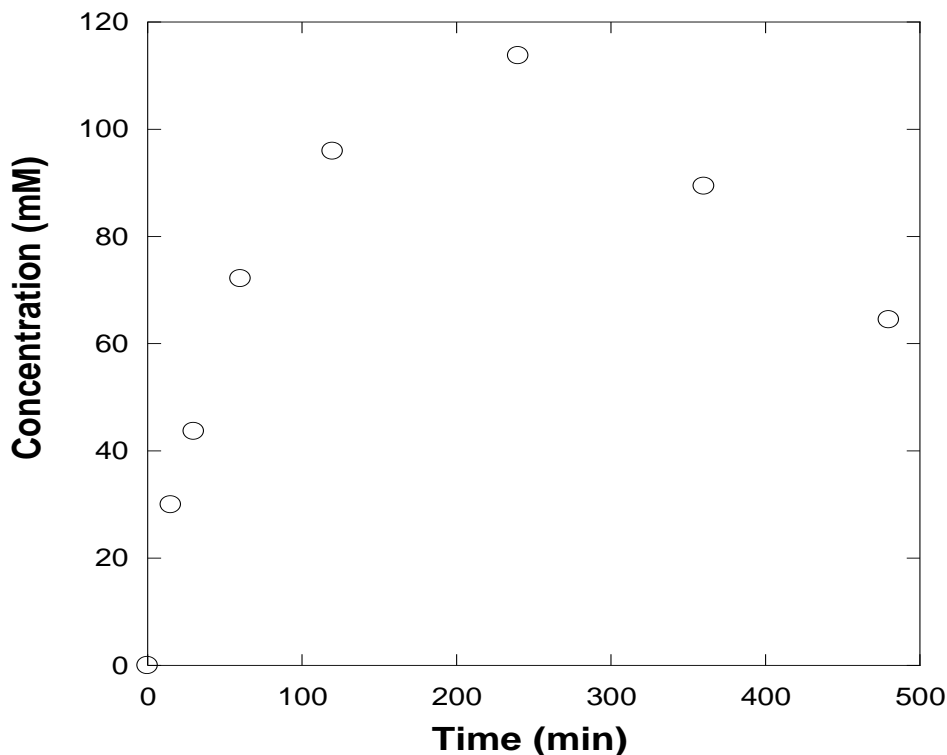
Figure 7.18: Reactive crystallization scale-up to 250 mL(6-APA 0.20 M, D-PGME 0.30 M, 25 °C, and pH 7.00).

Figures 7.19 and 7.20 show FBRM data for the same run. In Figure 7.19 the increase in chord counts at around 200 minutes is thought to result from secondary nucleation, which is consistent with the concentration profiles shown before as the concentration of ampicillin starts to decay at that point. Additionally we note that 30 to 60 minutes after nucleation, the number of small particles (0 to 50 μm) starts to decay while the number of big particles (50-300 μm) keeps increasing. Hence, after that point supersaturation is being depleted by crystal growth rate rather than nucleation. This is reflected by the evolution of chord length distribution (Figure 7.20) where the CLD shifts on the x-axis meaning an increase on the mean size of the particles.
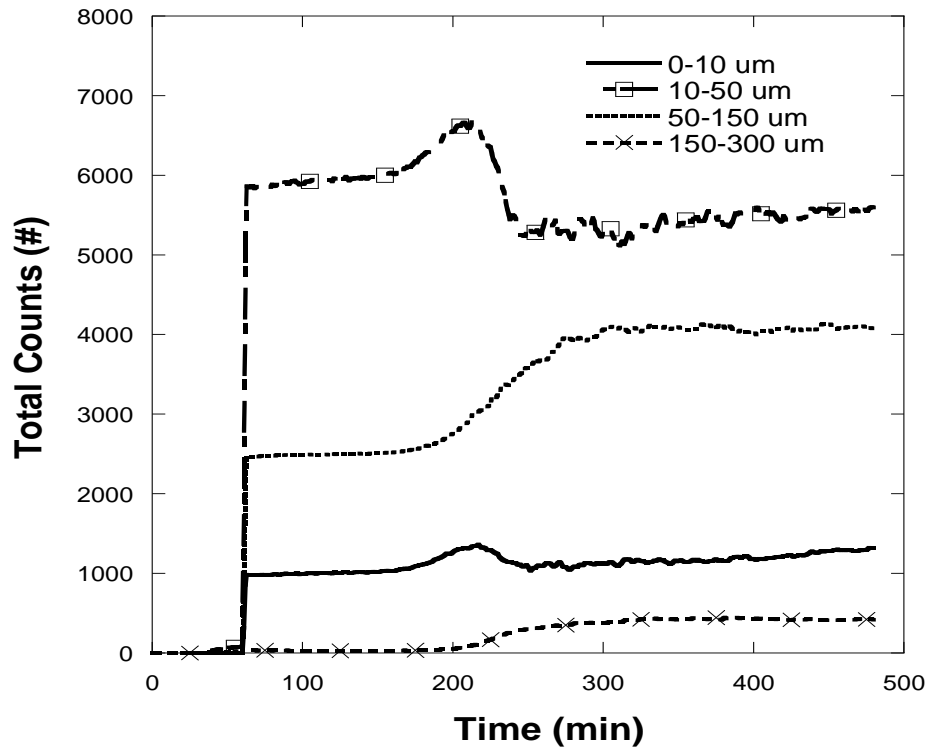
Figure 7.19: Counts evolution as a function of time.
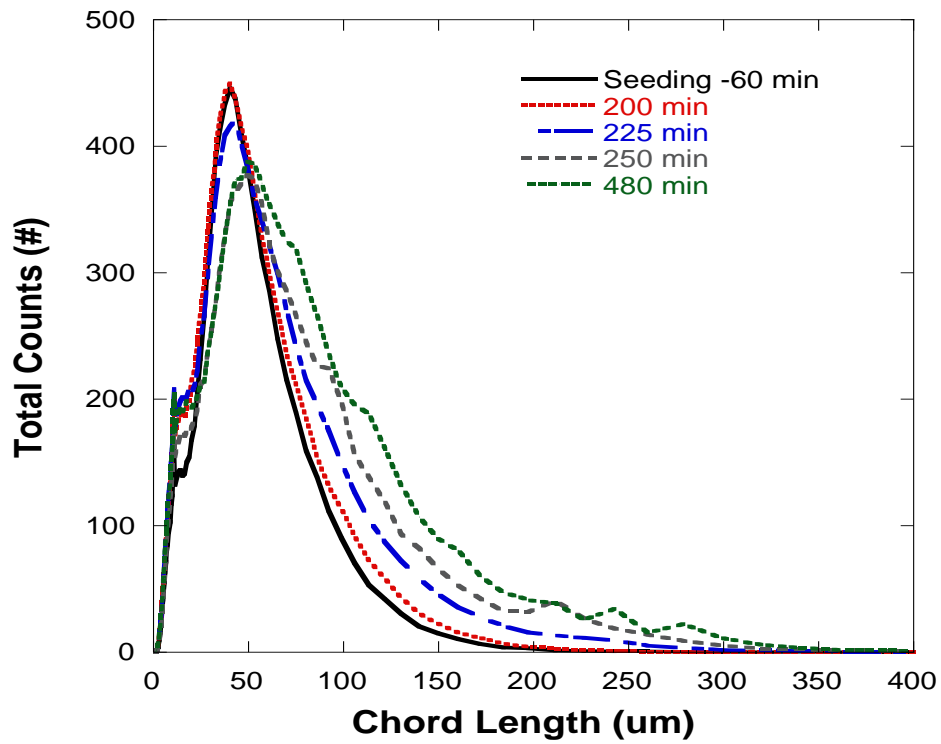
Figure 7.20: Chord length distribution (CLD) evolution.

134

Finally, the mass of recovered crystals was quantified after filtration and drying of the cake. In this case a total mass of 8.5 g was recovered from the process. This mass includes 2.5 g of seed crystals, thus 6.0 g of solid ampicillin were produced in the process. Additionally, solid-phase purity was determined by HPLC to be 99.05 wt% ampicillin. Ampicillin crystals yield should be slightly higher as some ampicillin was lost through the process as a result of samples withdrawing, filtration, drying, and a portion that remained stick to the vessel, baffles, and probes.

7.4 Conclusions

In this work we have demonstrated the advantage of performing a reactive seeded crystallization towards the manufacture of ampicillin. First, we demonstrated that unseeded reaction did not show product crystallization even after reaching high supersaturation (i.e. supersaturation of 5). In order to induce product precipitation without the presence of seed crystals, substrates initial concentrations were raised even more. However, this led mainly to crystallization of D-phenylglycine obtaining 5% wt. solid phase purity with respect to ampicillin. This problem was successfully resolved by the addition of seed crystals into the reaction vessel as crystallization of ampicillin was possible in all the runs. Solid phase purity analyses demonstrated that very high purities are possible with such an approach. Additionally, the effects of multiple seeding protocols were demonstrated in this work. Hence, in contrast to other heterogeneous reactive synthesis, seeding provides a selective separation in which crystallization of the desired product is promoted. As do other reactive crystallization processes, this operation has the advantage of reducing the rates of secondary hydrolysis because ampicillin is protected from the enzyme whenever it is in the solid phase. Additionally, the total manufacturing time is reduced as synthesis and separation and purification are performed in a single stage.

CHAPTER 8

Future Work

8.1 Reactive crystallization towards the manufacture of chiral compounds

8.1.1 Extension to multiple substrates

In Chapter 3 the possibility of performing chemoenzymatic stereoinversions at conditions at which crystallization of enantiomerically pure crystals was possible was demonstrated. This process was demonstrated by resolving mixtures of DL-methionine and DL-phenylalanine, where in both cases enantiomeric purities over 99% wt. were obtained. In addition, D-amino acid oxidases can be used to oxidize a broad range of amino acids. Alexandre et al. discussed the efficacy of multiple reducing agents in the chemo-enzymatic stereoinversion of amino acids (Alexandre et al., 2002). In the same work, 10 other amino acids are converted to single enantiomers but their success was not the same for all the amino acids tested.

Another enzyme that has shown great oxidation enantioselectivity is sec-alcohol oxidase (Fantin et al., 1993; Muller et al., 1991). This enzyme shows great enantioselectivity towards the oxidation of sec-alcohols. Following a similar scheme to the one used for the conversion of chiral amino acids to a single enantiomer, stereoinversion of sec-alcohols it is possible. Kroutil et al. developed a mathematical framework that can be employed to predict the stereoinversion of sec-alcohols through cyclic chemo-enzymatic stereoinversion (Kroutil et al., 1998). Upon the availability of thermodynamic information about the solubility of these compounds in their respective media, a reactive crystallization scheme can be developed.

8.1.1 Alternative of reactors design

The work presented in Chapter 3 was performed in a batch reactor. Batch reactors are the standard in the manufacture and purification of specialty chemicals and pharmaceutical products. In the work presented in Chapter 3, a reaction-crystallization scheme was developed using a single batch unit to decrease reactor volume and reduce operational time. The time of the operation was reduced as both reaction and separation could be performed in parallel. However, this has some potential disadvantages. For example, conditions that favor the reaction do not necessarily favored crystallization. As discussed before, relatively high temperatures enhance the rate of reaction. However, these temperatures increase the solubility of the substrates which reduced crystallization rates.

It is possible to transform this operation into a continuous operation where one section of the process used for reaction while the other is used for separation. Using this approach is possible to run both reaction and crystallization at their optimal point. As shown in Figure 8.1, the reaction can be run using two stages where in the first stage the reaction is run until the desired enantiomeric excess is achieved while in the second stage crystallization of the enantiopure product will take place.
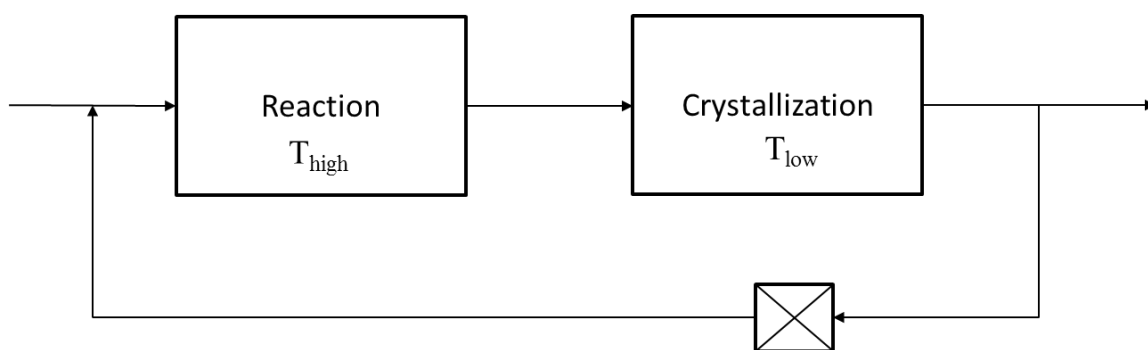
Figure 8.1: 2-stage reaction-crystallization.

8.2 Reactive crystallization towards the manufacture of β-lactam antibiotics

8.2.1 Extension to multiple substrates

In Chapter 7 a strategy towards the synthesis and recovery of ampicillin in a single stage was demonstrated. This was achieved by performing a seeded reactive crystallization in which ampicillin was produced and recovered with high purity in the solid phase. However, this process was only demonstrated for ampicillin as a target product. Nevertheless, penicillin G acylase has shown activity towards a wide range of β-lactam that can be utilized to produce other antibiotics such as amoxicillin, cephalexin, cefadroxil, and others (Wegman et al., 2001). Hence, a reactive crystallization towards the manufacture of these antibiotics is viable. In fact, if amoxicillin is the target product, co-product precipitation can be alleviated as the solubility of D-(hydroxyl)-phenylglycine is higher than the one of D-phenylglycine (Rudolph et al., 2001).

8.2.2 Reaction optimization

In Chapter 5 an experimental design consisting of 6 concentration levels at 5 pH values was performed. Our results demonstrated that pH has a significant effect on the rates of reactions, but not necessarily on the selectivity. However, in the case of reactive-crystallizations the pH value will not only affect the rates of reaction, but it will also affect solid-liquid equilibria and crystallization kinetics. In Chapter 4 a generic model for optimization of temperature-dependent reactive crystallizations was developed. In that case, at high temperatures the rates of reaction were favored, while at low temperatures the rate of crystallization was enhanced. The objective of such optimization was to maximize the productivity of the operation by finding the optimal temperature that yields the best overlap between reaction and crystallization. The

optimization embodied both reaction and crystallization kinetics, and their respective dependence on temperature. Using these relations, an optimal temperature path was developed.

As mentioned before, in Chapter 5 reaction kinetics were addressed through a variety of experiments. Additionally, in Chapter 6 crystallization kinetics of ampicillin were developed. Using reaction and crystallization kinetics a dynamic optimization like the one presented in Chapter 4 is possible. In this case, pH can be used to control substrate concentrations, which in turn control the rates of reaction. On the other hand, supersaturation can be controlled by manipulating the pH value in solution. Therefore, an optimal pH path can be developed such that process or product attributes are enhanced.

8.2.2 Effect of impurities on ampicillin crystallization

Ottens et al. developed models to predict crystallization kinetics of ampicillin with or without impurities (Ottens et al., 2001, 2004). In their work, the effect of substrates and by-products concentration on the crystallization of ampicillin were quantified. However, the only way in which concentrations of ampicillin can be obtained is if high concentrations of substrates are used. Unfortunately, the results in Ottens et al. do not represent the conditions at which the reaction is performed nor the concentration of substrate that are commonly used.

In the work presented in Chapter 7, information from Ottens et al. was used and extrapolated to process conditions (Ottens et al., 2004). However, the extrapolation was not addressed experimentally. It is possible that nucleation inhibition does not follow a linear relationship with substrate concentration as at some point surfaces might be saturated with impurities.

8.2.3 Classification of seed loads

In Chapter 7 a reaction crystallization scheme was developed in which seeds were used to promote secondary nucleation. However, for simplification purposes, these experiments were based on crystal mass. It is well known that crystal surface can influence the rate of secondary nucleation (Doki et al., 2002; Tseng et al., 2014). To quantify the effect of crystal surface area, quantification of seeds crystal size distribution is required. This information can be used to estimate the total available surface area and relate it to the rate of secondary hydrolysis. An alternative to this approach is seed classification. Seeds can be classified into multiple lengths, and these classes can be used as seeds in the process. Hence, the effect of increasing or decreasing seed length (while maintaining mass constant) can be quantified.

Appendix

A.1 Analytical methods

A.1.1 HPLC analysis for chiral compounds

HPLC analyzes were performed to calculate the concentration of species in solution. For illustration purposes, calibrations of semi-synthetic β-lactam substrates and products will be shown. Regardless the component of interest, the procedure will be similar. First, a stock solution of each component was prepared. Since most of the reactions performed in this thesis were at high concentrations, stock solutions were prepared to a concentration close to solubility. Stock solutions were used to prepare solutions at lower concentrations by diluting it with the desired solvent (water or buffer). Finally, an aliquot of 50 μL of each solution was diluted into 1 mL of HPLC buffer. An illustration of a typical chromatogram is shown in Figure A1 while their respective calibration curves are shown in Figure A2.
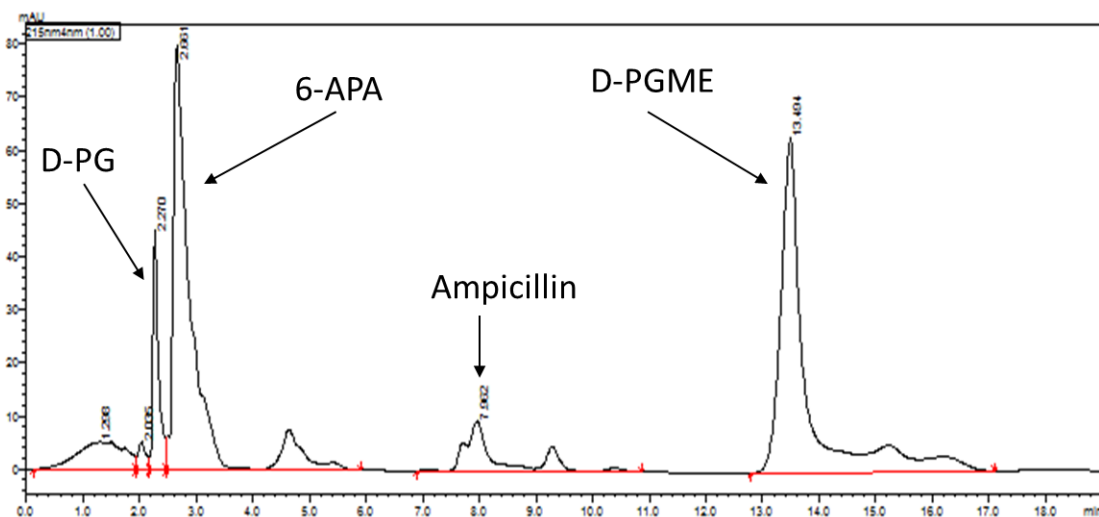
Figure A.1.1: HPLC chromatogram of β-lactam antibiotics substrates and products at a pH of 6.5 and 298K.

(a)

(b)
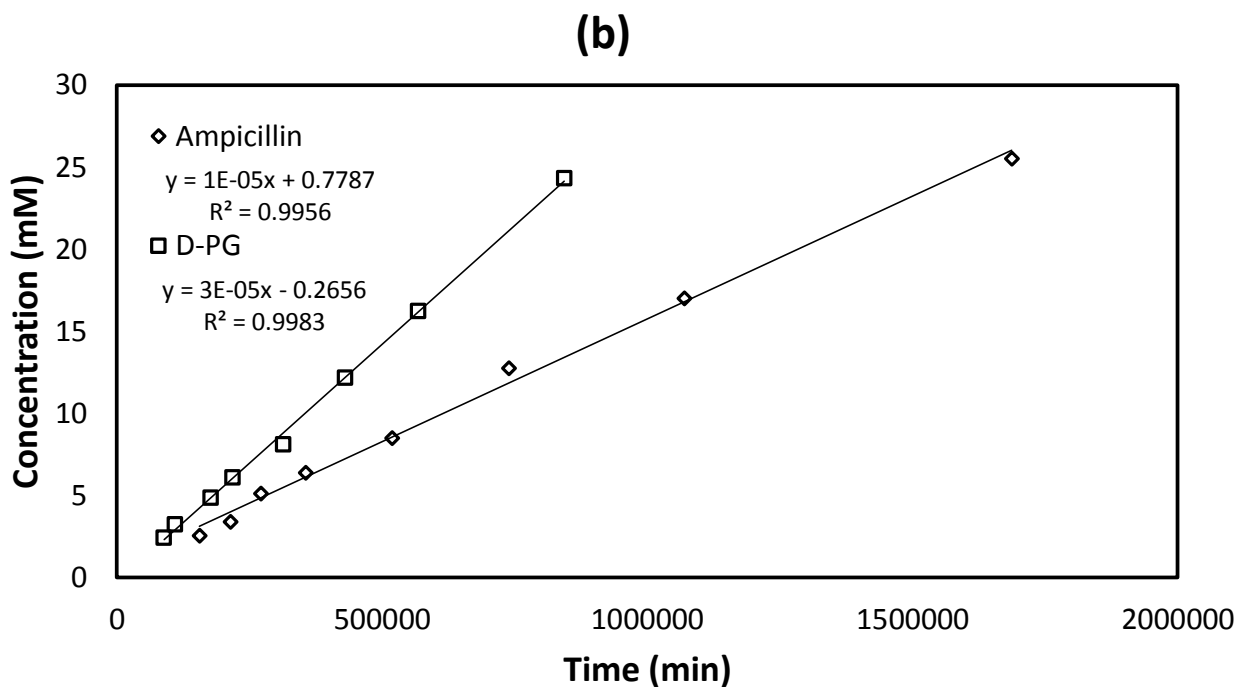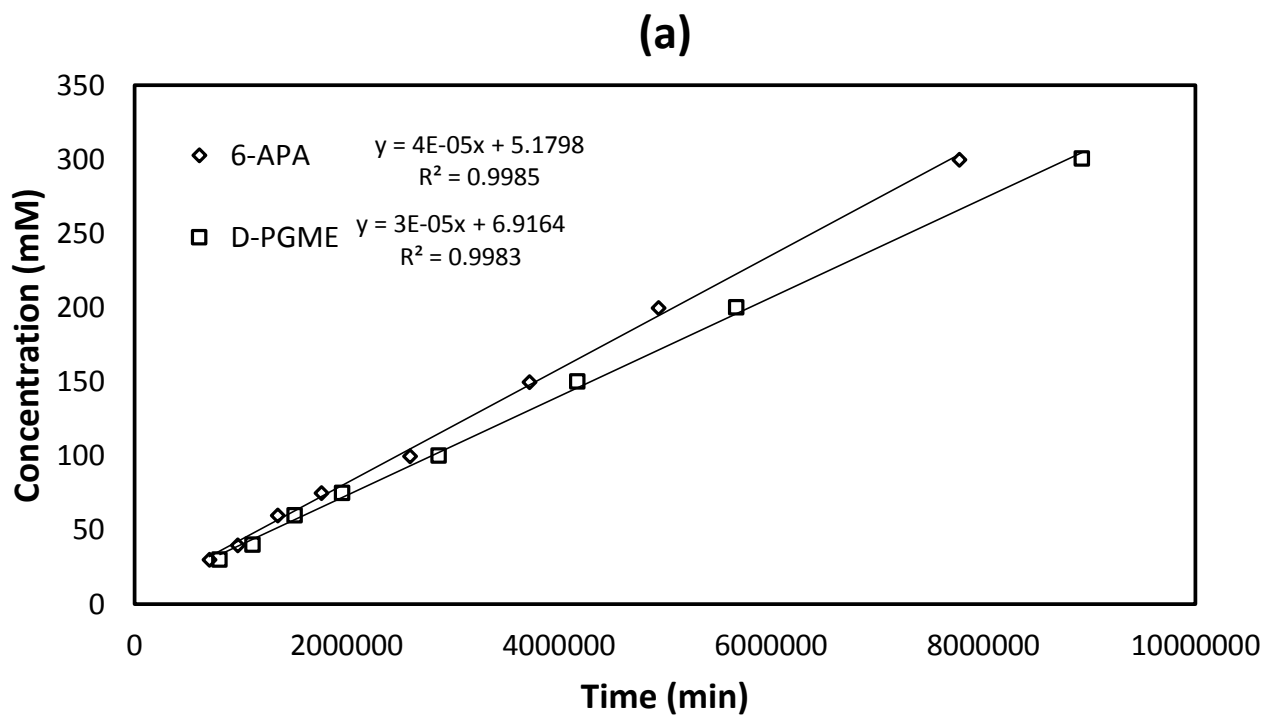
Figure A.1.2: Calibration curves of (a) 6-APA and D-PGME and (b) ampicillin and D-phenylglycine at pH of 6.5 and 298K.

In order to verify the effect of pH to the calibrations curves, the same procedure was done but the pH in solution was raised to 7.0. As it can be seen in Figure A.3, there is only some deviation in peaks retention time. However, data from calibrations performed at a pH of 6.5 and 7.0 were combined and shown in Figure A.4. As it can be seen the concentration at both pHs lie on the same linear trend.
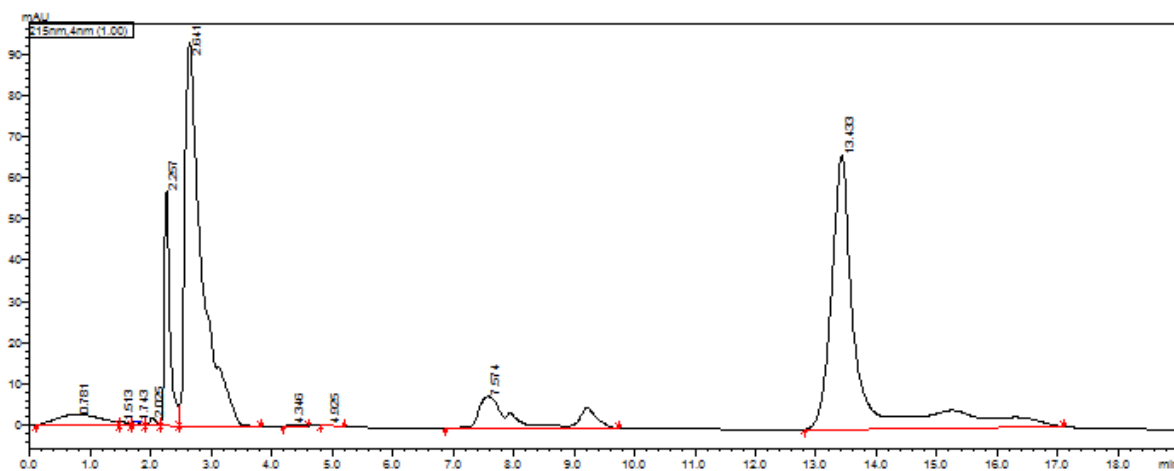
Figure A.1.3: HPLC chromatogram of β-lactam antibiotics substrates and products at a pH of 6.5 and 298K.

(a)

(b)
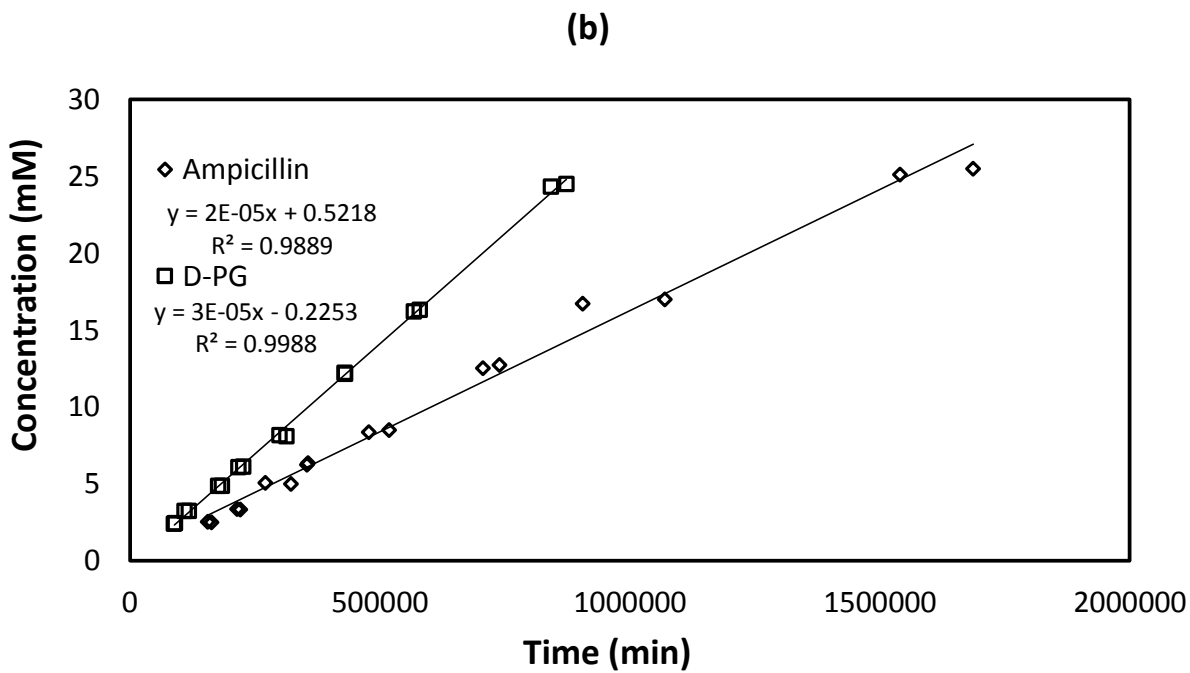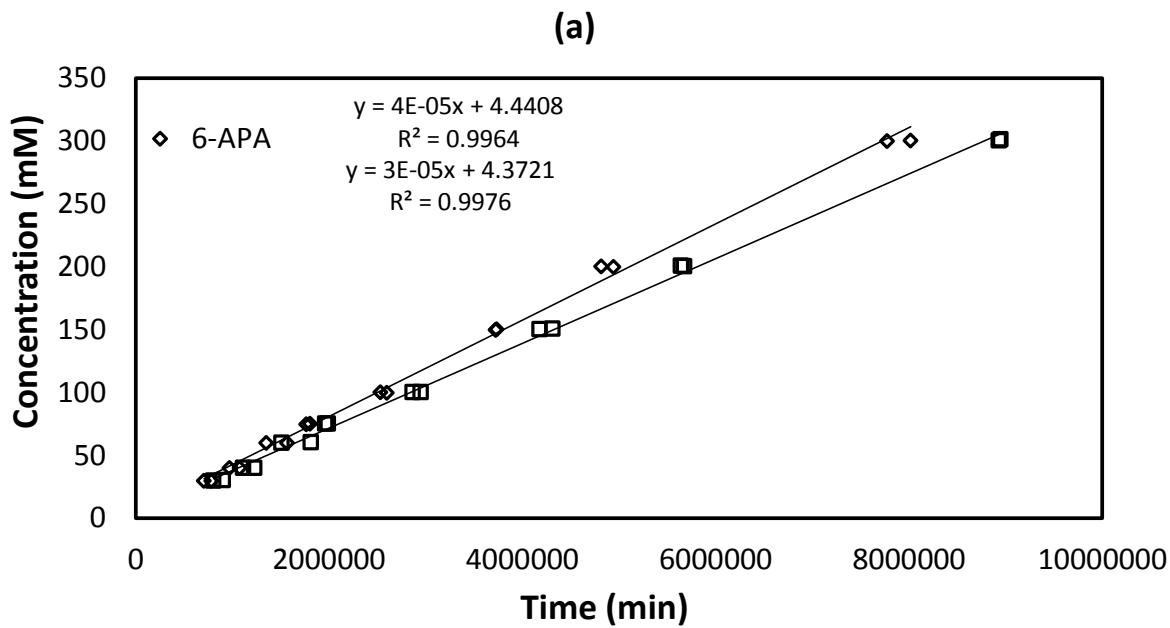
Figure A.1.4: Calibration curves of (a) 6-APA and D-PGME and (b) ampicillin and D-phenylglycine at pH of 6.5 and 7.0 and 298K.

A.1.2 Utilization of polarimetry and refractometry

In chapter 3 and 6, polarimetry and refractometry were used as part of an online monitoring system that allows real time concentration measurements. As mentioned in these chapters, a small portion of crystallizer solution was continuously recirculated through a polarimeter and refractometer. In order to estimate concentration from these signals, a calibration curve was necessary. Figure A.5 shows an example of ampillin calibration curves using polarimetry and refractometry. The calibration curve was prepared by adding a known weight of solute to the crystallizer and measuring the respective increment in polarimetric signal and regractive index. As it can be seen, both unit give a linear relation between signal and concentration.

(a)

(b)

$y = 4737.5x - 6314.9$
$R^2 = 0.9993$
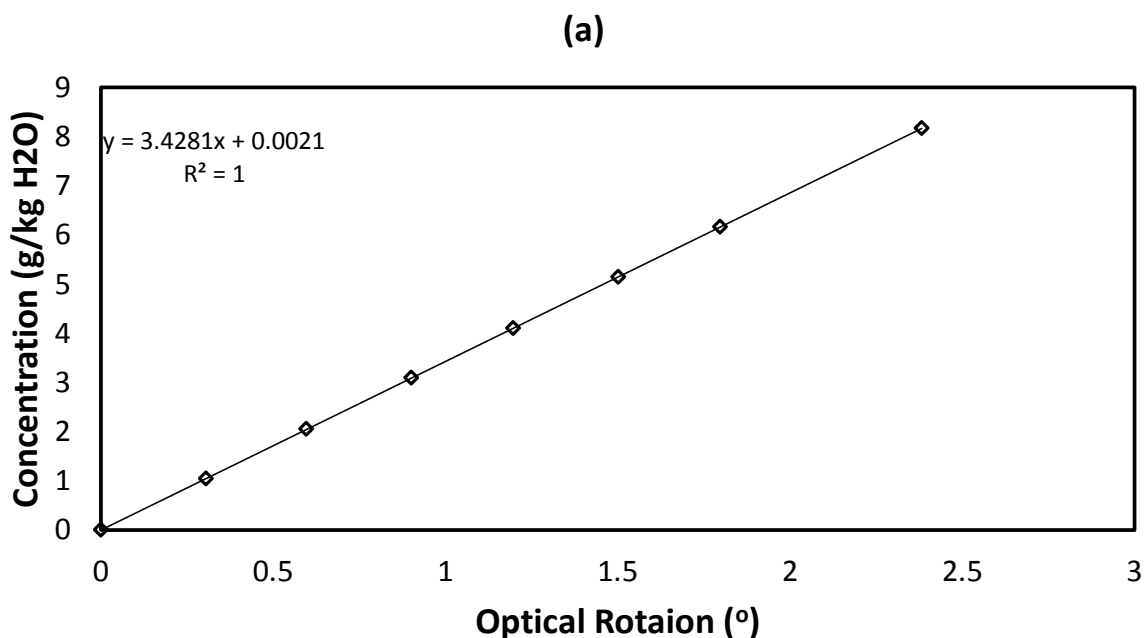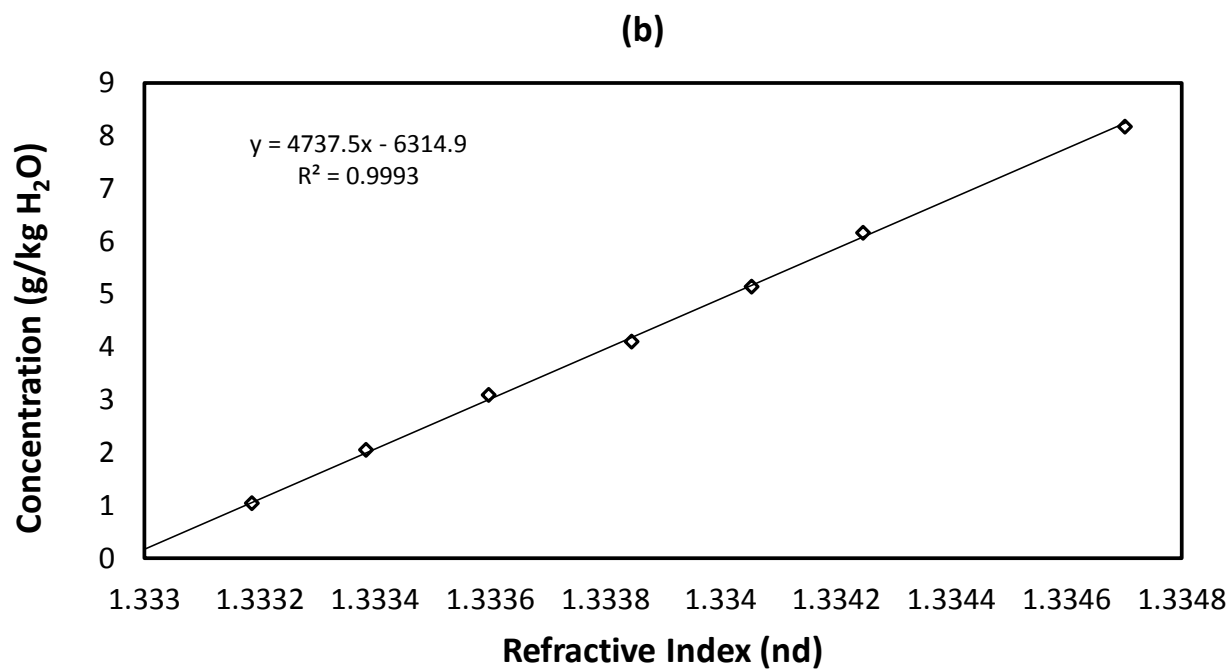
Figure A.1.5: Calibration curves of ampicillin using a (a) polarimeter and (b) refractometer.

A.2 Supporting Information

A.2.1 Optimization initial conditions

Table A.2.1: Optimization initial conditions

DL-phenylalanine (g/kg H_2O)	Temperature (°C)	Mass of Crystals (g)	Moments μ_i
60.0	60.0	0.0	0.0

A.2.2 Effect of changing the substrates ratio at different pH values

In order to verify if the pH value significantly affects the selectivity as a function of substrate

ratio, the slopes of synthesis vs. hydrolysis ratio as a function of substrate concentration has been

plotted at different pH values. It can be seen that the slope of this graph is significantly smaller to

the ones that quantify the effect of substrate concentration. In fact, depending on the specific pH

value the substrate ratio is in the range of 3.7 to 6.0 more significant than the pH value.

Table A.2.2: Analysis of substrate ratio and pH value slopes

pH	Slopes of Figure 5.3	Slopes Figure 5.3 divided by slope of Figure 5.4
6.00	1.49	5.96
7.00	1.052	4.21
7.50	1.16	4.64
8.00	0.93	3.72

A.2.3 Ampicillin crystallization kinetics covariance matrices

Table A.2.3: Covariance matrix for a single experiment (Run f).

	k_{B1}	k_G	g	k_{B2}	b	s
k_{B1}	1.06E+21	-35752.7	-3.3E+09	-2.1E+20	-2.8E+09	-5.2E+11
k_G	-35752.7	5.28E-12	-1.9E-07	-11389	-5.7E-07	-5.5E-05
g	-3.3E+09	-1.9E-07	0.037376	2.14E+09	0.069852	7.053434
k_{B2}	-2.1E+20	-11389	2.14E+09	1.31E+20	4.4E+09	4.34E+11
b	-2.8E+09	-5.7E-07	0.069852	4.4E+09	0.399479	11.77837
s	-5.2E+11	-5.5E-05	7.053434	4.34E+11	11.77837	1569.756

Table A.2.4: Covariance matrix for seeded experiments.

	k_{B1}	k_G	g	k_{B2}	b	s
k_{B1}	1.54E+20	-10764.1	1.31E+08	-1.3E+18	7649648	-1.4E+08
k_G	-10764.1	7.93E-13	-5.3E-09	87.76328	-1.6E-09	6.33E-09
g	1.31E+08	-5.3E-09	0.001519	-463040	-0.00026	-0.00127
k_{B2}	-1.3E+18	87.76328	-463040	1.14E+16	-426921	60641.8
b	7649648	-1.6E-09	-0.00026	-426921	0.000267	0.000194
s	-1.4E+08	6.33E-09	-0.00127	60641.8	0.000194	0.002895

Table A.2.5: Covariance matrix for all experiments.

	k_{B1}	k_G	g	k_{B2}	b	s
k_{B1}	2E+18	-90.3629	-2771924	-1.3E+16	-3154326	-7165773
k_G	-90.3629	9.71E-15	5.03E-10	0.24867	1.17E-10	2.3E-10
g	-2771924	5.03E-10	0.000102	61968.39	-1.8E-05	-7.4E-05
k_{B2}	-1.3E+16	0.24867	61968.39	2.44E+14	-12692.2	-24844.5
b	-3154326	1.17E-10	-1.8E-05	-12692.2	4.31E-05	-2.1E-05
s	-7165773	2.3E-10	-7.4E-05	-24844.5	-2.1E-05	0.000408

A.2.4 Effect of cosolute to the solubility of ampicillin at low pH

In order to understand the effect of cosolutes to the solubility of ampicillin, solutions with different cosolute concentrations were prepared and the solubility of ampicillin in theses was measured. The fist column of Table A.2.4 shows the concenteration of colute, the second column shows the solubility of ampicillin, and the last column shows the ratio of the solubility compared with a solution wihout cosolute. In that column we can clearlyu see if the cosolute increases, decrease, or does not affect the solubility of ampicillin. All the samples were taken at 25 ºC and in a pH range of 5-6.5. In that range ampicillin is arounf its isoelectric point and the solubility is barely affected by the pH value.

Table A.2.6: Ampicillin solubility at different cosolute concentration.

PG (mM)	Ampicillin Solubility (mM)	Ratio (mM/mM)
0.00	44.27	1.00
3.13	35.34	0.80
6.26	40.95	0.93
12.52	38.03	0.86
25.05	33.28	0.75

6-APA (mM)	Ampicillin Solubility (mM)	Ratio (mM/mM)
0.00	41.09	1.00
25.05	51.95	1.26
50.09	54.18	1.32
100.18	53.64	1.31
200.36	59.67	1.45

PGME (mM)	Ampicillin Solubility (mM)	Ratio (mM/mM)
0.00	40.76	1.00
24.34	40.22	0.99
48.69	37.80	0.93
97.37	38.70	0.95
194.74	45.13	1.11

References

Abian, O., Mateo, C., Fernandez-Lorente, G., Guisan, J. M., & Fernandez-Lafuente, R. (2003).
Improving the industrial production of 6-APA: Enzymatic hydrolysis of penicillin G in
the presence of organic solvents. *Biotechnology Progress, 19*(6), 1639-1642. doi: Doi
10.1021/Bp0340786

Abrahamson, M. J., Bommarius, A. S., Vazquez-Figueroa, E., Moore, J. C., & Wong, J. W.
(2012). Novel amine dehydrogenases for the production of chiral amines. *Abstracts of
Papers of the American Chemical Society, 243*.

Abrahamson, M. J., Vazquez-Figueroa, E., Woodall, N. B., Moore, J. C., & Bommarius, A. S.
(2012). Development of an amine dehydrogenase for synthesis of chiral amines.
Abstracts of Papers of the American Chemical Society, 244.

Alexandre, F. R., Pantaleone, D. P., Taylor, P. P., Fotheringham, I. G., Ager, D. J., & Turner, N.
J. (2002). Amine-boranes: effective reducing agents for the deracemisation of DL-amino
acids using L-amino acid oxidase from Proteus myxofaciens. *Tetrahedron Letters, 43*(4),
707-710.

Berry, D. A., & Ng, K. M. (1997). Synthesis of reactive crystallization processes. *Aiche Journal,
43*(7), 1737-1750.

Blackmond, D. G. (2010). The Origin of Biological Homochirality. *Cold Spring Harbor
Perspectives in Biology, 2*(5). doi: ARTN a002147

DOI 10.1101/cshperspect.a002147

Blum, J. K., & Bommarius, A. S. (2010). Amino ester hydrolase from Xanthomonas campestris

    pv. campestris, ATCC 33913 for enzymatic synthesis of ampicillin. *Journal of Molecular*

    Catalysis B-Enzymatic, 67(1-2), 21-28. doi: DOI 10.1016/j.molcatb.2010.06.014

Boehm, M. F., & Bada, J. L. (1984). Racemization of Aspartic-Acid and Phenylalanine in the

    Sweetener Aspartame at 100-Degrees-C. *Proceedings of the National Academy of*

    Sciences of the United States of America-Physical Sciences, 81(16), 5263-5266.

Bommarius, A. S., Schwarm, M., & Drauz, K. (1998). Biocatalysis to amino acid-based chiral

    pharmaceuticals - examples and perspectives. *Journal of Molecular Catalysis B-*

    Enzymatic, 5(1-4), 1-11.

Bommarius, A. S., Schwarm, M., & Drauz, K. (2001). Comparison of different chemoenzymatic

    process routes to enantiomerically pure amino acids. *Chimia, 55*(1-2), 50-59.

Chaaban, J. H., Dam-Johansen, K., Skovby, T., & Kiil, S. (2014). Separation of Enantiomers by

    Preferential Crystallization: Mathematical Modeling of a Coupled Crystallizer

    Configuration. *Organic Process Research & Development, 18*(5), 601-612. doi: Doi

    10.1021/Op400286q

Chang, S. C. (1995). The Method of Space-Time Conservation Element and Solution Element - a

    New Approach for Solving the Navier-Stokes and Euler Equations. *Journal of*

    Computational Physics, 119(2), 295-324.

Doki, N., Kubota, N., Yokota, M., & Chianese, A. (2002). Determination of critical seed loading

    ratio for the production of crystals of uni-modal size distribution in batch cooling

    crystallization of potassium alum. *Journal of Chemical Engineering of Japan, 35*(7), 670-

    676. doi: Doi 10.1252/Jcej.35.670

Elander, R. P. (2003). Industrial production of β-lactam antibiotics. *Appl Microbiol Biotechnol, 61*, 385-392.

Eliel, E. L. (1983). Enantiomers, Racemates, and Resolutions - Jacques,J, Collet,a, Wilen,Sh. *American Scientist, 71*(4), 428-428.

Elsner, M. P., Ziomek, G., & Seidel-Morgenstern, A. (2009). Efficient Separation of Enantiomers by Preferential Crystallization in Two Coupled Vessels. *Aiche Journal, 55*(3), 640-649. doi: Doi 10.1002/Aic.11719

Encarnacion-Gomez, L. G., Bommarius, A. S., & Rousseau, R. W. (2015). Reactive crystallization of selected enantiomers: Chemo-enzymatic stereoinversion of amino acids at supersaturated conditions. *Chemical Engineering Science, 122*, 416-425. doi: DOI 10.1010/j.ces.2014.09.055

Fantin, G., Fogagnolo, M., Medici, A., Pedrini, P., Poli, S., & Gardini, F. (1993). Microbial Oxidation with Bacillus-Stearothermophilus - High Enantioselective Resolution of 1-Heteroaryl and 1-Aryl Alcohols. *Tetrahedron-Asymmetry, 4*(7), 1607-1612.

Ferreira, A. L. O. (2007). Nonconventional reactor for enzymatic synthesis of semi-synthetic beta-lactam antibiotics. *Industrial & Engineering Chemistry Research, 46*(23), 7695-7702.

Findrik, Z., Vasic-Racki, D., Geueke, B., Kuzu, M., & Hummel, W. (2005). Kinetic modeling of amino acid oxidation catalyzed by a new D-amino acid oxidase from Arthrobacter protophormiae. *Engineering in Life Sciences, 5*(6), 550-555. doi: DOI 10.1002/elsc.200520105

Franco, L. F. M., Mattedi, S., & Pessoa, P. D. (2013). A new approach for the thermodynamic modeling of the solubility of amino acids and beta-lactam compounds as a function of pH. *Fluid Phase Equilibria, 354*, 38-46. doi: DOI 10.1016/j.fluid.2013.06.009

Francotte, E. (2009). Enantioselective Chromatography: From its Emergence to its Successful Implementation in the Pharmaceutical Environment. *Chimia, 63*(12), 867-871. doi: DOI 10.2533/chimia.2009.867

Francotte, E., Leutert, T., La Vecchia, L., Ossola, F., Richert, P., & Schmidt, A. (2002). Preparative resolution of the enantiomers of tert-leucine derivatives by simulated moving bed chromatography. *Chirality, 14*(4), 313-317. doi: Doi 10.1002/Chir.10042

Francotte, E. R. (2001). Enantioselective chromatography as a powerful alternative for the preparation of drug enantiomers. *Journal of Chromatography A, 906*(1-2), 379-397. doi: Doi 10.1016/S0021-9673(00)00951-1

Franks, M. E., Macpherson, G. R., & Figg, W. D. (2004). Thalidomide. *Lancet, 363*(9423), 1802-1811. doi: Doi 10.1016/S0140-6736(04)16308-3

Fujiwara, M., Nagy, Z. K., Chew, J. W., & Braatz, R. D. (2005). First-principles and direct design approaches for the control of pharmaceutical crystallization. *Journal of Process Control, 15*(5), 493-504. doi: DOI 10.1016/j.jprocont.2004.08.003

Giordano, R. C., Ribeiro, M. P. A., & Giordano, R. L. C. (2006). Kinetics of beta-lactam antibiotics synthesis by penicillin G acylase (PGA) from the viewpoint of the industrial enzymatic reactor optimization. *Biotechnology Advances, 24*(1), 27-41. doi: DOI 10.1016/j.biotechadv.2005.05.003

Gruber, C. C., Lavandera, I., Faber, K., & Kroutil, W. (2006). From a racemate to a single

    enantiomer: Deracemization by stereoinversion. *Advanced Synthesis & Catalysis,*

    348(14), 1789-1805.

Hamad, B. (2010). The antibiotics market. *Nature Reviews Drug Discovery, 9*(9), 675-675.

Hoeben, M. A., van Hee, P., van der Lans, R. G. J. M., Kwant, G., & van derWielen, L. A. M.

    (2009). Design of a Counter-Current Interfacial Partitioning Process for the Separation of

    Ampicillin and Phenylglycine. *Industrial & Engineering Chemistry Research, 48*(16),

    7753-7766.

Illanes, A., Anjari, S., Arrieta, R., & Aguirre, C. (2002). Optimization of yield in kinetically

    controlled synthesis of ampicillin with immobilized penicillin acylase in organic media.

    Applied Biochemistry and Biotechnology, 97(3), 165-179. doi: Doi

    10.1385/Abab:97:3:165

Kelkar, V. V., & Ng, K. M. (1999). Design of reactive crystallization systems incorporating

    kinetics and mass-transfer effects. *Aiche Journal, 45*(1), 69-81.

Kim, M. G., & Lee, S. B. (1996). Penicillin acylase-catalyzed synthesis of pivampicillin: Effect

    of reaction variables and organic cosolvents. *Journal of Molecular Catalysis B-*

    Enzymatic, 1(2), 71-80. doi: Doi 10.1016/1381-1177(95)00009-7

Klussmann, M., White, A. J. R., Armstrong, A., & Blackmond, D. G. (2006). Rationalization and

    prediction of solution enantiomeric excess in ternary phase systems. *Angewandte*

    Chemie-International Edition, 45(47), 7985-7989. doi: DOI 10.1002/anie.200602520

Kroutil, W., & Faber, K. (1998). Deracemization of compounds possessing a sec-alcohol or -

    amino group through a cyclic oxidation-reduction sequence: a kinetic treatment.

    Tetrahedron-Asymmetry, 9(16), 2901-2913. doi: Doi 10.1016/S0957-4166(98)00306-1

Larson, M. A., & Garside, J. (1986a). Solute Clustering and Interfacial-Tension. *Journal of Crystal Growth, 76*(1), 88-92. doi: Doi 10.1016/0022-0248(86)90013-8

Larson, M. A., & Garside, J. (1986b). Solute Clustering in Supersaturated Solutions. *Chemical Engineering Science, 41*(5), 1285-1289. doi: Doi 10.1016/0009-2509(86)87101-9

Leyssens, T., Baudry, C., & Hernandez, M. L. E. (2011). Optimization of a Crystallization by Online FBRM Analysis of Needle-Shaped Crystals. *Organic Process Research & Development, 15*(2), 413-426. doi: Doi 10.1021/Op100314g

Li, H. Y., Kawajiri, Y., Grover, M. A., & Rousseau, R. W. (2014). Application of an Empirical FBRM Model to Estimate Crystal Size Distributions in Batch Crystallization. *Crystal Growth & Design, 14*(2), 607-616. doi: Doi 10.1021/Cg401484d

Lorenz, H., & Seidel-Morgenstern, A. (2014). Processes To Separate Enantiomers. *Angewandte Chemie-International Edition, 53*(5), 1218-1250.

Ma, D. L., Chung, S. H., & Braatz, R. D. (1999). Worst-case performance analysis of optimal batch control trajectories. *Aiche Journal, 45*(7), 1469-1476. doi: DOI 10.1002/aic.690450710

Massey, V., Curti, B., & Ganther, H. (1966). A Temperature-Dependent Conformational Change in D-Amino Acid Oxidase and Its Effect on Catalysis. *Journal of Biological Chemistry, 241*(10), 2347-&.

Miller, S. M., & Rawlings, J. B. (1994). Model Identification and Control Strategies for Batch Cooling Crystallizers. *Aiche Journal, 40*(8), 1312-1327. doi: DOI 10.1002/aic.690400805

Muller, H. G., Guntherberg, H., Drechsler, H., Mauersberger, S., Kortus, K., & Oehme, G. (1991). Stereoselectivity in the Enzymatic Oxidation of Racemic Alkyl Methylcarbinols - a New Approach to the S-Enantiomers. *Tetrahedron Letters, 32*(18), 2009-2012.

Mullin, J. W. (2001). *Crystallization* (Fourth ed.). Boston, MA: Elsevier Butterworth-Heinemann.

Nagy, Z. K. (2008). A population balance model approach for crystallization product engineering via distribution shaping control. *18th European Symposium on Computer Aided Process Engineering, 25*, 139-144.

Nagy, Z. K., & Braatz, R. D. (2004). Open-loop and closed-loop robust optimal control of batch processes using distributional and worst-case analysis. *Journal of Process Control, 14*(4), 411-422. doi: DOI 10.1016/j.procont.2003.07.004

Nagy, Z. K., & Braatz, R. D. (2012). Advances and New Directions in Crystallization Control. *Annual Review of Chemical and Biomolecular Engineering, Vol 3, 3*, 55-75. doi: DOI 10.1146/annurev-chembioeng-062011-081043

Nagy, Z. K., Fevotte, G., Kramer, H., & Simon, L. L. (2013). Recent advances in the monitoring, modelling and control of crystallization systems. *Chemical Engineering Research & Design, 91*(10), 1903-1922. doi: DOI 10.1016/j.cherd.2013.07.018

Nagy, Z. K., Fujiwara, M., Woo, X. Y., & Braatz, R. D. (2008). Determination of the kinetic parameters for the crystallization of paracetamol from water using metastable zone width experiments. *Industrial & Engineering Chemistry Research, 47*(4), 1245-1252.

Ospina, S., Barzana, E., Ramirez, O. T., & LopezMunguia, A. (1996). Effect of pH in the synthesis of ampicillin by penicillin acylase. *Enzyme and Microbial Technology, 19*(6), 462-469. doi: Doi 10.1016/S0141-0229(96)00032-4

Ottens, M., Lebreton, B., Zomerdijk, M., Rijkers, M. P. W. M., Bruinsma, O. S. L., & van der Wielen, L. A. M. (2001). Crystallization kinetics of ampicillin. *Industrial & Engineering Chemistry Research, 40*(22), 4821-4827.

Ottens, M., Lebreton, B., Zomerdijk, M., Rijkers, M. P. W. M., Bruinsma, O. S. L., & van der Wielen, L. A. M. (2004). Impurity effects on the crystallization kinetics of ampicillin. *Industrial & Engineering Chemistry Research, 43*(24), 7932-7938.

Pessoa, P. D., & Maurer, G. (2008). An extension of the Pitzer equation for the excess Gibbs energy of aqueous electrolyte systems to aqueous polyelectrolyte solutions. *Fluid Phase Equilibria, 269*(1-2), 25-35. doi: DOI 10.1016/j.fluid.2008.04.019

Polenske, D., & Lorenz, H. (2009). Solubility and Metastable Zone Width of the Methionine Enantiomers and Their Mixtures in Water. *Journal of Chemical and Engineering Data, 54*(8), 2277-2280.

Prausnitz, J. M., Lichtenthaler, R. N., & Azevedo, E. G. d. (1999). *Molecular thermodynamics of fluid-phase equilibria* (3rd ed.). Upper Saddle River, N.J.: Prentice-Hall PTR.

Qamar, S., Elsner, M. P., Angelov, I. A., Warnecke, G., & Seidel-Morgenstern, A. (2006). A comparative study of high resolution schemes for solving population balances in crystallization. *Computers & Chemical Engineering, 30*(6-7), 1119-1131.

Qiu, Y. F., & Rasmuson, A. C. (1994). Estimation of Crystallization Kinetics from Batch Cooling Experiments. *Aiche Journal, 40*(5), 799-812.

Randolph, A. D., & Larson, M. A. (1988). *Theory of particulate processes*. San Diego, CA: Academic Press.

Rodrigo, A. A., Lorenz, H., & Seidel-Morgenstern, A. (2004). Online monitoring of preferential crystallization of enantiomers. *Chirality, 16*(8), 499-508. doi: Doi 10.1002/Chir.20067

Rudolph, E. S. J., Zomerdijk, M., Ottens, M., & van der Wielen, L. A. M. (2001). Solubilities and partition coefficients of semi-synthetic antibiotics in water+1-butanol systems.

Industrial & Engineering Chemistry Research, 40(1), 398-406. doi: Doi 10.1021/Ie000089h

Santana, M., Ribeiro, M. P. A., Leite, G. A., Giordano, R. L. C., Giordano, R. C., & Mattedi, S. (2010). Solid-Liquid Equilibrium of Substrates and Products of the Enzymatic Synthesis of Ampicillin. *Aiche Journal, 56*(6), 1578-1583. doi: Doi 10.1002/Aic.12082

Schroer, J. W., Wibowo, C., & Ng, K. M. (2001). Synthesis of chiral crystallization processes. *Aiche Journal, 47*(2), 369-387.

Shi, B., Frederick, W. J., & Rousseau, R. W. (2003). Effects of calcium and other ionic impurities on the primary nucleation of burkeite. *Industrial & Engineering Chemistry Research, 42*(12), 2861-2869. doi: Doi 10.1021/Ie020845e

Simon, H., Bader, J., Gunther, H., Neumann, S., & Thanos, J. (1985). Chiral Compounds Synthesized by Biocatalytic Reductions. *Angewandte Chemie-International Edition in English, 24*(7), 539-553.

Soda, K., Oikawa, T., & Yokoigawa, K. (2001). One-pot chemo-enzymatic enantiomerization of racemates. *Journal of Molecular Catalysis B-Enzymatic, 11*(4-6), 149-153. doi: Doi 10.1016/S1381-1177(00)00181-8

Sohnel, O., & Mullin, J. W. (1988). Interpretation of Crystallization Induction Periods. *Journal of Colloid and Interface Science, 123*(1), 43-50. doi: Doi 10.1016/0021-9797(88)90219-6

Svang-Ariyaskul, A., Koros, W. J., & Rousseau, R. W. (2012). Chiral purification of glutamic acid enantiomers using a size-selective barrier membrane and dual-vessel crystallization. *Chemical Engineering Science, 77*, 35-41. doi: DOI 10.1016/j.ces.2012.01.004

Tseng, Y. T., & Ward, J. D. (2014). Critical seed loading from nucleation kinetics. *Aiche Journal, 60*(5), 1645-1653. doi: Doi 10.1002/Aic.14366

Wegman, M. A., Janssen, M. H., van Rantwijk, F., & Sheldon, R. A. (2001

). Towards Biocatalytic Synthesis of β-Lactam Antibiotics. *Adv. Synth. Catal, 343*(6-7), 559-
576.

Wegman, M. A., Janssen, M. H. A., van Rantwijk, F., & Sheldon, R. A. (2001). Towards
biocatalytic synthesis of beta-lactam antibiotics. *Advanced Synthesis & Catalysis, 343*(6-
7), 559-576.

Wibowo, C., Chang, W. C., & Ng, K. M. (2001). Design of integrated crystallization systems.
Aiche Journal, 47(11), 2474-2492.

Wolf, C. (2007). Dynamic Stereochemistry of Chiral Compounds Principles and Applications
Introduction. *Dynamic Stereochemistry of Chiral Compounds: Principles and
Applications*, 1-5. doi: Book_Doi 10.1039/9781847558091

Youshko, M. I., Chilov, G. G., Shcherbakova, T. A., & Svedas, V. K. (2002). Quantitative
characterization of the nucleophile reactivity in penicillin acylase-catalyzed acyl transfer
reactions. *Biochimica Et Biophysica Acta-Proteins and Proteomics, 1599*(1-2), 134-140.

Youshko, M. I., & Svedas, V. K. (2000). Kinetics of ampicillin synthesis catalyzed by penicillin
acylase from E-coli in homogeneous and heterogeneous systems. Quantitative
characterization of nucleophile reactivity and mathematical modeling of the process.
Biochemistry-Moscow, 65(12), 1367-1375. doi: Doi 10.1023/A:1002896621567

Youshko, M. I., van Langen, L. M., de Vroom, E., Moody, H. M., van Rantwijk, F., Sheldon, R.
A., & Svedas, V. K. (2000). Penicillin acylase-catalyzed synthesis of ampicillin in
"aqueous solution-precipitate" systems. High substrate concentration and supersaturation
effect. *Journal of Molecular Catalysis B-Enzymatic, 10*(5), 509-515. doi: Doi
10.1016/S1381-1177(00)00091-6

Youshko, M. I., van Langen, L. M., de Vroom, E., van Rantwijk, F., Sheldon, R. A., & Svedas, V. K. (2001). Highly efficient synthesis of ampicillin in an "aqueous solution-precipitate" system: Repetitive addition of substrates in a semicontinuous process. *Biotechnology and Bioengineering, 73*(5), 426-430. doi: Doi 10.1002/Bit.1076

Youshko, M. I., van Langen, L. M., de Vroom, E., van Rantwijk, F., Sheldon, R. A., & Svedas, V. K. (2002). Penicillin acylase-catalyzed ampicillin synthesis using a pH gradient: A new approach to optimization. *Biotechnology and Bioengineering, 78*(5), 589-593.